COMBINED TROPOSPHERIC ATTENUATION ALONG SATELLITE PATH AT SHF AND EHF BANDS IN SUBTROPICAL REGION

By

Elijah Olusayo Olurotimi

Submitted in the fulfilment of the requirements of the degree of

Doctor of Engineering in Electronic Engineering in the

Faculty of Engineering and the Built Environment at the

Durban University of Technology

MARCH 2019

ABSTRACT

The traffic flow of information across the globe is crucial in today's communication systems, where about 88% population are connected via several smart devices, hence resulting into constraints on the limited available radio resources. Due to the limitations of terrestrial connectivity affecting communication systems, in terms of geographical coverage area and system capacity, which have become serious issues globally. Therefore, there is a need for communication industries to embrace the use of satellite systems. Satellite services have many advantages some of which includes availability, wide coverage area and the ability to accommodate most of the limitations of the terrestrial systems. However, Earth-to-satellite systems, especially those operating at higher frequencies above 7 GHz, usually suffer from degradation due to hydrometeors which are mainly produced in the troposphere. Hydrometeors include rainfall, hail, gases, clouds and snow among others; of which rainfall is the principal factor which contributes highest impairment along the propagation paths, simply termed as rain attenuation. Moreover, the scenario in the tropical and subtropical regions become more pronounced due to the degree of occurrence of precipitation when compared to the temperate region. Other significant factor that usually affects the propagation of signals is attenuation by scattering and absorption due to rain, water vapour, cloudiness and other gases in the atmosphere.

Thus, in order to estimate accurate rain attenuation of a location, there is a need for accurate measurements of rain attenuation components such as rain height, rain rate, altitude, slant-path length, among others; of which rain height plays a significant role in the case of satellite links. However, the attenuation due to other tropospheric components cannot be negligible at higher frequencies over any location in order to proffer solution or cater for impairments that may arise as a result of any atmospheric perturbation in a satellite communications system. The significance of rain height in estimating rain attenuation along the satellite path, is

crucial and this important component has been extensively dealt with in the temperate region, partially in tropical region with no record in subtropical regions.

This study, therefore, focuses on the measurement of rain height to assess the degree of attenuation due to precipitation over several locations across South Africa, a subtropical region. In spite of the extensive works that have been carried out on prediction of rain attenuation based on the recommended rain height by the International Telecommunication Union-Regulation over some of the studied locations, the contribution of local rain height data for rain attenuation prediction will enable better results which are the focus of this study. Hence, this thesis presents 5-year rain height measurements based on zero-degree isotherm height (ZDIH) obtained from the Tropical Rainfall Measuring Mission-Precipitation Radar (TRMM-PR) over a subtropical region-South Africa.

The component of this work encompasses rain height cumulative distribution, percentage of exceedances, development of the contour maps of rain heights for South Africa, modeling of rain height, tropospheric attenuation prediction due to gas, cloudiness, scintillation, application of rain height for rain attenuation prediction, estimation of total attenuation and prediction of quality of service based on signal to noise ratio.

Findings from this work show that the ZDIH distribution is location dependent. Rain heights value ranges from about 4.305 km from the southern region to 5.105 km in the northern region of South Africa. The parameters of the ZDIH distribution models developed with the use of maximum likelihood estimation technique show a wider variation over some selected locations observed. Finally, attenuation due to rain, gas, cloudiness and scintillation were estimated. In addition, the total attenuation and the quality of service based on the propagation signals at SHF and EHF over some selected stations were evaluated and presented in this work.

DECLARATION

I hereby declare that this dissertation is my original work, every cited or text have been properly referenced and has not been previously submitted in part or totality for another degree in this or any other University.

Submitted by:

……. ……..……..

E. O. Olurotimi Date

Student Number: 21556553

Approved for Final Submission by:

……. …….

Supervisor: Dr. A. O. Sokoya Date

……. …….

Co-Supervisor: Prof. J. S. Ojo Date

…….. …….

Co-Supervisor: Prof. P. A. Owolawi Date

DEDICATION

This work is dedicated to:

God Almighty, my Creator, King, my all in all;

The blessed memory of my late father and ever supportive my mother;

My siblings; and

My children.

ACKNOWLEDGEMENTS

Firstly, I give all glory to the Almighty God for His infinite mercy, care, love, protection, and the opportunity given to me ever since the commencement of this program.

My profound gratitude goes to Dr. A. O. Sokoya, Prof. J. S. Ojo, and Prof. P. A. Owolawi for their commitments, invaluable comments, and useful suggestions for this research. I thank them for their times, guidance, financial supports, encouragements, and valuable inputs with thorough supervision in order to make this work a success.

I will like to extend my gratitude to the Durban University of Technology for the financial assistance via the Doctoral Scholarship Scheme, this support assisted me in completing my program.

I express my gratitude to the former Head of Department, Electronic Engineering, Durban University of Technology, Mr. K. E. Moorgas, as well as members of staff most especially Mr. S. Sewdass, Dr Poobie (of blessed memory), for their assistance and encouragements.

I will like to thank Erasmus+ for the scholarship and exposure, also the members of staff and colleagues at the University of Valladolid.

I deeply appreciate my parents and siblings for their moral supports, prayers, understanding, patience and encouragements.

Lastly, I wish to thank all my friends (most especially Mr. Niyi and Banjo for their assistance in proofreading this work) and well-wishers in the Electronic Engineering Department, Faculty of the Engineering and the Built Environment, the entire University, and beyond for their insightful advice and encouragements.

TABLE OF CONTENTS

Title **Page**

LIST OF FIGURES

LIST OF TABLES

LIST OF ABBREVIATIONS

BSS	Broadcast Satellite Service
CCIR	International Radio Consultative Committee
CDF	Cumulative Distribution Function
CERES	Cloud and Earth Radiant Energy Sensor
DTH	Direct-To-Home
EHF	Extremely Higher Frequency
ENSO	El Nino Southern Oscillation
FSS	Fixed Satellite Service
HDF	Hierarchical Data Format
H_r	Rain height
ICTs	Information and Communication Technologies
IFOV	Instantaneous Field of View
ITU	International Telecommunication Union
ITU-D	International Telecommunication Union-Development
ITU-R	International Telecommunication Union-Radio communication
ITU-R Rec.	ITU-R Recommendation
ITU-T	International Telecommunication Union- Telecommunication
JAXA	Japan Aerospace Exploration Agency
K-S test	Kolmogorov Smirnov Test
LIS	Lightning Imaging Sensor
LMDS	Local Multipoint Distribution Services
LOS	Line of Sight
LWC	Liquid Water Content
MLE	Maximum Likelihood Estimation
MSS	Mobile Satellite Service
MVD	Microwave Video Distribution Services
NASA	National Aeronautics and Space Administration
PDF	Probability Density Function

PMB	Pietermaritzburg
QoS	Quality of Signal/ Service
RH	Relative Humidity
RMSE	Root Mean Square Error
Rx	Receiver
SAM	Simple Attenuation Model
SCADA	Supervisory Control and Data Acquisition
SHF	Super High Frequency
SNR	Signal to Noise Ratio
TRMM	Tropical Rainfall Measuring Mission
TMI	TRMM Microwave Imager
TRMM-PR	TRMM-Precipitation Radar
Tx	Transmitter
USATs	Ultra Small Aperture Terminals
VIRS	Visible and Infrared Scanner
VSATs	Very Small Aperture Terminals
ZDIH	Zero-Degree Isotherm Height (0^{o} C Isotherm Height)

CHAPTER ONE

GENERAL INTRODUCTION

1.1 Introduction

The massive demands of satellite communication services in recent times have resulted in the expansion of frequency band in the spectrum [1]. Hence, scientists, system engineers and satellite communication system designers are improving on the microwave and millimeter wave systems to enhance good Quality of Service (QoS) to the end users. Higher frequency band occupancy is one of the characteristics of this spectrum, which is capable of accommodating the ever-increasing consumers' demands by providing higher data rate, wide capacities, better bandwidth, improved coverage and decongesting the lower frequency bands [2].

Studies have also revealed that satellite communication services using Ultra Small Aperture Terminals (USATs) and Very Small Aperture Terminals (VSATs), especially those operating above 10 GHz required necessary measurements to deliver good QoS to the end-users [3-5]. The services rendered by such satellite are Direct-to-Home (DTH), internet access, real-time video conferencing, telemedicine, tele-education, defense, electronic banking, oil exploration, Supervisory Control and Data Acquisition (SCADA), fixed and mobile telephony, among others.

Over the years, the increased usage of satellite communication has brought congestion in the frequencies up to about 6 GHz (known as lower frequency bands) of the radio frequency spectrum. This has led to the usage of the higher frequency bands. These bands are now available for use in the radio communication and radar systems [6]. Hence, it is of great importance to systems designers and service providers due to the available bandwidths in this frequency range. However, the reliability of the radio wave propagation systems in these

bands is severely degraded by several atmospheric perturbations such as rain, ice, snowflakes, fog, cloud, hail, atmospheric gases, among others [7, 8]. Among these perturbations, rain is known to be the primary factor causing attenuation, while other attenuations that may arise are regarded as the secondary effect on the radio wave via absorption, scattering and heating [9, 10]. In order to establish the grade of service and systems' satisfactorily work [11, 12], the need for signal attenuation parameters to be examined under the chosen weather is necessary. It has been reported that the rainfall incidence on the radio link, which resulted in rain attenuation, became significant at the frequencies of about 10 GHz in the temperate climates, while it can be significant as low as about 7 GHz in the tropical and subtropical climates [13-16]. In addition, statistical information of attenuation on satellite communication signals operating above these frequencies by precipitation is very important in the development of satellite communication systems. Rain height is also known as an important parameter in accurate estimation of rain attenuation and in some applications of satellite communication systems [17-19].

In the temperate climates, the information on effect of rain in microwave and millimeter wave propagation is available due to the availability of large data bank in the region. As a result of several measurement campaigns in the temperate region and enormous database, the developed global climate zone classification was proposed and established [20, 21]. The extension of the process to tropical and subtropical were based on interpolation and extrapolation due to data scarcity in those mentioned regions [20, 21]. As a result of extrapolation and interpolation of data, this assumption has led to over- or under-estimation of the attenuation in those two regions, hence the need to study diverse propagation factors that are peculiar with those regions are crucial for accurate calculation of attenuation [13]. Rain is known as a natural phenomenon that varies yearly and from location to location. Therefore, propagation measurement should be made to create the desired database for a geographical location. For the tropical region, rain height

data are available in only a very few locations, while the measurement is yet to receive attention in subtropical regions. Tropospheric disturbances such as rain, atmospheric gases, cloudiness and scintillation have strong effects on the propagation of radio wave signals. Hence, there is a need to take proper measurements of these tropospheric parameters by estimating accurate attenuation of a location in order to provide better QoS to the end-users.

1.2 Problem Formulation

The transmission impairments arising from the signal attenuation due to rain, gaseous absorption, cloudiness and tropospheric scintillation adversely compromise the reliability of SHF and EHF band signals resulting in noticeable digital transmission errors. These propagation impairments, characterized by variations in the signal amplitude and phase, are commonly known as rain fade [22], which has an adverse effect on the QoS of satellite communication applications. A decision support system becomes essential for satellite service providers in accurately predicting rain fade and establishing mitigation planning by adaptively selecting the suitable power levels, coding, and the modulation schemes.

Propagation impairments produced by the troposphere are known to be the limiting factors affecting the effective use of high-frequency bands. Studies show that the atmospheric effects and its impact on satellite communications are well pronounced, especially at frequencies above 10 GHz [14]. The case of the tropical and sub-tropical regions become more serious because the rain patterns at such locations are characterized by high-intensity rainfall, the increase in the degree of the rain occurrence, and the increased occurrence of large raindrops when compared with the temperate climates in the regions.

In addition, it is a well-known fact that rain is a natural phenomenon with varied attributes, that is time dependent, location dependent and yearly dependent. For

this reason, there is a need for a solid database of propagation measurements to be made as nearly as possible in the intended topographical area of operations. Some efforts have been made with the use of the classification of climate zones on the worldwide basis in order to extend existing data to a wider range of the circumstances. However, most of the dimensions in the databases have been made in the Northern Hemisphere in temperate zones [20]. Much evidence proposes that in the tropical and subtropical zones, the factors that make significant contributions to propagation impairment are different [13]. In addition, the location variation is built on selected point rainfall data and radar reflectivity data collected around the world. And the influence of rain intensity often leads to degradation of radio propagation signals at very high frequencies, most especially SHF and the EHF bands [23].

It is well established that rain attenuation is the principal propagation impairment at the frequencies above 10 GHz, while attenuation from other hydrometeors is regarded as a secondary impairments contributor [14, 24]. This assumption may be possible at the lower frequency, even up to Ku band. However, with the advent of modern communication systems operating at higher frequency bands, other attenuations that may arise from the so-called secondary impairment contributor (other hydrometeors) must be taken into consideration [25]; in order to guarantee the end-users a good and highly acceptable QoS. It should be noted that the empirical calculation of attenuations is regionally based. Hence, local or regional data are needed.

The empirical modeling of rain attenuation along the satellite path consists of rain rate at lower integration time (point of rainfall) and rain height measurements. These parameters are very important in accurate estimation of rain attenuation in a satellite link.

Also, due to the growing demand for better QoS in satellite services, the need for the accurate estimation of rain attenuation along the satellite path become crucial and important. Consequently, there is an increasing need to determine the accurate rain height of a location to counter the several degradations that arise due to tropospheric attenuation. The combination of prediction models with the task to majorly determine the amount of the individual models of propagation impairments is also required. Rain attenuation, depolarization, and melting layer models are generally correlated or interdependent. Several authors have worked on the aforementioned areas of combined attenuation except in the measurement and modeling of the rain height, which is an important component to calculate rain attenuation [26-29].

Moreover, there is limited information on the measurement of rain height over the studied locations in Southern Africa, a subtropical region. South Africa is one of the countries with diverse climate patterns. Much information on the statistical attenuation of the satellite communication signals by precipitation will be very useful in the development of satellite communication systems, especially those that are operated at frequencies above 10 GHz as earlier stated.

1.3 Research Objectives of the Work

The objectives of this research are:

1. To measure and estimate rain height based on 0^{o} C isotherm height (covering about 18 locations across the country) across South Africa, a subtropical region;
2. To develop contour maps of rain height across South Africa;
3. To evaluate the statistics and modeling of rain height;
4. To estimate rain attenuation based on measured rain height and make comparisons with attenuation obtained based on ITU-R recommendation value;
5. To predict gas, cloud attenuation, and tropospheric scintillation;

6. To determine combined attenuation (total attenuation); and QoS based on the propagation signals at SHF and EHF.

1.3.1 Research Scope of the Work

This research proposed the study of rain height in a subtropical region, observed the tropospheric disturbances on satellite links, and predicted the combined attenuation along the satellite path at Super High Frequency (SHF) and Extremely High Frequency (EHF).

1.4 Overview of the Thesis

In general, this thesis contains six chapters. Each of the chapters proffers an insight into the contents, objectives and the intensity of work accomplished during this study. Thus, the organization of this thesis starts with **Chapter one**. This chapter discusses the general introduction of the thesis: introduction, frequency bands in communication systems, problem formulation, the scope of the work, own contribution, and publications. The outline of the remaining chapters in this thesis is presented as follows:

Chapter two focuses on the propagation phenomena which usually impairs the propagation of radio signals on satellite communication systems. The interaction techniques of radio wave propagation and the transmission effects on Earth-satellite links were presented. It also looks into the categorization of rainfall and the climate observed over South Africa. **Chapter three** deals with the rain height measurement across stations in South Africa. This aspect gives the detailed analysis of rain height measured across South Africa, which is known as an important parameter for several applications of satellite communication. The contour map of rain height was also developed. The modeling and estimation method of rain height was also presented. **Chapter four** provides the mathematical methods of tropospheric attenuation prediction, such as the

amplitude of tropospheric scintillation, atmospheric gaseous attenuation, and cloud attenuation.

Chapter five observes the effects of rain height on rain attenuation in South Africa. This led to the prediction of rain-induced attenuation on satellite links, and further to the total attenuation prediction which comprises of the atmospheric components that causes impairments in the satellite communication links. The QoS-based on signal to noise ratio at SHF and EHF observed to understand the performances of the communication systems at the receiver's end are also presented. Lastly, **Chapter six** is the conclusion of the study carried out in this research. This chapter highlights the description of the research information and achievements, together with possible future research areas in order to improve in the rain height campaign measurement over subtropical region.

1.5 Research Contribution

In this thesis, the following are the contributions to the body of existing knowledge:

1. Determination of rain height over several locations in South Africa;
2. Developing rain height modeling and contour maps of rain heights for South Africa;
3. Reviewing and improving on the ITU-R rain height recommendations for the region;
4. Deduce rain attenuation based on local data of rain heights;
5. Improvement of the QoS of the satellite signals as a result of 1 and 2; and
6. Generating a set of data that will be useful in the area of link budgeting, especially for the radio network planning at higher frequencies with a specific focus on the Southern region of Africa.

1.7 Publications

The publications in this section are materials forming part of this thesis with appearances in peer-reviewed conference proceedings and accredited journals.

Journals:

1. Observation of Bright-Band Height Data from TRMM-PR for Satellite Communication in South Africa, Journal of Atmospheric and Solar-Terrestrial Physics. Vol. 160, pp. 24-33.

2. Distribution of rain height over subtropical region: Durban, South Africa for satellite communication systems, IOP Conference Series: Materials Science and Engineering, Vol. 321, No. 1, p. 012006.

3. 0^{o} C isotherm height distribution in South Africa for satellite communication systems. (Submitted to Advances in Space Research).

Conferences:

1. Analysis of Bright-Band Height Data from TRMM-PR for Satellite Communication in Durban, South Africa, IEEE AFRICON 2015 and available in IEEE Xplore Digital Library.

2. Modeling Freezing Height Level for Satellite Link Communication: Durban, South Africa, IEEE AFRICON 2017 and available in IEEE Xplore Digital Library.

3. Freezing Height Level Distribution over Durban, South Africa for Satellite Communication, IEEE Radio and Antenna Days of the Indian Ocean (RADIO- 2017) and available in IEEE Xplore Digital Library.

CHAPTER TWO

Propagation Impairments and Rain Rate Characterization

2.1 Introduction

The impact of atmospheric events on propagated waves over Earth-satellite links is a continuous concern for the performance and designing of satellite communications systems. The presence of these events on the Earth-satellite links often leads to an unrestrained variation in the amplitude signal, polarization, phase, and angle of arrival. Thus, the outcome of this variation in signal properties will increase the error rate of the digital transmissions and reduce the quality of the analog transmissions propagated through an open space channel. The atmospheric parameters, which are in various forms of water, include raindrops, cloud, hail, fog, snow and water vapor and are generally known as hydrometeors. Some other parameters exist as atmospheric parameters. All these parameters are mainly produced in the troposphere and are known to be the limiting factors for the effective use of high-frequency bands. That is, at frequencies above 3 GHz, attenuation due to the effect of these parameters are significant, whereas the attenuation is negligible at lower frequencies below 3 GHz. Hence, this chapter reviews the frequency bands in communication systems, tropospheric propagation, propagation impairments, and characterization of rain rate.

2.2 Frequency Bands in Communication Systems

Frequency bands are useful in many industries such as telecommunication, hospital, manufacturing, construction, meteorology, transportation and many more. The frequency bands range between 300 Hz to about 3000 THz and different parts of these bands are allocated for different applications of radio transmission and technology, which are classified and designated by an authorized organization, such as Radio Regulation of International Telecommunication Union-Radio communication (ITU-R) [23]. Also, the area of

interest of this study lies between the EHF and SHF range, for the bands below this range is highly congested and these bands of interest have the ability to carry a large collection of terrestrial and satellite services such as internet, Direct-to-Home (DTH), wireless mobile telephone, marine communication systems, critical military logistics and support, and recently with interplanetary communications. The designation of the frequency bands is depicted in Table 2.1.

Table 2.1 Frequency band descriptions [23].

Band No.	Abbreviation	Band name	Name	Symbol	Frequency
3	ULF	Ultra-low frequency	Hectokilo m		300 - 3000 Hz
4	VLF	Very low frequency	Myria m		3 - 30 kHz
5	LF	Low frequency	Km		30 - 300 kHz
6	MF	Medium frequency	Hm		300 - 3000 kHz
7	HF	High frequency	Dam		3 - 30 MHz
8	VHF	Very high frequency	M		3 - 30 MHz
9	UHF	Ultra-high frequency	Dm		300 - 3000 MHz
				L-band	1 - 2 GHz
				S-band	2 - 4 GHz
10	SHF	Super high frequency	Cm		3 - 30 GHz
				C-band	4 - 8 GHz
				X-band	8 - 12 GHz
				Ku-band	12 - 18 GHz
				K-band	18 - 27 GHz
				Ka-band	27 - 40 GHz
11	EHF	Extremely high frequency	Mm		30 - 300 GHz
				V-band	40 - 75 GHz
				W-band	75 - 110 GHz
12	THz (or THF)	Terahertz (Tremendously high frequency)	Deci mm		0.3 - 3 THz.
13			Centi mm		3 - 30 THz
14			Micrometric		30 - 300 THz
15			Decimicrometric		300 - 3000 THz

2.3 Overview of Tropospheric Propagation

The process by which radio signals propagate from the radio transmitters to the receivers is of great importance in planning a radio network. The radio path is governed by the atmospheric region through which the radio signal passes. Without the help of the atmosphere, it would have been very difficult for the radio signal to travel around the globe either on the short-wave bands or at higher frequencies. In view of the importance of the atmosphere, an overview of its makeup is presented in the next sub-section.

2.3.1 Earth's Atmosphere and its Structure

The Earth's atmosphere is the layer where different gases, meteors, vapors, dust particles and hydrometeors surrounded the planet [30]. These are cumulatively combined in different percentages till about 500 km above sea level by the force of gravity. These compositions of the Earth's atmosphere are categorized by various complex photochemical reactions such as nitrogen, oxygen, argon, carbon dioxide, water vapor and the traces of gases (helium, neon, xenon, and krypton). Due to the precipitation and the evaporation process, water is being transported from the ocean to the atmosphere.

The Earth's atmosphere is known to be divided into some distinct layers, with each layer comprises of their specific characteristics such as temperature and other compositions. The division into various layers is known as stratification and it's brought by gravity. The Earth's atmospheric layers consist of the following: the troposphere, the stratosphere, the mesosphere, the thermosphere, and the exosphere. The structure of Earth's atmospheric layers is presented in Figure 2.1 [31].

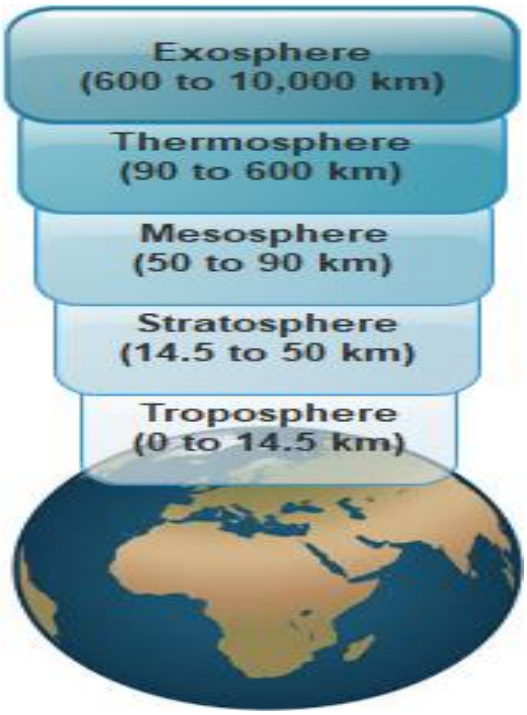

Figure 2.1 The Earth's atmospheric layers [31].

2.3.1.1 The Troposphere

The term "troposphere" was first used in 1908 by Treisserenc de Bort, which literally means the region of the Earth where air "turns over" with reference to the appreciable vertical mixture of the air in the lowermost zone [32]. In this layer, the steady temperature decreases with height and the lapse rate of the layer is noteworthy [33]. Also, the troposphere is an exact thermodynamic environment which does not relate much with the overlying layer of the stable air, or the stratosphere [34].

The troposphere is known to spread from the Earth's surface and extends up to about 8 to 14.5 km high. An assumption of these altitudes established that clouds transpire at the altitudes between 2 and 10 km. This region of the atmosphere is known as the denser and where the entire Earth's weather phenomenon originated. The region also contains about 80% percentage of the mass of the atmosphere. The pressure, temperature, and density of the air in the troposphere

decreases constantly as the altitude increases. The troposphere also contains about 99% of the water vapor in the atmosphere, with which its concentrations vary with the latitude (from North to South).

The refractive index of the air also plays a leading role in radio signal propagation in the troposphere, which depends on the pressure, temperature, and humidity [35]. In addition, the absorption, radiation, turbulence, diffusion, convection together with several complex and interactions of meteorological occurrences resulted in non-linear and random procedures in the troposphere. At the altitude of about 2 km, the radio signals are frequently affected while at low and mid-latitude areas of the world, tropospheric propagation circumstances are frequently existed. The interaction of these phenomena on satellite and terrestrial communications systems, especially those operating in the high-frequency bands, have called for the precise propagation predictions. It is also compulsory to know that either over or under-prediction of the propagation effect can result in an expensive or unreliable design of a communication system [14].

Hence, this work focuses on the assessment of the combined tropospheric attenuation along satellite paths at SHF and EHF in subtropical region. The effect of the troposphere on the electromagnetic waves in the higher frequency bands, due to clouds and precipitation are considered.

2.3.1.1.1 Tropospheric Components

The absorption effects of the troposphere are mainly caused by its composition. For example, the dry part (that is, oxygen, nitrogen, argon, carbon dioxide, water vapor); liquid water (fog, clouds, hydrometeors); aerosol and pollution. The clear-sky attenuation is due to oxygen, gases, and water vapor. Water vapor is mainly found in the troposphere. Definitely, about 50% of the water vapor in the atmosphere can be found between 0 and 1.5 km, while less than about 5-6% of water vapor can be found above 5 km, and less than about 1% can be found in

the stratosphere. The oxygen can be assumed to be constant without losing its generality, while the source of attenuation is always present, and the water vapor is highly variable during the year [36, 37].

Also, the attenuation due to hydrometeors (such as cloud, fog and raindrop) is dependent on two factors. That is, the absorption of energy caused by Joule effect and the diffusion wave induced by the particles. The attenuation generated by hydrometeors can be classified as rain and cloud attenuation. The rain attenuation is due to bigger hydrometeors precipitation and is known as the principal source of attenuation, although it is limited to time and space. While the cloud attenuation is dependent on small hydrometeors or liquid water that is suspended in the troposphere in forms of fog or clouds.

2.3.1.1.2 Troposphere Parameters

In the troposphere, quite a few parameters that can affect the formation of hydrometeors are further characterized here, and each of these could have its potential influence on the characteristics of the hydrometeors. The parameters considered are as follows:

2.3.1.1.2.1 Liquid Water Content

Liquid Water Content (LWC) is said to be the amount of the mass of water in the cloud in a specified quantity of dry air. It is also measured per the volume of air or the mass of air (g/m^3). LWC is important in figuring out the type of clouds that are likely to form and this strongly linked to the cloud microphysical variables [38].

2.3.1.1.2.2 Temperature

Temperature is a physical extent of expressing hotness and coldness. Also, it is a quantification of the internal energy (that is, the average kinetic energy) of a substance. Temperature is the most important quantity measured in the atmosphere. It is given in degrees Celsius (^oC), Fahrenheit (^oF) and in Kelvin (K).

The troposphere is generally marked by a decrease in temperatures with increasing height.

2.3.1.1.2.3 Humidity

Atmospheric humidity is the quantity of water vapor present in the air. While water vapor is known as the gaseous state of water, which is invisible to the human eye and indicates the likelihood of precipitation, fog or dew. Humidity consists of several measurements such as absolute humidity, relative humidity, humidity ratio and specific humidity [38].

Absolute humidity is the quantity of water vapor in a volume or mass of air. It can be measured in kg/m^3 and expressed as AH in (2.1):

$$AH = \frac{mass\ (water\ vapour)}{volume\ (air)} \tag{2.1}$$

Relative humidity (RH) is the ratio of partial pressure of water vapor to the saturated vapour pressure at a specified temperature; and it is measured in % and given by:

$$RH = \frac{e}{e_s} \times 100 \tag{2.2}$$

where e is the pressure due to water vapour and e_s is the saturated vapour pressure.

Humidity ratio**,** $H_{r,}$is the ratio of a mass of water vapor in the dry air; as given in (2.3):

$$H_r = \frac{m_v}{m_d} \tag{2.3}$$

where m_v is the mass of water vapour and m_d is the mass of dry air.

Specific humidity, Q, is the ratio of the mass of water vapor (m_v) to the total mass of water vapor and dry air ($m_v + m_d$). As given in (2.4):

$$Q = \frac{m_v}{m_v + m_d} \tag{2.4}$$

2.3.1.1.2.4 Atmospheric Pressure

Atmospheric pressure is initiated by the gravitational attraction of the earth on the atmospheric gases above the Earth's surface, which is a function of the surface radius, the mass of the planet and its vertical distribution in the Earth's atmosphere. Also, it can be defined as the product of the mass of the unit area above the point of air and the gravitational acceleration. That is the force per unit area applied to the above surface of the weighed air. It is measured in Pascal's (where 1 Pa = 1 Newton per square meter - N/m^2). Pressure is known to exponentially decrease from the surface of the Earth to the mesosphere.

2.3.1.2 Stratosphere

The stratosphere layer is the layer which extends just above the troposphere and extends to about 50 km high. In this layer, the airflow is mostly horizontal, and the temperature increases due to the strong absorption of the solar ultraviolet radiation by the ozone layer, which is located close to about 25 km above the surface of the Earth.

2.3.1.3 Mesosphere

The mesosphere is a layer located just above the stratosphere and extends up to about 90 km high. Also, it is the coldest region of the atmosphere because temperature decreases with height in this layer. Meteors also burn up in this layer

2.3.1.4 Thermosphere

The thermosphere can be found just above the mesosphere and extends to about 600 km high. Due to absorption of extremely energetic solar radiation in this layer,

the temperature increases with altitude. Aurora and satellites are positioned in this layer.

2.3.1.5 Exosphere

This is the uppermost region of the Earth's atmosphere, and this extends from the peak of the thermosphere up to about 10,000 km, as it gradually fades into the vacuum of the space.

2.3.1.6 Ionosphere

The ionosphere is known as a rich layer that contained ionized atoms, electrons, and molecules as it stretches from about 48 km above the surface of the Earth to the edge of space at about 1,000 km and overlap into the mesosphere and the thermosphere. This region grows and shrinks based on solar conditions and divides further into the sub-regions (such as D, E, and F), which are based on the wavelength absorption of the solar radiation. The ionosphere has a critical link in the chain of the Sun to Earth interactions, which makes the radio communications possible.

2.4 Radio Wave Propagation

In the space, the propagation of radio wave is as faster as electrons travel at the speed of light (that is, $\approx 3 \times 10^8$ m/s). During the propagation of radio wave signals from a transmitting antenna, three modes of propagation paths are formed, which are surface, sky and space wave propagation, as presented in Figure 2.2 (where the Tx and Rx is transmitting and receiving antenna respectively) [39]. Also, the

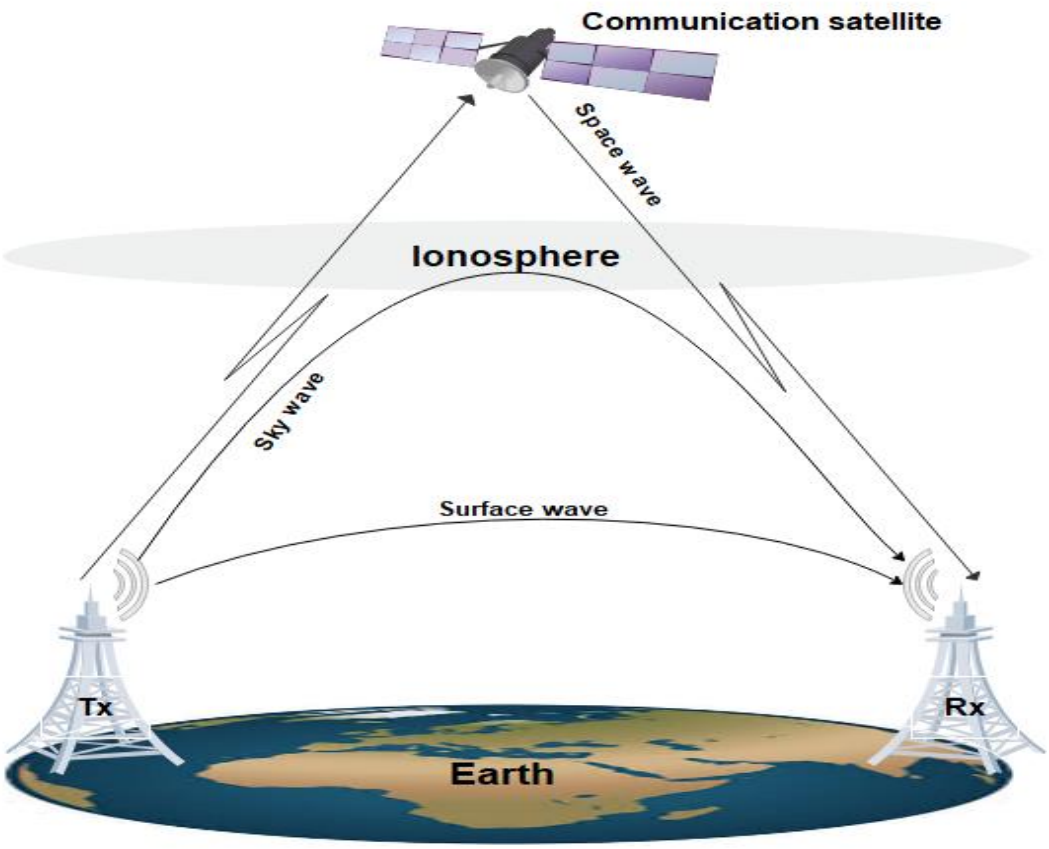

Figure 2.2 The modes of radio wave propagation [39].

transmissions of radio waves from an antenna are generally omnidirectional, which can be altered in a directional path with the use of antenna arrays or a directional dish. However, the **surface wave** mode of propagation is the type of radio wave that is being modified by the nature of the environment of which it travels; it can also be predominated by all radio frequencies between the ULF and MF bands. Whereas, the **sky waves** are strictly influenced by the action of the free electrons (known as ions) in the upper atmosphere (the ionosphere); and these usually cause attenuation, reflection and returning the ions back to the Earth's surface. Also, the propagation of sky wave dominates the HF band. While, the mode of propagation of radio wave by the **space wave** predominated the waves above the HF bands. During the propagation of space wave by Earth

station radio into the troposphere (which varies between 30 and 300 MHz), the variation of the wave is subjected to deflection as it passes through the refractive index of the air, which normally causes the radio wave in the short distance of about 100 km to follow the Earth's curvature. However, the wave above the frequencies of about 300 MHz is usually propagated upward, leaving the troposphere, this type of waves is very useful in satellite communications and can be termed as **free space** waves [39].

2.5 Interaction Techniques of Radio Wave

The introduction of general terms for better description of the propagation phenomena or interaction techniques that can affect the radio wave characteristics is very important in this research. These techniques are usually described in terms of variability of signal wave characteristics within the atmosphere through the following interactions [35, 40-42]:

2.5.1 Absorption and Scattering

Absorption can be defined as the reduction in the amplitude of a radio wave signal caused by an irreversible transfer of energy between the radio wave and the propagation path, while scattering can be defined as the process in which the energy of a radio wave is isolated or scattered during the incidence of radio wave on an ionic particle of inhomogeneous medium during the radio propagation [43-45]. Due to different components contained in the atmosphere (such as gases, water, and particles), there is an absorption and scattering on transmission of several wavelengths of electromagnetic radiation in the atmosphere, causing attenuation (reduction of signal strength) by introducing unwanted signals into the communication systems, this usually affect the desired signal at the receiver end [46]. Figure 2.3 shows the radio wave due to the absorption and the scattering effects, when transmitting during the rain-filled event. Figure 2.3 reveals the way by which absorption and scattering of signals depend on the raindrop shape, size, and other components [47]. The effect experienced by signals when passing

through rainy medium is given by the total sum of the separate contributions of the raindrop components. From the fact that raindrop consists of several magnitudes, the specific attenuation can be estimated by integrating the contributions of each raindrop [14, 43, 48].

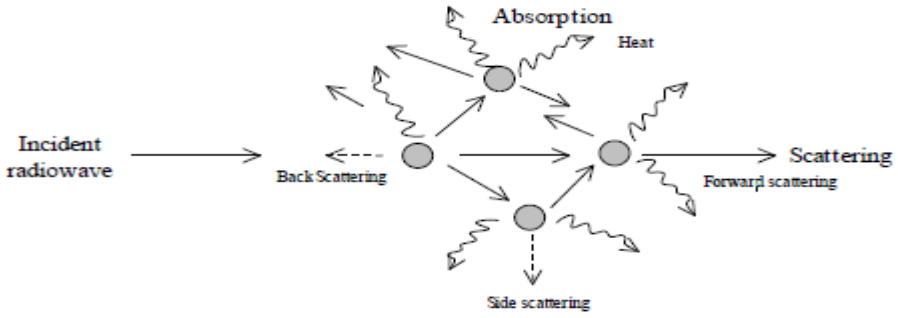

Figure 2.3 The absorption and scattering of radio wave during rain-filled event.

2.5.2 Refraction and Reflection

Refraction is a change in the direction of dissemination of a radio wave, resulting from the spatial variation of the refractive index of the medium. Reflection occurs when a signal encounters a large surface relative to the signal wavelength. Radio waves can be reflected from several substances or objects they encounter during their propagation between the transmission and receiving sites. Figure 2.4 shows the illustration of refraction and reflection of the signals.

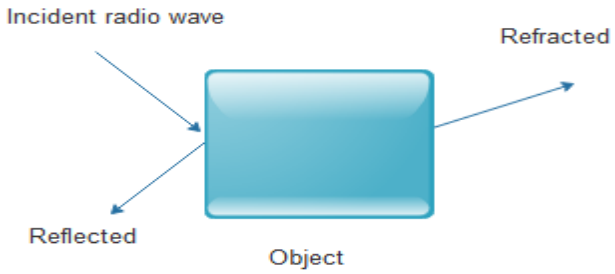

Figure 2.4 The Refraction and Reflector of radio wave.

2.5.3 Diffraction and Multipath

A change in the propagation direction of a radio wave signal, as a result of the presence of an obstacle, a restricted aperture, or other objects in a medium is denoted as diffraction. The condition of propagation as a result of the transmission of the radio wave by two or more propagation paths to the receiving antenna is called multipath. This effect arises due to the refractive index anomalies in the troposphere or in the ionosphere, or from the structural and terrain scattering on the surface of the Earth.

2.5.4 Scintillation

An electromagnetic wave that experiences the rapid variations in its phase, amplitude, and direction of arrival, due to the presence of irregularities inside a medium. These variations are known as scintillations. They are usually characterized by their period, depth, and speed of variation.

2.5.5 Fading

The variation of the amplitude in the radio wave propagation caused by changes in the transmission path with respect to time is termed as fading. Fading and scintillation is used substitutable, though, scintillation differs by referring more to rapid variations on the duration of second fractions order, while fading referred to the time variations of seconds or minutes order slowly.

2.5.6 Frequency Dispersion

Frequency dispersion can be defined as the change in the phase and frequency components caused by a dispersive medium across the radio wave bandwidth. A dispersive medium is a medium that constitutes components (such as permeability, permittivity, and conductivity) and depends on wave direction (spatial dispersion) or frequency (temporal dispersion).

Some of the interaction described in this **section** 2.4 can be presented on the propagation path at the same time, and it might be extremely difficult to identify

the techniques that produced the change in the characteristics of the propagation signal. Hence, Figure 2.5 briefly presents the situation that indicates how various techniques affect the observable parameters of the signal in a communication system [49].

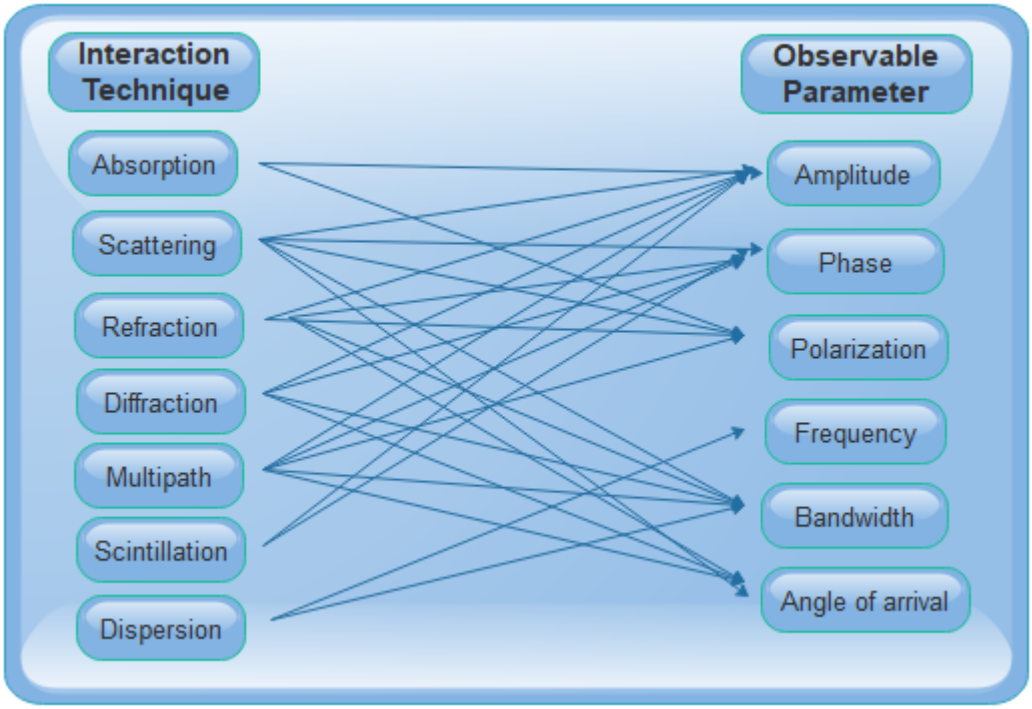

Figure 2.5 The interaction techniques and their influence on the communication signal parameters [42].

2.6 Transmission Impairments in the Earth-satellite Link and Measurement

Generally, radio waves from the frequencies of about 3 GHz and above are usually affected by the following propagation factors, which are primarily produced in the troposphere, and these frequencies are where numerous satellite communications operate [40, 41, 50]. Satellite applications that operate in the frequencies above 3 GHz include the following:

i. Broadcast Satellite Service (BSS);
ii. Mobile Satellite Service (MSS);
iii. Fixed Satellite Service (FSS);

iv. Military communication links; and
v. Deep space communication.

In this section, besides free space attenuation, the propagation impairment on the Earth-space links that is primarily involved in the effect of regularities of refractive index in the troposphere and the ionosphere is the absorption due to atmospheric gases (that is, oxygen and water vapour), and the attenuation caused by hydrometeors (such as cloud, fog, rain, snow, and ice) [40, 51]. Some other effects are blockage, shadowing and multipath scintillation, which might be involved on mobile terminal links. But the focus here are those impairments along the line of sight link, which are really crucial to Earth-satellite link propagation. These briefly discussed as follows:

2.6.1 Free Space Attenuation

The propagation loss experienced by radio waves due to the dispersion of energy that takes place as the signal wave travels from the transmitter, is known as free space attenuation. This free space attenuation, A_o, can be measured in dB and is given by:

$$A_o = 20 \log_{10} \left(\frac{4\pi d}{\lambda} \right) \tag{2.5}$$

where d and λ expressed in (m), are the distance and wavelength travelled between the transmitter and receiver respectively.

2.6.2 Phenomenon Associated with Refractive Index

The way in which refractive index of the media varies along the propagation direction in respect with height has a massive effect on the propagation of a radio wave. The variations of the atmospheric refractive index transpire in the lower Earth layer (tropospheric) due to changes in pressure, humidity and temperature. The tropospheric refractive index generally decreases with height.

Radio refractivity, N, can be used to magnify the change in the refractive index from the vacuum or free space (unity). Atmospheric refractive index, n, can be written as:

$$n = 1 + N \times 10^{-6} \tag{2.6}$$

where refractivity of a radio N, is given as:

$$N = \frac{77.6}{T}\left(p + \frac{4810e}{T}\right) \tag{2.7}$$

where T is temperature (K), e is the water vapor pressure (hPa), and p is the atmospheric pressure (hPa) [52].

2.6.3 Scintillation

Scintillation is known as the state of rapid fluctuations of the radio wave signal parameters in the propagation path, due to the time dependent irregularities [53]. The affected signal parameters include phase, amplitude, polarization, and angle of arrival. Also, scintillation effect can be produced in the troposphere and ionosphere. The concerned effect in this study is tropospheric scintillation, which will be discussed briefly in this subsection.

Tropospheric scintillation is the refractive index irregularities due to gradients of high humidity and the inversion of temperature layers in the first few kilometers of the altitude of the troposphere. These effects depend on daily, seasonal, and the local climate. It can be observed from above 10 GHz over line-of-site links [42].

2.6.3.1 Scintillation Parameters

The scintillation described in this part will be based on the received power of the radio wave transmission, since the interest of this work is on radio wave frequencies.

The received power log (dB) can be defined as:

$$x_{dB} = 20\log_{10}\left(\frac{A}{A_o}\right) \tag{2.8}$$

where $A_o = \langle A \rangle$ is the mean of the received amplitude, while A is the received signal amplitude.

Also, scintillation strength in the applications of a communication system is often specified by the variance of received power log of the transmission parameters and can be given as:

$$\sigma^2{}_x = 42.25\ (2\pi/\lambda)^{7/6} \int_o^L C_n^2(x)\ x^{5/7} dx \tag{2.9}$$

where λ is the wavelength (m), L is the total path length, C_n^2 is the structure constant of refractive index, and x is the distance along the path [42].

2.6.4 Atmospheric Gaseous Effect

Electromagnetic wave propagation through a clear atmosphere along the surface of the Earth is subjected to the attenuation by oxygen and water vapor due to absorption [43]. These effects can be noticeable at some certain frequencies, coinciding with the mechanical resonant frequencies of gas molecules such as oxygen and water vapor [54]. Some other gases such as O_3, SO_2, N_2O, NH_3, and NO_2 can also display resonant lines, though their effects are negligible on the propagation of signals due to their low density in the Earth's atmosphere [11]. This attenuation is dependent on the humidity, atmospheric pressure and temperature. Figure 2.6 shows the typical plot of specific attenuation due to water vapor and oxygen as a function of frequency. The computation of this figure consists of temperature measurement at about 15^o C, pressure at about 1013 hPa, and water vapor density of about 7.5 g/m^3 [55]. A single line of absorption due to water vapor

(H_2O) occurs at about 22.25 GHz and the complexity of the oxygen (dry air) lines was between 30 – 70 GHz frequency bands [55].

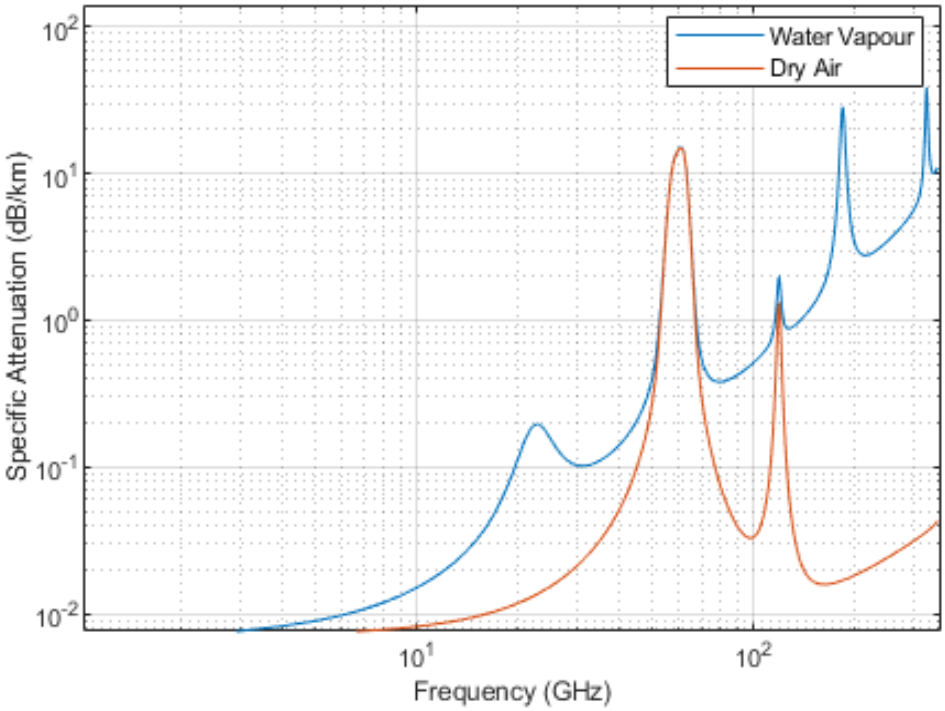

Figure 2.6 Specific attenuation due to atmospheric gases [55].

For this present technology, the significance of the peaks of absorption transpire at about 24 and 60 GHz [54]. The frequency regions between the absorption lines or the complexities of the lines are called atmospheric windows [46]. The regions of the spectra between the peaks of absorption provide the windows where propagation can more readily occur. The propagation windows are about 35, 94, 140 and 220 GHz [54]. As the windows become overfilled from the distribution of a large number of systems, the system designers are forced to drift towards higher frequencies. At frequencies above 100 GHz, where the structure of the line of absorption becomes more complex with significantly stronger water vapour lines occurring at about 183, 325, and 380 GHz [56].

2.6.5 Cloud Effect

Cloud effect is considerably less severe than rain effect. Nevertheless, this must be considered in the satellite link design, especially for frequencies above 15 GHz where the attenuation can approach up to about 4 dB, which may increase as the frequency increases, while the cloud attenuation can be ignored for the lower frequencies [57]. Also, attenuation due to cloudiness can be determined based on the total water content per unit volume. Scattering caused by the very small liquid water droplets which make up the liquid water in the clouds are higher in the Earth's atmosphere and can cause a significant attenuation at higher frequency bands. In the mid-latitude thunderstorms, clouds are assumed to consist of excess liquid water content of about 5 g/m^3. Similarly, in the atmosphere, the heights of the liquid water existence ranges from about 0 km up to about 6 km above the surface of the Earth in the convective clouds of the strong updrafts [57]. Figure 2.7 presents the specific attenuation due to water droplets as a function of frequency at several temperatures. It can be seen from the figure that the attenuation increases monotonically with the frequency. In order to derive attenuation due to cloudiness, the curve corresponding to 0^o C should be used as stipulated by [58].

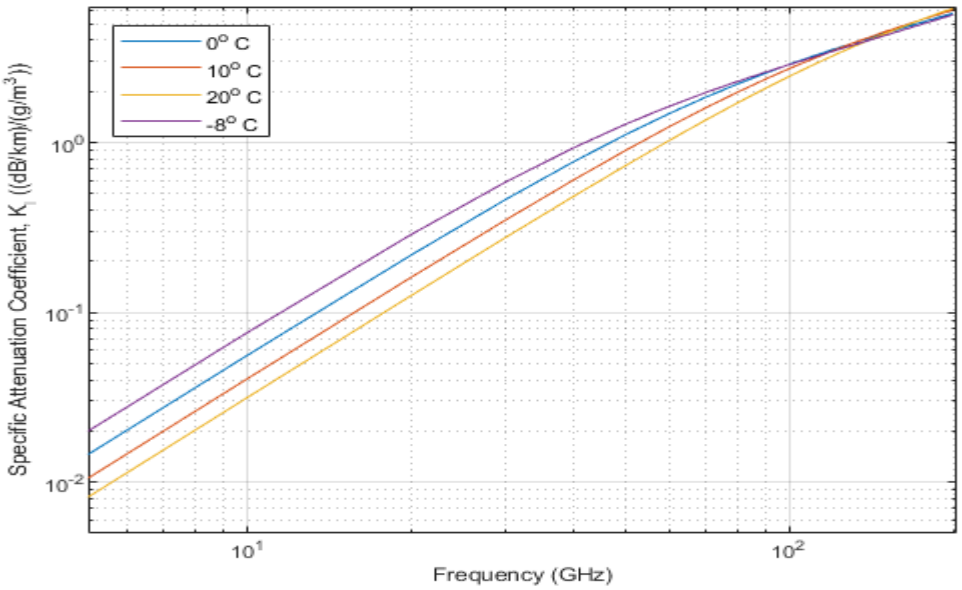

Figure 2.7 Specific attenuation due to water droplets at several temperatures as a function of frequency [58].

2.6.6 Rain Effect

Rain attenuation is known as the dominant impairment in the satellite communication systems operating above 10 GHz. Due to the condensation of water vapor, the droplet diameter from the formation of cloud increases, either by the absorption of the water vapor or the coalescence around them. The fall speed increases with the increase in size. Raindrops both absorb and scatter energy. Rain also causes depolarization, phase fluctuations and rapid amplitude, bandwidth coherence reduction and antenna gain degradation. The signal losses due to rainfall experienced over Earth-satellite links are an integral of all the individual attenuation increments, which are caused by the raindrops as encountered along the propagation path. This process could be termed as rain attenuation prediction. The rain attenuation prediction relies mostly on rain rate (mm/h), which is highly variable in term of space and time [59].

There is a standard developed for the rain attenuation determination for the radio wave transmission, which must assume the following:

1. The strength of the transmitted wave decays exponentially as it passes through the volume of the rain;

2. Rain drops are presumed to be spherical in shape, which both absorb and scatter energy from the incident of radio waves; and

3. The contributions of the individual drops to attenuation are independent and additive of the other drops, which signifies a single energy scattering, although, multiple energy scattering effects are acceptable in the classification development of the empirical results.

The atmospheric impairments encountered by a radio signal are significant along the path between a satellite and Earth-station and are briefly described in Table 2.2 [60].

The value of the total attenuation can only be estimated from the knowledge of the characteristics at each point of the propagation path of the raindrops because rain is highly variable in space and time. Also, rain attenuation measurements can be realized, by either radiometers or satellite beacons. These measurements are spatially and temporally scattered and are severely limited by frequency. So, they cannot be generalized at all the locations around the world. The basic reason has led to the development of various rain attenuation models based on the physical processes and the meteorological data observed over the region. More particularly, the models have been based on cumulative distribution of rain intensities and for the estimation of the link margins, which is crucial in the deployment of telecommunication systems [50].

Table 2.2 Propagation concerns for satellite communication systems [60]

Propagation impairment	**Physical cause**	**Prime importance**
Attenuation and sky noise	Atmospheric gases, cloud, rain	Frequencies above 10 GHz
Signal depolarization	Rain, ice crystals	Dual-polarization systems at C and Ku bands (depends on system configuration)
Refraction, atmospheric multipath	Atmospheric gases	Communication and tracking at low elevation angles
Signal scintillations	Tropospheric and ionospheric refractivity fluctuations	Tropospheric at frequencies above 10 GHz and low-elevation angles; ionospheric at frequencies below 10 GHz
Reflection multipath, blockage	Earth's surface, objects on the surface	Mobile satellite services
Propagation delays, variations	Troposphere, ionosphere	Precise timing and location systems; time division multiple access system
Inter-symbol interference	Ducting, scatter, diffraction	Mainly C band, rain scatter may be significant at higher frequencies

2.6.6.1 Specific Rain Attenuation

The fundamental quantity used in the estimation of rain attenuation statistics for Earth-space and terrestrial paths is known as specific attenuation, γ [61]. Two universal approaches have been used to estimate γ, as stated by various authors:

(1) A theoretical method using a uniform distribution of raindrops modeled such as water spheres, or more complex shapes; and

(2) An empirical technique based on the estimated relation between specific attenuation, γ, and rain rate, R, given as [61]:

$$\gamma = kR^{\alpha} \tag{2.10}$$

Equation (2.10) is known as the power-law form of specific rain attenuation [62], where R is the rain rate in mm/h, coefficients k and α are power law parameters, which depend on the raindrop size distribution, frequency, polarization, and rain temperature. This method is adopted in this research to compute the specific attenuation. The values for k and α for the frequency range 1 - 1000 GHz was provided for raindrops by [63] for consideration, with the presumed shape of oblate spheroids, at the temperature of 20^{o} C, using the drop size distribution proposed by [64], terminal velocity [65], and refractive index values according to the model of Ray [66]. However, several researchers computed values of the parameters for different rain types for linear and circular polarizations. The values computed by ITU-R Recommendations in [63] is adopted in this work. To determine the total path attenuation due to rain, it is compulsory to know the specific attenuation of the rain rate exceeded for the percentage of time of interest upon which the coefficients k and α depend [14]. The specific attenuation, γ, (dB/km) is obtained from the rain rate, R (mm/h) using the power-law relationship as stated in (2.10). However, the k and α used in this study were based on the [63].

For the linear and circular polarization, and for all geometric, the coefficients in (2.10) can be calculated using the following equations:

$$k = \frac{[k_H + k_V + (k_H - k_V)\cos^2\theta\cos 2\tau]}{2} \tag{2.11}$$

$$\alpha = \frac{[k_H\,\alpha_H\ +\ k_V\alpha_V\ +(k_H\,\alpha_H -\ k_V\alpha_V)\cos^2\theta\cos 2\tau]}{2k} \qquad (2.12)$$

where the path elevation angle is θ and τ is the polarization tilt angle with relative to the horizontal (τ = 45° for circular polarization). The summary of the horizontal polarization coefficients are the pairs (k_H and α_H) and vertical polarization coefficients (k_V and α_V), also with coefficients k and α for the frequencies used in this research are presented in Table (2.3). The actual k and α for the frequencies of interest to be used for the specific attenuation are derived using (2.11) and (2.12). The frequency used for this study is also asterisked in Table 2.3.

Table 2.3 Frequency-dependent coefficients for estimating the specific rain attenuation [63].

Frequency (GHz)	**Linear Polarization**				**Circular Polarization**	
	k_H	α_H	k_V	α_V	k	α
10	0.01796	1.13320	0.01519	1.1297	0.0166	1.2083
*12	0.03020	1.11270	0.02584	1.1120	0.0280	1.1147
14	0.04230	1.08540	0.03820	1.0814	0.0402	1.0835
16	0.06101	1.10661	0.05274	1.0603	0.0569	1.0634
18	0.07821	1.05270	0.06774	1.0421	0.0729	1.0478
*20	0.09629	1.04490	0.08340	1.0303	0.0898	1.0381
*30	0.20451	1.01740	0.17536	1.0023	0.1898	1.0104
35	0.26997	0.99190	0.23169	0.9818	0.2507	0.9872
*40	0.33879	0.96180	0.29255	0.9559	0.3155	0.9591

***** refers to the frequencies used in this work.

2.7 Rainfall

Rainfall exists in the form of droplets of the liquid water, which have condensed from the atmospheric water and thereafter become substantial enough to fall under gravity. Rain is also a major component of the water cycle and accounting for deposition of the fresh water on the Earth. Moisture is the main source of rain production, moving in the three-dimensional zones of the moisture contrasts and temperature, this phenomenon is known as weather fronts.

2.7.1 Types of Rainfall

Due to variability in time, space and frequency, the description of rainfall is known to be very complex [67], and are classified by meteorologists into two major types: stratiform and convective rainfall. These classifications are based on their physical characteristics [14, 20, 68-71]. These two categories are basically the types observed across the globe and they are also based on the nature of the cloud formation, condensation and strength of the rainfall [67-69, 72]. Stratiform rainfall is produced from weak nimbostratus clouds [73] which results in light drizzle and widespread rain usually over a large area. It also extends up to 1 km across the vertical profile of the 0^{o} C isotherm height with rain rates, which is usually less than 10 mm/h [14, 74].

Convective rainfalls, on the other hand, are produced from robust cumulonimbus clouds which are often local and reach up to about 100 km/h with the general formation below 0^{o} C isotherm height [14, 72]. They are mainly responsible for shower and thunderstorm rainfalls where rainfall rates exceed 10 mm/h [69, 75-78]. It falls rapidly with changes in intensity with large drops spread over a specific area for a moderately short time, for convective clouds only have limited horizontal range. Some researchers such as [14, 68] indicated in their work that these types of rainfall are naturally common in the equatorial and tropical climates and extends towards subtropical climates.

However, some other researchers apply three rainfall regimes of drizzle, shower, and thunderstorm to classify the rainfall as stated in [79], while others apply four rainfall regime, that is, drizzle, widespread, shower, and thunderstorm for efficient propagation modeling and prediction [76, 79, 80]. Only recently, the Southern African researchers embarked on rainfall campaigns over the subtropical region, and discovered that the rainfall over the area shared the same approach with the four rules which are, drizzle (< 5 mm/h), widespread (extended from 5 to 10 mm/h), shower (from 10 to 40 mm/h), and thunderstorm (> 40 mm/h) by [81, 82].

2.7.2 Categorization of Rainfall in the Climatic Zones

The categories of rainfall are based upon the intensity, amount, frequency or return period, and the seasonal distribution of rainfall, which varies from location to location, day to day, month to month, and year to year. The precise knowledge of these categories is important to provide some important information for planning and management, by which the full utilization can proffer solution or minimize problems that may arise in several sectors (such as hydrology, meteorology, communication systems, among others) over each climate. For example, the rainfall characteristics of the tropical regions differ substantially from the ones in temperate regions. However, it has been recorded that the empirical relationships obtained in the temperate regions may not be suitable for the propagation predictions in the tropical or subtropical regions [14, 20]. And, these are categorized as follows:

2.7.2.1 Rainfall Rate

Rainfall rate is a measure of rainfall intensity which corresponds to the amount of rain falling over a given time interval. This rate can be typically expressed in terms of length (that is the depth) per unit time, such as millimeters per hour (mm/h), or inches per hour [83]. Rain rate data are mostly presented in units of mm/h. Also, rainfall rate is highly variable in terms of locations and time, which includes diurnal, seasonal and yearly variations.

2.7.2.2 Rain Height

Rain height is the altitude in the free atmosphere at which temperature is at 0^{o} C. It also referred to the freezing point of water and known as 0^{o} C isotherm height as used by ITU-R Rec. [84]. The rain height is an important parameter for the prediction of hydrometeor scattering and rain attenuation that occur in the satellite radio links [85]. It is presumed that rain cells extend vertically up to the 0^{o} C isotherm height in the climate such as temperate region, where rain is mostly stratiform and widespread; while on the other hand, it is associated with the convective cells in the tropical and subtropical climates. This research is based on the measurement of rain height based on 0^{o} C isotherm height; hence, the detailed information of measurement of 0^{o} C isotherm height used in this work will be discussed in the next chapter.

2.7.2.3 Rain Drop-size Distribution

The raindrop-size distribution is the quantity of concentration of raindrops together with equivolume diameter in a specified volume of space. It can be used to estimate rainfall rate and radio wave attenuation. It also varies significantly with time and height, and the modal size increases as it decreases with height. Rain drop-size distribution is a single parameter useful for many purposes as its representing a given distribution of the volume of the median diameter (that is, the diameter for which the total quantity of all the drops having greater diameters is equivalent to the primary factors involved in determining the radar reflectivity of rainfall) [86].

2.8 Radio Noise

Radio noise is the occurrence of unwanted signals in the frequency band along the propagation path of a communication system, which can be generated by either natural sources or artificial sources. The interaction of the natural absorbing medium with the transmitted signal of a radio wave in the atmosphere will not produce attenuation (signal amplitude reduction) but can as well be the source of

thermal noise radiation power. Therefore, the noise related to these sources is known as sky noise or radio noise, which can be added directly to the noise of the system by increasing the temperature of the receiver's antenna. In the design and performance of the communication system for very low noise communication receivers, radio noise can be the limiting factor. Radio noise can be emitted from several sources, such as in both artificial and natural (which consist of terrestrial and extra-terrestrial source). Here are what the sources are made of:

a) Artificial sources include:

i. Emission from other communication systems;
ii. Power transmission lines;
iii. Internal combustion engine ignition; and
iv. Unintended radiation from electrical and electronic equipment, or electrical machinery.

b) Terrestrial sources include:

i. Emissions from hydrometeors (such as rain, fog, clouds among other);
ii. Emissions from atmospheric gases (oxygen or dry air and water vapour);
iii. Re-radiation from the ground or any other obstructions within the beam of the antenna; and
iv. Radiation lightning discharges (that is atmospheric noise due to lightning)

c) Extra-terrestrial sources include:

i. Celestial radio source radiation (radio star);
ii. Solar and lunar radiation; and
iii. Cosmic background radiation.

All these sources produce radio noise which usually affects the fidelity of good signals of the communication systems.

2.9 Overview of South Africa Climate

South Africa is positioned on the latitude 29º00'S and longitudinal 24º00'E in the most southern tip of the African continent. By this positioning in the world, South Africa is therefore classified as a subtropical region, since the subtropics include all parts of the world just outside 23.4°N and 23.4°S latitude [87]. South Africa share borders with some other Southern African countries such as Zimbabwe and Botswana in the central north, Namibia in the north-west, and Mozambique in the north-east. Lesotho and Swaziland are embedded in the South Africa as shown in the Figure 2.8. South Africa is moderated climatically by its surrounding with oceans; that is, the Indian Ocean in the eastern part and the Atlantic Ocean in the western part. Since the country is surrounded by oceans, on the two sides of a triangle-shaped and ranges from the Mediterranean to the temperate of the interior highland. This accounts for the warm, sunny, temperate conditions

Figure 2.8 The map of South Africa showing the locations of study.

exhibition within the country, together with a broader variety of climates than all other sub-Saharan countries in Africa Continent. Rainfall and temperature patterns vary with respect to the movement of the high-pressure belt that encircles the globe in the southern latitude during the winter season and the low-pressure systems that occur in summer. Rainfall usually occurs during summer except for the southwest (Cape Town) where rainfall occurs in winter; and experience lower average temperatures due to the influence in the area, elevation and ocean currents more than other countries in the same range of latitude [88]. Table 2.4 depicted the detailed information about the geographical locations of this research [89].

The country (South Africa) comprises of four different types of climate which are summer, autumn, winter and spring. Summer season is characterized by hottest, sunny weather with average temperatures rising above 30^{o} C; autumn has very little rainfall during its season over the whole country with warm weather but not too hot and colder as the season advances; the winter is characterized by dry, sunny, cold nights, and sometimes with heavy frosts; and the spring [82, 84, 88, 89]. Table 2.5 depicted the detailed calendar dates of the climate [84].

Table 2.4 The detailed geographical information of the studied locations [89].

Serial number	Location	Latitude (°S)	Longitude (°E)	Altitude (m)	Climatic Region
1	Bhisho	35.21	27.26	594	Cold semi-arid
2	Umthatha	31.5	28.6	732	Warm Temperate
3	Bethlehem	28.23	28.3	1666	Steppe
4	Johannesburg	26.12	28.2	1694	Sub-tropical Highland
5	Pretoria	25.7	28.11	1330	Temperate
6	Durban	29.58	30.57	8	Coastal Savannah
7	Pietermaritzburg	29.37	30.23	613	Inland Savannah
8	Ladysmith	28.5	29.7	1015	Warm temperate
9	Polokwane	23.54	29.27	1230	Tropical Semi-arid
10	Tshipise	22.6	30.1	502	Subtropical Steppe
11	Ermelo	26.4	29.4	1766	Sub-tropical
12	Nelspruit	25.25	30.55	671	Sub-tropical
13	Klerksdorp	26.8	26.6	1334	Semi-arid
14	Lichtenburg	26.09	26.1	1459	Semi-arid
15	Kimberley	28.7	24.7	1198	Continental
16	Brandvlei	30.27	20.29	923	Desert
17	Cape Town	33.58	18.36	42	Mediterranean
18	Mossel bay	34.11	22.08	59	Mild Sub-tropical

Table 2.5 The detailed calendar dates of the climates [84].

Southern Hemisphere	Calendar dates
Autumn	mid-February to April
Winter	May to July
Spring	August and mid-October
Summer	mid-(October to February)

2.10 Review of Rain Rate Measurement in the South Africa Climate

Several researchers have carried out several measurement campaigns which have been instituted on rainfall in South Africa and constitute to the rainfall campaign measurement in South Africa, with the goal of achieving the best performing model for a specific geographical zone. Some of the widely known researchers with the detail description of their models are not discussed here and are accessible in [13, 21, 46, 90-94]. Over a few decades, the focus of researchers was much on the temperate zone and later on the tropical regions, then subtropical regions due to insufficient propagation research over this region. However, much attention has been drawn over the subtropical region in recent years, which includes a research work based on 4-year data [95]; modeling of rain attenuation for different climatic rain zones [96-98]; using power law expression for conversion of 60-minute to 1-minute equivalent; also using statistical distributions to convert 5-minute rainfall data to 1-minute equivalent due to lack of 1-minute rain rate data [99-101]. Others include developing a model based on the refined parameters to describe 1-minute rain rate distribution both in tropical and subtropical, besides South Africa consists of mixed climate (such as tropical, temperate and subtropical) [91] of rainfall $R_{0.01}$ across the locations which this research is based on was obtained from 5-minute rainfall data provided by [102], and the detailed information and the method of conversion to 1-minute can be found in [89]. Table 2.6 presents the location parameters with the 1-minute point of rainfall across South Africa [89].

Table 2.6 Location parameters with 1-minute point of rainfall across South Africa [89]

Serial number	Location	Latitude (°S)	Longitude (°E)	$R_{0.01}$
1	Bhisho	35.21	27.26	76.15
2	Umthatha	31.5	28.6	83.54
3	Bethlehem	28.23	28.3	77.55
4	Johannesburg	26.12	28.2	85.87
5	Pretoria	25.7	28.11	84.45
6	Durban	29.58	30.57	95.21
7	Pietermaritzburg	29.37	30.23	90.29
8	Ladysmith	28.5	29.7	87.14
9	Polokwane	23.54	29.27	76.25
10	Tshipise	22.6	30.1	75.86
11	Ermelo	26.4	29.4	82.93
12	Nelspruit	25.25	30.55	85.80
13	Klerksdorp	26.8	26.6	76.44
14	Lichtenburg	26.09	26.1	74.74
15	Kimberley	28.7	24.7	73.06
16	Brandvlei	30.27	20.29	52.01
17	Cape Town	33.58	18.36	77.96
18	Mossel bay	34.11	22.08	73.32

2.11 TRMM Overview

The Tropical Rainfall Measuring Mission (TRMM) is known as the first Earth research satellite and the one of the most powerful meteorological equipment that is designed to study and improve the understanding of the distribution and variability of precipitation within the tropical, subtropical and temperate regions of the Earth. By covering these regions, the TRMM provides abundant information required on rainfall and several related parameters that can help the researchers to account for atmospheric circulation with an improved ability to carry out and predict the consequence of the parameters over a day to day activities globally. Due to this fact, the satellite is regarded as one of the most powerful

meteorological equipment. In 1997, the TRMM satellite was launched in collaboration with Japan Aerospace Exploration Agency (JAXA) by the National Aeronautics and Space Administration (NASA) of America. This satellite consists of five sensors, due to the mission of designing multiple instruments that can provide a better physical parameter estimation on only a single equipment [103-105]. The sensors include TRMM-Precipitation Radar (TRMM-PR), Visible and Infrared Scanner (VIRS), TRMM Microwave Imager (TMI), Lightning Imaging Sensor (LIS), and Cloud and Earth Radiant Energy Sensor (CERES); and the sensors have been in operation since the inception. Figure 2.9 and Table 2.7 present the observation concept and the parameters of the TRMM sensors respectively.

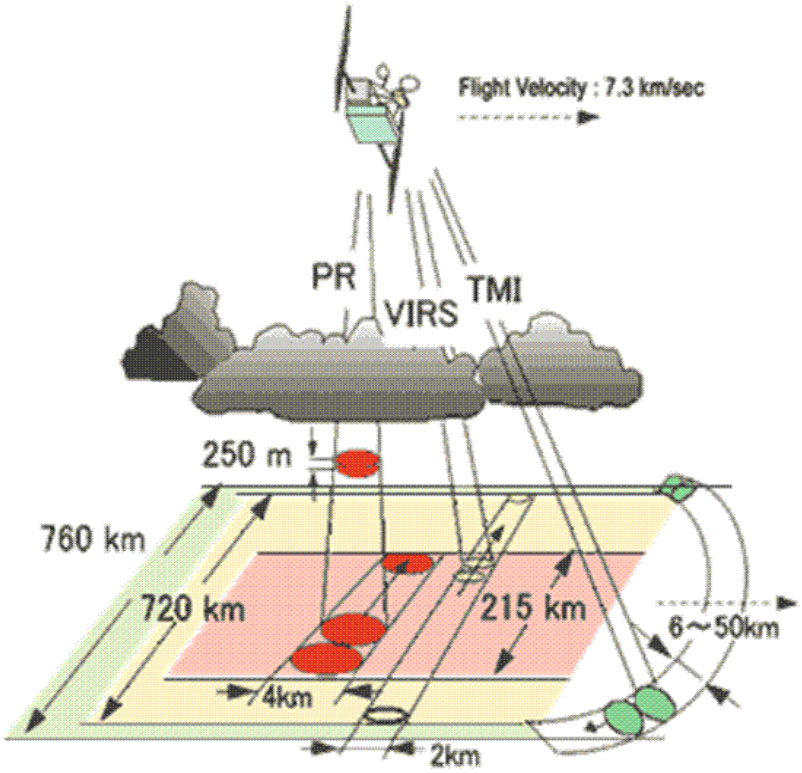

Figure 2.9 The observation concept of the TRMM sensors [106].

Table 2.7 The system parameters of the TRMM sensors [106].

Sensors	PR	TMI	VIRS	CERES	LIS
Observation frequency	13.796 and 13.8 GHz	10.65, 19.35, 21.3, 37 and 85.5 GHz	0.63, 1.6, 3.75, 10.8, and 12 µm	0.3 – 5; 8 – 12; and 0.3 - 100 µm	0.77765 µm
Polarization – V/H (Vertical/Horizontal)	H	V/H (21.3 GHz is V only)			
Scan mode	Cross track	Conical	Cross track	Cross track	
Horizontal resolution (km)	4.3 ± 0.12 (nadir)	6 – 50	2	10 (nadir)	4 (nadir)
Swath width (km)	220	≈ 760	720		≈ 600
Data rate (kbps)	93.5	8.8	50	8.5	6
Weight (kg)	465	50	49	45.5	18
Power (W)	213	39	53	47	42

2.11.1 TRMM-PR

The TRMM-PR is the most important sensor and the foremost space-borne which can directly detect vertical compositions of rain (such as detailed rain rate and rain height information); radar reflectivity as a function of latitude and height; and provides three-dimensional records of storm structure with the frequency of about 13.8 GHz [19, 84, 106-111]. One of the most important features of TRMM-PR is the ability to deliver vertical profiles of snow and rain from the surface of the Earth up to a height of about 20 km. These measurements give way to very useful information on the concentration and distribution of the rain, the storm depth, the rain type, and also the height at which the snow melts into rain. Also, the estimation of which heat is released into the atmosphere at diverse heights based on these measurements can be adopted to improve models of the global atmospheric circulation. TRMM-PR also has the ability to split out rain echoes for the vertical sample sizes, of about 250 m when looking down directly, and only

use about 224 W of electric power to carry out all these measurements. In addition, the size of the footprint of the satellite is sufficient for the study of the inhomogeneous effect of rainfall upon the comparatively common footprints of the small occurrences microwave radiometer channels [106, 108, 111-117]. Figure 2.10 presents the TRMM-PR standard algorithm flow [106].

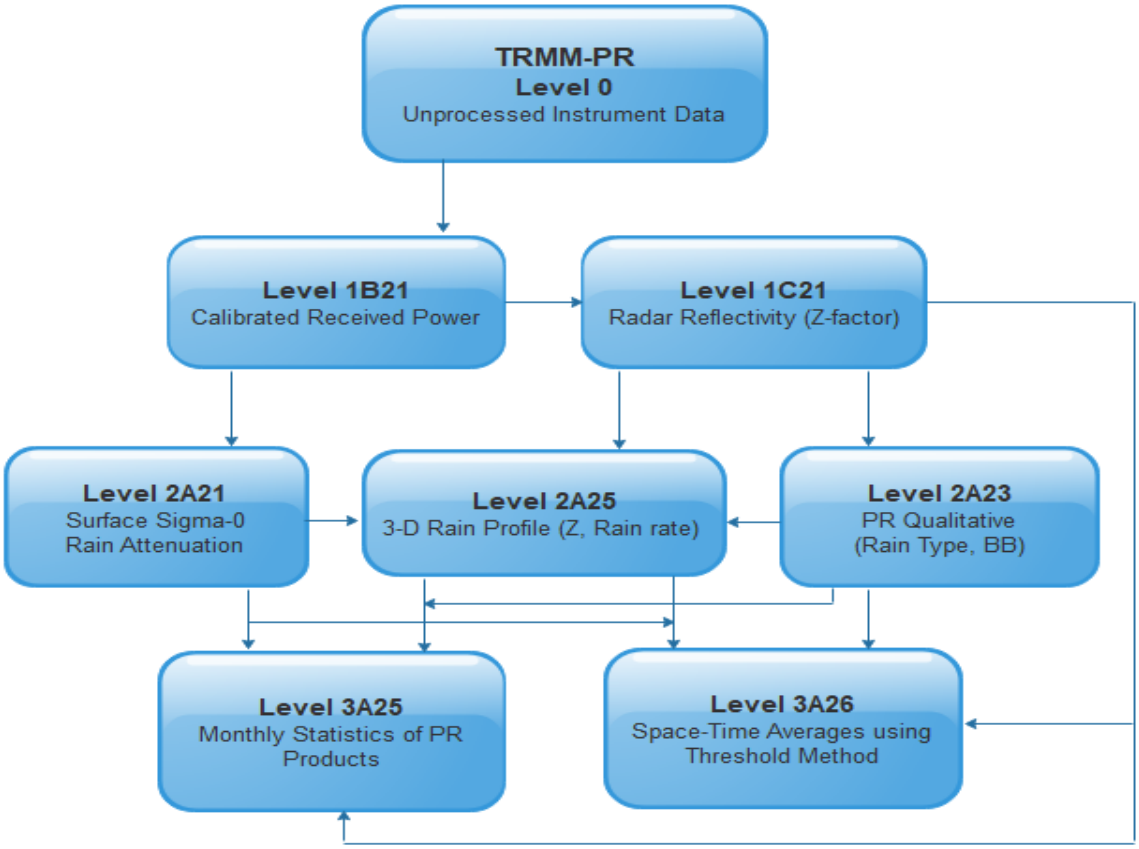

Figure 2.10 The standard algorithm flow of TRMM-PR [106].

2.12 ITU Overview

The International Telecommunication Union is an organization established in 1865, from the day of telegraphy through the modern world satellites, internet, and mobile phones - means it has been the center of the developments of communications; and as well responsible for any matters regarding Information and communication technologies globally. Also, ITU is the authorized organization

to allocate global radio spectrum, satellite orbits, and also develop technical standards that ensure technologies and networks seamlessly interconnect, and endeavor to improve the access of information and communication technologies (ICTs), and to underserved communities worldwide. Due to the growth, liberalization and globalization of telecommunication markets, ITU was structured into three sectors, which are Telecommunication Standardization (ITU-T), Radio communication (ITU-R), and Development (ITU-D). Figure 2.11 shows the ITU sectors together with ITU-R structure [118].

ITU-R is the sector in charge of Radio communication, which plays a vibrant role in the global administration of the radio-frequency spectrum and satellite orbits resources and provides international standards for radio communication systems. This sector contains about four departments, where some technical standard was developed from the result undertaken by study groups called ITU-R Recommendations and some of these Recommendations were widely used in this work.

ITU-T is the sector that assembles the specialists from around the world to improve the international standards known as ITU-T Recommendation, which act as defining the fundamentals of global infrastructure of ICTs.

ITU-D is the one that strives to spread reasonable access to telecommunications, as a means of motivating broader social and economic development.

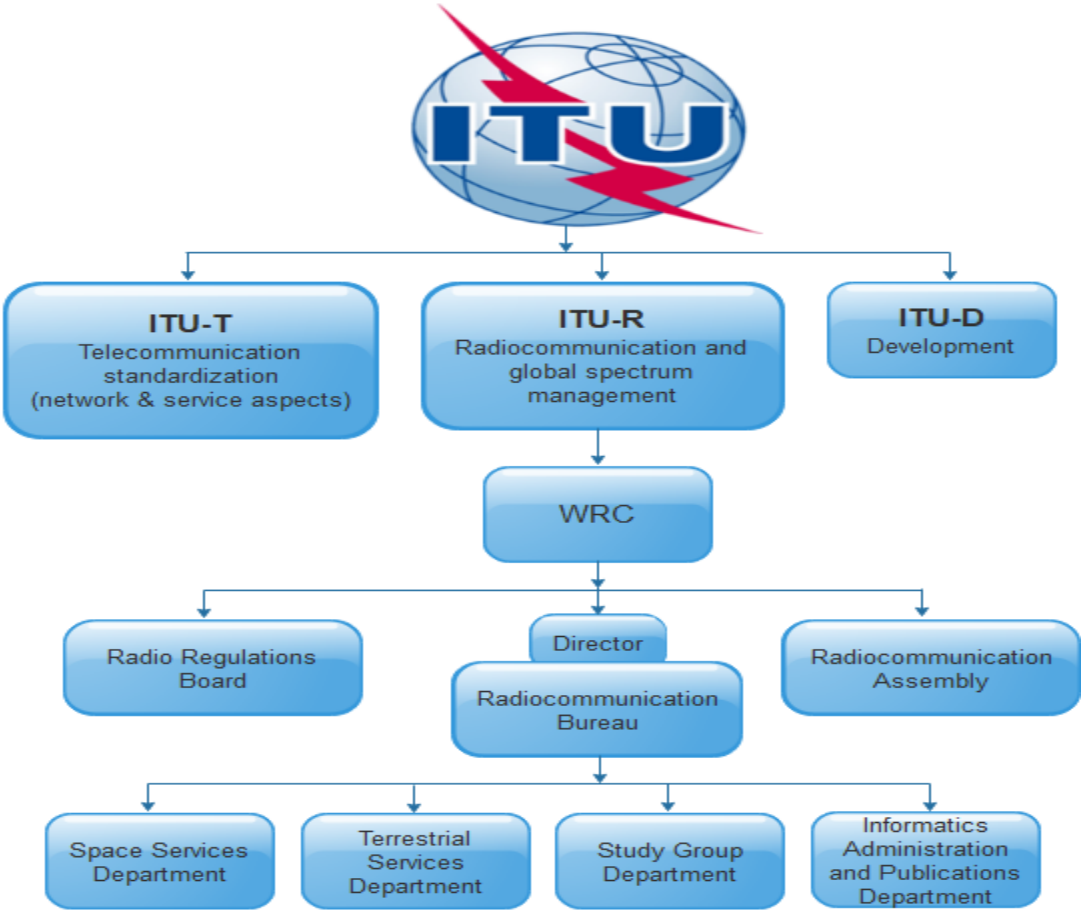

Figure 2.11 The ITU sectors showing the structure of ITU-R [118].

2.13.1 ITU-R Recommendations

The ITU-R Recommendations institute a set of international technical standards established by the ITU-R Sector. The Recommendations are developed by the experts from the operators, the administrations, the industry and other organizations in charge of radio communication matters from all over the world, with a high status and are instigated worldwide. Also, the recommendations are the result of studies undertaken by their study groups based on the use of a massive range of wireless services. These include the current new mobile communication technologies, the efficient use of the radio-frequency spectrum for all radio communication services, the management of the satellite orbits and radio-frequency spectrum, terrestrial and satellite radio communication

broadcasting, systems and networks for the fixed-satellite service, radio wave propagation, the fixed service and the mobile service, Earth exploration-satellite, space operation, meteorological-satellite and the radio astronomy services.

The ITU-R Recommendations are divided into several series according to their covering subjects as presented in Table 2.8 [119]. Quite a few numbers of the recommendations made from the asterisked (*) series were broadly used as a standard in this research and compared with the real measurement data. All the recommendation used will be discussed in the next chapter.

Table 2.8 The list of ITU-R Recommendations Series [119]

Series	Subject
BO	Satellite delivery
BR	Recording for production, archival and play-out; film for television
BS	Broadcasting service (sound)
BT	Broadcasting service (television)
F	Fixed service
M	Mobile, radio determination, amateur and related satellite services
P*	Radiowave Propagation
RA	Radio Astronomy
RS	Remote sensing systems
S	Fixed-satellite service
SA	Space applications and meteorology
SF	Frequency sharing and coordination between fixed-satellite and fixed service systems
SM	Spectrum management
SNG	Satellite news gathering
TF	Time signals and frequency standard emissions
V	Vocabulary and related subjects

2.14 Chapter Summary

This chapter has specified the general introduction and some basic concepts required for this research work. A survey of tropospheric propagation, radio wave propagation, interaction techniques of radio wave, and several transmission impairment phenomena in satellite communication systems is conversed. In addition, this chapter looked into the specific rain attenuation as the fundamental quantity of calculating rain attenuation. “Rainfall” being the main phenomenon in the framework of this study, and its categorization in the climatic zones is presented. South African climate overview and rain rate measurement, together with TRMM and ITU overviews are discussed in this chapter.

The next chapter presents the detailed information of rain height, which include its review, measurement, and modeling across the locations of study in a subtropical region.

CHAPTER THREE

Review, Measurement and Modeling of Rain height

3.1 Introduction

Rain height has a serious impact on the designing and performance of satellite communication services operating at higher frequencies (above 10 GHz). It is also a well-established fact that rain attenuation is the principal propagation impairment at the frequencies above 10 GHz [89, 99, 120-133]. The need for advanced technology service within satellite network communication systems requires not only the design mechanism but also accuracy in rain attenuation prediction, where rain height is an important factor. Therefore, to predict reliable and accurate rain attenuation for a specified location, there is a need to investigate annually, monthly and seasonal rain height, the variability over the location of interest. This chapter presents the review of rain height measurement across the globe, the distribution of rain height accumulation across several locations in South Africa; development of contour map of rain height; and modeling of the rain height in South Africa.

3.2 Review of Rain Height across the Globe

Rain height plays a significant role in the assessment of attenuation in both lines of sight and satellite communications in the region.

Since rainfall is known as a time-varying and natural phenomenon. Efforts have been made by several researchers to study the seasonal and yearly variability of rain height across the globe, which only temperate and tropical regions had only reported their findings, while the subtropical region is just receiving attention with an on-going measurement campaign over the region. Also, this research is taking a huge part in the measurement campaign over a subtropical region, a case study of South Africa. Hence, the comparative studies of the cumulative distribution of

rain height measured based on ZDIH over South Africa is presented in this section.

Several researchers have been working on rain height based on ZDIH measurements across the globe. Findings show that changes in ZDIH can cause deleterious effects on microwave and millimeter wave systems. Also, global warming generally contributes to the changes in ZDIH, and different trends of ZDIH can be observed in different regions across the globe [134-136]. Besides, ZDIH is known as a major parameter needed for accurate estimation of rain attenuation at SHF and EHF for Earth-satellite communication. Hence, there is a need for accurate measurement and detailed information of ZDIH of a region in order to proffer solution to any problems that may arise due to rain height effects.

ZDIH is also known as freezing height level, this is referred to the altitude at which the temperature is at freezing point of water, that is at 0^{o} C in the free atmosphere [84]. ZDIH information can be obtained indirectly in the melting layer region of the atmosphere [84, 137, 138]. Table 3.1 presents the annual average of rain height, $H_{r,}$ in relation to ZDIH as previously measured across the globe.

Table 3.1 Annual mean of rain height measured across the globe

Source	Location	Coordinates	Climatic region	Average Hr (km)
Ajayi & Barbaliscia [131]	Santa Rosa, Argentina	36.34S, 64.16W	Temperate	3.45
	Roma, Italy	41.8N, 12.2E		2.31
	Dares Salam, Tanzania	6.88S, 39.7E	Tropical	4.65
Ajayi & Odunewu [139]	Oshodi, Nigeria	6.5N, 3.4E	Tropical	4.85
	Minna, Nigeria	9.6N, 6.5E		4.75
	Kano, Nigeria	12.1N, 8.5E		4.74
Ojo et al. [140]	Akure, Nigeria	7.18N, 5.12E	Tropical	4.682
	Abuja, Nigeria	9.04N, 7.28E		4.697
	Bauchi, Nigeria	10.18N, 9.46E		4.686
	Enugu, Nigeria	6.24N, 7.24E		4.684
	Kaduna, Nigeria	10.32N, 7.25E		4.695
	Port Harcourt, Nigeria	4.43N, 7.02E		4.676
Mandeep [18, 141]	Subang, Malaysia	3.07N, 101.33E	Equatorial	5.02
	Penang, Malaysia	5.25N, 100.24E		5.1
	Kluang, Malaysia	2.02N, 103.32E		4.7
	Ipoh, Malaysia	4.34N, 101.4E		4.9
	Kuala Lumpur, Malaysia	3.1N, 101.42E		5.1
	Melaka, Malaysia	2.28N, 102.5E		4.8
	Terengganu, Malaysia	4.13N, 103.2E		4.95

3.3 Importance of Rain Height

As stated in section 1.3 of this thesis, that rain height is a significant input parameter which is highly required in accurate estimation of satellite communication performance and remote sensing application. It also has an important effect in some other applications such as hydrology, meteorology, among others. In the context of this research, rain height is a parameter which can be used to determine accurate attenuation due to rain over a satellite path. Also, ITU-R recommended the use of rain height as one of the crucial input parameters to estimate their various impairments in radio wave propagation [84], this includes:

1. The propagation data and the prediction methods required for the designing of Earth-space telecommunication systems [142];
2. The propagation data required for the evaluation of the coordination distances in the frequency range 100 MHz - 105 GHz [143];
3. The prediction procedure for evaluation of interference between stations on the surface of the Earth at frequencies above 0.1 GHZ, accounting for both clear-air and hydrometeor scattering interference mechanisms [144]; and
4. The method for the determination of the coordination area in an Earth station in the frequency bands between 100 MHz and 105 GHz [145].

Although, the accuracy of the global method of prediction by the ITU-R has always been under- or over-estimated due to availability of exact data points for numerous regions of the world which includes Africa. The ITU.R Rec. [146] is a model used to predict rain height with the consideration based on the knowledge of the ZDIH during rainy conditions, and it is required in several models especially in the design of space communication systems as earlier stated. Hence, the rest of this chapter presents the accurate rain height measurement and modeling across a subtropical region (a case study of South Africa).

3.4 Rain Height Data Description and Collection

The rain height data analyzed in this research is based on 0^{o} C isotherm height (ZDIH) acquired from the Tropical Rainfall Measuring Mission-Precipitation Radar (TRMM-PR) level 2 algorithms (both in 2A23 and 2A25), over 18 locations across 9 provinces of South Africa, a subtropical region for the period of 5 years (2011 - 2015). Figure 3.1 presents the topography of the location of study.

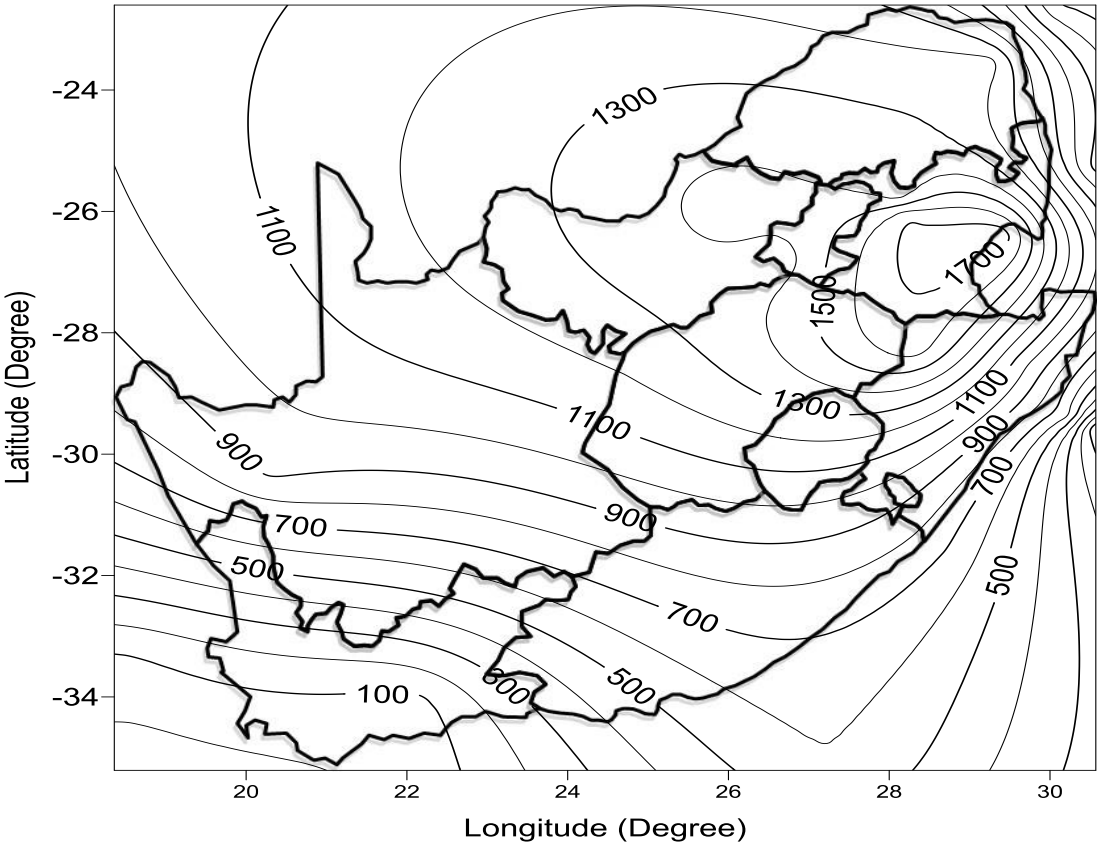

Figure 3.1 The topography of South Africa, showing the locations of study and their altitude (m).

3.4.1 Description of TRMM-PR Instrument

The ZDIH data used in this research were obtained from TRMM-PR, this subsection presents the operation and the detailed description of the instrument. TRMM-PR antenna beam during normal observational mode scans in the cross-tracking direction over the angle of about $\pm 17^{o}$, with observation angle of about

49 bins, average scan per orbit of about 9250 from end to end of swath width, and this result to about 247 km in a temporal resolution of about 92.5 minutes per orbit, with the coverage area of about 16 orbits per day. Also, the footprint size of the horizontal resolution of the TRMM-PR is around 4.3 km with the scan edge of about 5 km at the altitude of about 420 km. The vertical resolution is about 250 m, which is also equal to the range resolution at nadir [106, 147-149]. The detailed description of the parameters (PR system parameters) together with the observational geometry and the observation concept of TRMM-PR is presented in Figure 3.2 and the Table 3.2 respectively.

3.4.1.1 The TRMM-PR Radar Algorithms

The TRMM Science Team developed some algorithms for TRMM-PR and classified them into three levels, which are Level 1 (1B21, 1C21); Level 2 (2A21, 2A23, and 2A25); and Level 3 (3A25, 3A26). Where the products of data in Level 1 and Level 2 are in the instantaneous field of view (IFOV), while the Level 3 provides the monthly statistical in $5^{o} \times 5^{o}$ grid boxes required of rain parameters. This work makes use of the Level 2 algorithms Version 7 (that is 2A23 and 2A25), which is an improvement on earlier Version 6. These algorithms are very relevant, particularly to estimate rain height parameters such as freezing height level (ZDIH), bright-band height, the height of the storm, among others; which all serve as the main objectives of these algorithms. Also, the classification of events in TRMM radar was allocated with routine algorithms at this level. These algorithms are capable of categorizing each measured profile data on the vertical and horizontal distribution of the radar reflectivity factor [106, 147-149].

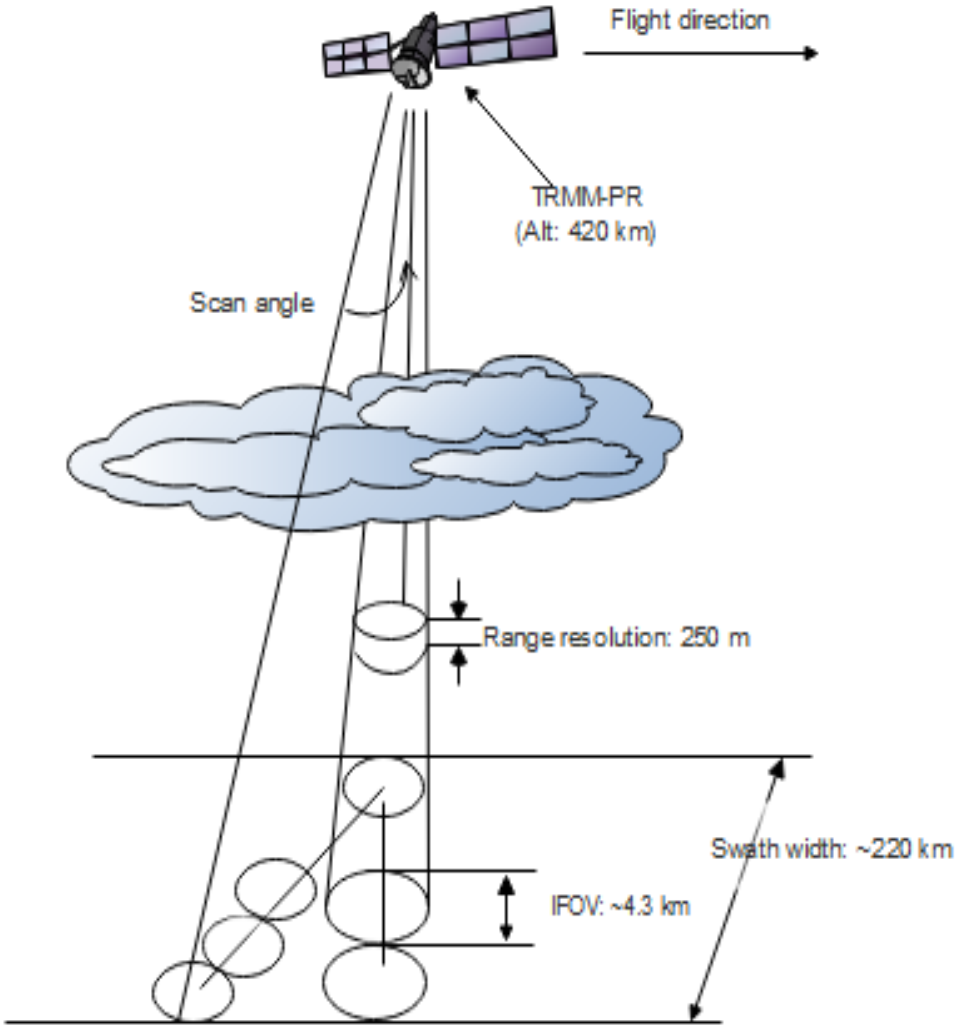

Figure 3.2 The observation concept of the TRMM-PR [106].

Table 3.2 The observatory parameters of TRMM-PR [106].

Items	Specification
Scanning mode	Cross track
Frequency	13.796 GHz and 13.802 GHz (Two-channel frequency agility)
Sensitivity	≤ ≈ 0.7 mm/h (S/N/pulse ≈ 0 dB)
Swath width	220 km (from end to end)
Observable range	Surface to 15 km altitude
Horizontal resolution	4.3 km (nadir)
Vertical resolution	0.25 km (nadir)
Antenna	
Type	128-element WG planar array
Beam width	$0.71^{o} \times 0.71^{o}$
Aperture	2.0 m × 2.0 m
Scan angle	± 71^{o} (Cross track scan)
Gain	≥ 47.4 dB
Transmitter/ Receiver	
Type	SSPA & LNA (128 channels)
Peak power	≥ 500 W (at antenna input)
Pulse width	1.6 μs × 2
PRF	2776 Hz
Dynamic range	≥ 70 dB
Number of Samples	64
Data rate	93.2 kbps
Mass	465 kg
Power	250 W

3.4.1.2 The Interpretation of TRMM-PR Algorithm

The ZDIH data used in this work was obtained from TRMM-PR algorithms 2A23 and 2A25 as stated in sub-section 3.41, which comprises of an average of about 16 data granules per day stored in a compressed Hierarchical Data Format (HDF). The average size of each of the compressed granule is about 6.70 MB. The data used was extracted from the compressed format which resulted to the average size to about 16 MB per file [106]. The HDF file of the TRMM-PR algorithm can be viewed by HDFView, a program developed by the HDF group specifically for reading the HDF file. Also, the use of some other software such as Microsoft Excel and MATLAB are also employed to analyze the data. Annexure (A-1) to (A-3) depicts a typical display of TRMM-PR data for each of the software used.

Also, the interpretation of TRMM-PR data comprises of valid and invalid data, which requires a need to distinguish between the valid and invalid value. The valid data is considered and known as the ZDIH value (m), this data is well used and as the main focus of this research. Table 3.3 presents the description of ZDIH data estimation from TRMM-PR (2A23 and 2A25).

Table 3.3 The description of ZDIH values of 2A23 and 2A25 [106].

Indication Value		**Description**
Invalid	-5555	Error estimation
	-9999	Missing value
Valid	> 0 (m)	Estimated 0^{o} C isotherm height

3.5 Rain Height Measurement Techniques

At EHF and SHF bands, rain fading is the most dominant factor [150]. Also, attenuation at these bands occurs due to scattering and absorption by rain [151]. Fading due to rain attenuation is defined empirically from the link tests, where rainfall data and rain height are the key factors to deduce the accurate attenuation of a satellite link over a location.

However, the rain height cannot be directly measured; hence, the simplest approximation of it is the 0° C isotherm height (ZDIH) during the rainy conditions which are available from radiosonde and satellite radar data. Although, some researchers such as [14, 131, 152] made use of some meteorological data such as temperature, pressure, and relative humidity to obtain ZDIH, and found out that ZDIH varies with altitude. While others measured ZDIH using radiosondes and satellite data and noted that both measurement instruments indicated that ZDIH varies yearly as per location [18, 131, 135, 139-141]. Also, the ITU-R Recommendations [146, 153] expressed a global and recommended version of predicting rain height, which is set as a standard for all researchers and provide for unknown location by means of extrapolation and interpolation of existing data points. This recommendation is used in this work as discussed in this section.

3.5.1 ITU-R Rec. P.839-2

In the design of satellite communication systems, the knowledge of the ZDIH throughout the rainy period is needed in numerous prediction models as earlier stated. Hence, the ITU-R recommended the following model in the global estimation of ZDIH [153]. This model is where the value of ZDIH originally estimated from, for different climate regions, and it is expressed as a function of latitudes as:

$$h_o = \begin{Bmatrix} 5 - 0.075(\varphi - 23) \\ 5 \\ 5 \\ 5 + 0.1(\varphi + 21) \\ 0 \end{Bmatrix} \quad \text{for} \quad \begin{cases} \varphi > 23 & \text{Northern Hemisphere} \\ 0 \leq \varphi \leq 23 & \text{Northern Hemisphere} \\ 0 \geq \varphi \geq -21 & \text{Southern Hemisphere} \\ -71 \leq \varphi < -21 & \text{Southern Hemisphere} \\ \varphi < -71 & \text{Southern Hemisphere} \end{cases} \tag{3.1}$$

where h_o is the mean of ZDIH above sea level (km) and φ is the latitude (°).

3.5.2 ITU-R Rec. P.839-4

This model is an improved version over [153], with the use of ZDIH in the prediction of the rain height for global use. It is clearly stated that the model can be adopted for the areas of the world where no specific information of data is available. So, the mean of the rain height, h_R, may be approximated by h_o, the ZDIH using the expression in (3.1) and presented as in (3.2):

$$h_R = h_o + 0.36 \quad (\text{km}) \tag{3.2}$$

where h_o is the mean of ZDIH in (km). Generally, it must be noted that h_R is different from h_o.

3.6 Cumulative Distribution of Rain Height in South Africa

In this section, the cumulative distribution of ZDIH measured data in accordance with Table 2.6 and Figure 3.1 are presented for yearly, monthly and seasonal distributions over the study locations.

3.6.1 Year-wise Variability of ZDIH Distribution

The year-wise variability of the ZDIH measured data over 18 locations and the observation years of study were presented in this sub-section. Generally, the annual measured ZDIH data over the study locations shows a strong variation over the years as it can be seen from Figure 3.3 to Figure 3.6; and the ZDIH observed increases as the year of observation increased. This shows that there is increasing trend in ZDIH measurement in the subtropical region. Also, the increasing trend in ZDIH could be as a result of general global warming associated with the variations in the climatological parameters, which is in agreement with the work of [135, 154, 155]. Global warming could be referred to as the climate change observed over a region due to changes in the temperature of the Earth's climatic system (that is, the Earth's atmosphere and the ocean). In addition, the highest observation value of ZDIH over the last year of observation (2015) might be as a result of the El Nino transition, which referred to the large-scale ocean-

atmosphere climatic interaction linked to a periodic warming in the sea temperatures across the Southern Africa region. This El Nino approached as a result of El Nino Southern Oscillation (ENSO) phase warming [84]. ENSO can be referred to as the atmospheric and oceanic effects which associated strongly with El Nino. Also, it is known that the location of study (South Africa) has different climatic regions which resulted in having a different correlation with ENSO [102].

Figure 3.3 presents the measured ZDIH over 5 locations of study, namely: Johannesburg, Tshipise, Emerlo, Mossel Bay and Nelspruit. It can be observed that Johannesburg recorded lowest values among the selected locations, with the trough and peak of about 4.311 km in the year 2012 and 4.357 km in the year 2014 respectively. Tshipise recorded the lowest value in the first three years (between 2011 - 2013) with the trough of about 4.282 km in the year 2011, which increases a bit during the last 2 years of observation (2014 - 2015) with the peak of about 4.408 km in the year 2015. This is followed by Mossel Bay and Emerlo with the trough and peak of about 4.330, 4.349, 4.464 and 4.460 km in the year 2011 and 2015 respectively; while Nelspruit only recorded trough values of about 4.328 km in the first year (2011) with extremely high values over the remaining 4 years of observation and has its peak in the year 2014 with the value of about 4.500 km.

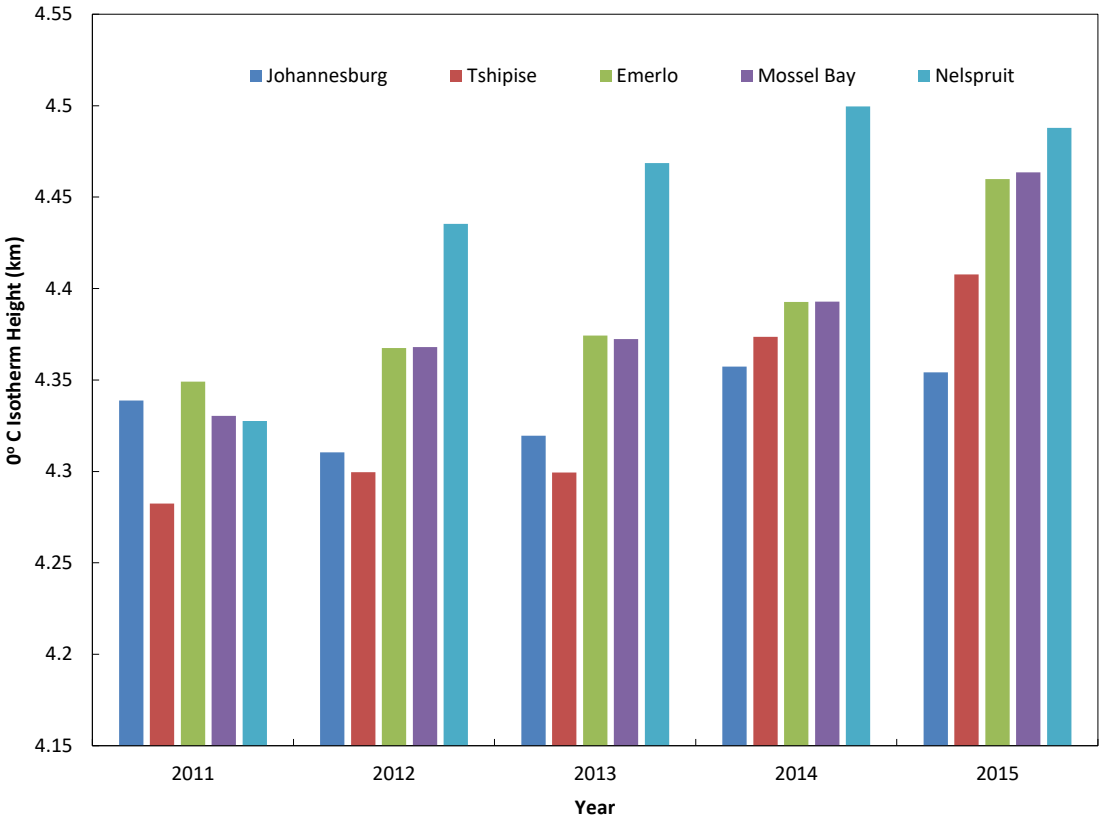

Figure 3.3 The measured ZDIH over Johannesburg, Tshipise, Emerlo, Mossel Bay and Nelspruit.

Figure 3.4 presents the measured ZDIH over Bethlehem, Durban, Pietermaritzburg, Kimberley and Cape Town. In Figure 3.4, Bethlehem, Durban, Pietermaritzburg shows same trends that the observed ZDIH increase as the year increases, its trough was observed in the year 2011 with about 4.312, 4.279, 4.307 km and its peak in the year 2015 with about 4.443, 4.411, 4.449 km respectively; while Kimberley and Cape Town presented different trends, that is its trough in the same year (in the year 2013) with about 4.294 and 4.371 km, and its peak also in the same year (in the year 2015) with about 4.430 and 4.416 km respectively.

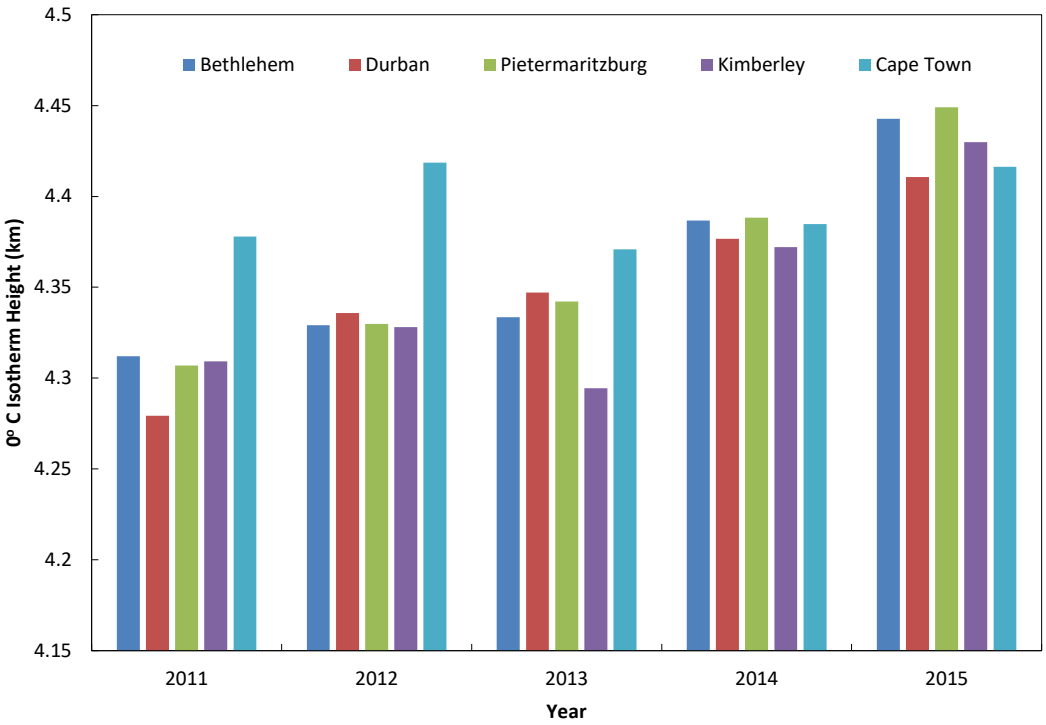

Figure 3.4 The measured ZDIH over Bethlehem, Durban, Pietermaritzburg, Kimberley and Cape Town.

Figure 3.5 also presents the measured ZDIH over Bhisho, Polokwane, Klerksdorp and Lichtenburg. The same trend could observe over these locations except Polokwane that recorded its trough in the second year of observation (2012) with about 4.259 km, while Bhisho, Klerksdorp and Lichtenburg in the first year (2011) with about 4.349 km, 4.229 km and 4.300 km respectively. Also, all the locations under this category recorded their peak in the same year (2015) with about 4.452, 4.399, 4.451 and 4.440 km over Bhisho, Polokwane, Klerksdorp and Lichtenburg respectively.

Figure 3.6 presents the measured ZDIH over Umthatha, Pretoria, Ladysmith and Brandvlei. It could be seen in Figure 3.6 that Umthatha and Ladysmith presented the same trend of the observations with trough in 2011 of about 4.315 and 4.212 km, together with the peak in 2015 of about 4.423 and 4.444 km respectively.

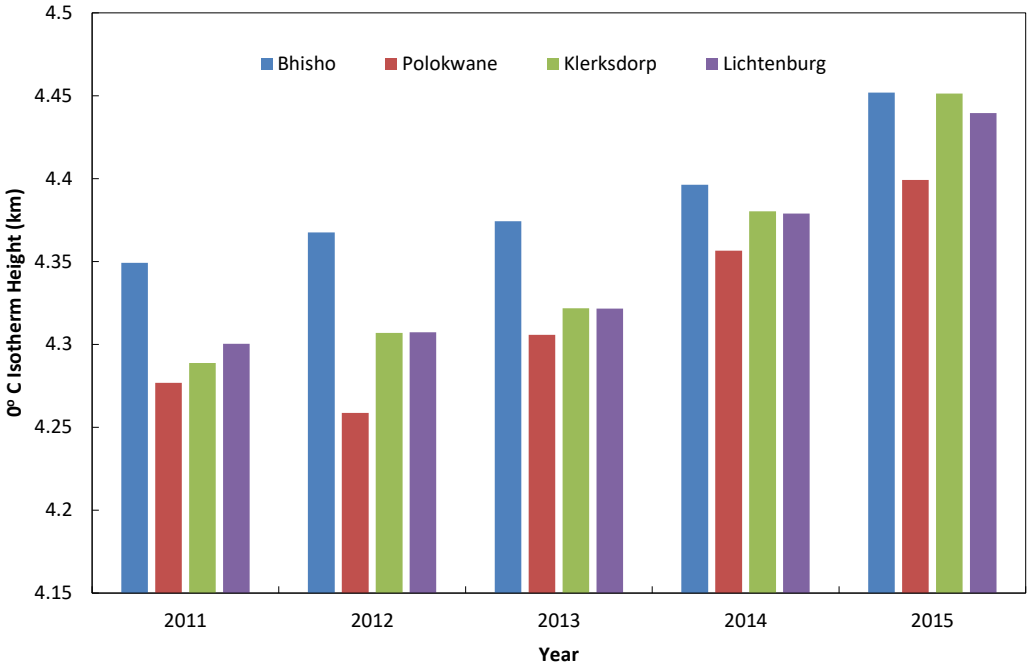

Figure 3.5 The measured ZDIH over Bhisho, Polokwane, Klerksdorp and Lichtenburg.

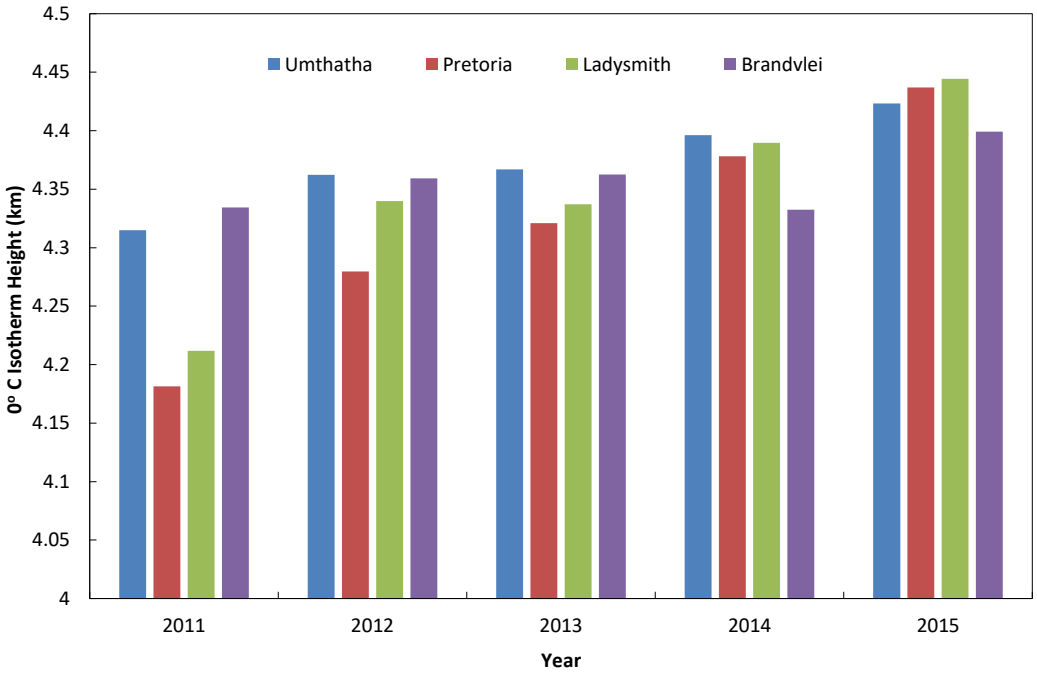

Figure 3.6 The measured ZDIH over Umthatha, Pretoria, Ladysmith and Brandvlei.

3.6.2 Monthly and Seasonal Variability of ZDIH Distribution

The monthly mean distribution of the ZDIH observed over the study locations is presented in this sub-section. It is known that South Africa has four seasons: autumn season (mid-February - April), winter season (May - July), spring season (August – mid-October), and summer season (mid-October – first mid-February). Generally, it can be noticed that each location recorded different values for different months of their average peak. Also, it can be seen that ZDIH values started rising from the beginning of the autumn season through to the middle of winter and fall towards the end of the winter, while the highest ZDIH was recorded at the beginning of the spring seasons, then falls from the middle of the season through the summer season to the end of the season.

Figure 3.7 presents the monthly ZDIH measured over Johannesburg, Tshipise, Emerlo, Mossel Bay and Nelspruit respectively. It can be observed from Figure 3.7 that Johannesburg and Tshipise consistently recorded the lowest values and then followed by Mossel Bay, although Johannesburg recorded the highest value of about 4.571 km, then followed by Nelspruit of about 4.478 km and then Emerlo of about 4.4325 km. The recorded values of the trough over Johannesburg, Tshipise, Emerlo, Mossel Bay and Nelspruit are 4.215 km (in the month of January), 4.210 km (in the month of January), 4.343 km (in the month of August), 4.314 km (in the month of January), 4.402 km (in the month of February) respectively.

Figure 3.8 presents the monthly ZDIH measured over Bethlehem, Durban, Pietermaritzburg (PMB), Kimberley and Cape Town respectively. It can be seen that Kimberley recorded highest values of ZDIH followed by Cape Town, Durban, PMB, and Bethlehem with about 4.5198, 4.4841, 4.4713, and 4.4648 km in September, July, August, and August respectively; while the lowest values were about 4.1404, 4.2044, 4.2747, 4.2843, and 4.3236 km in Kimberley, Durban, PMB, Bethlehem and Cape Town, respectively.

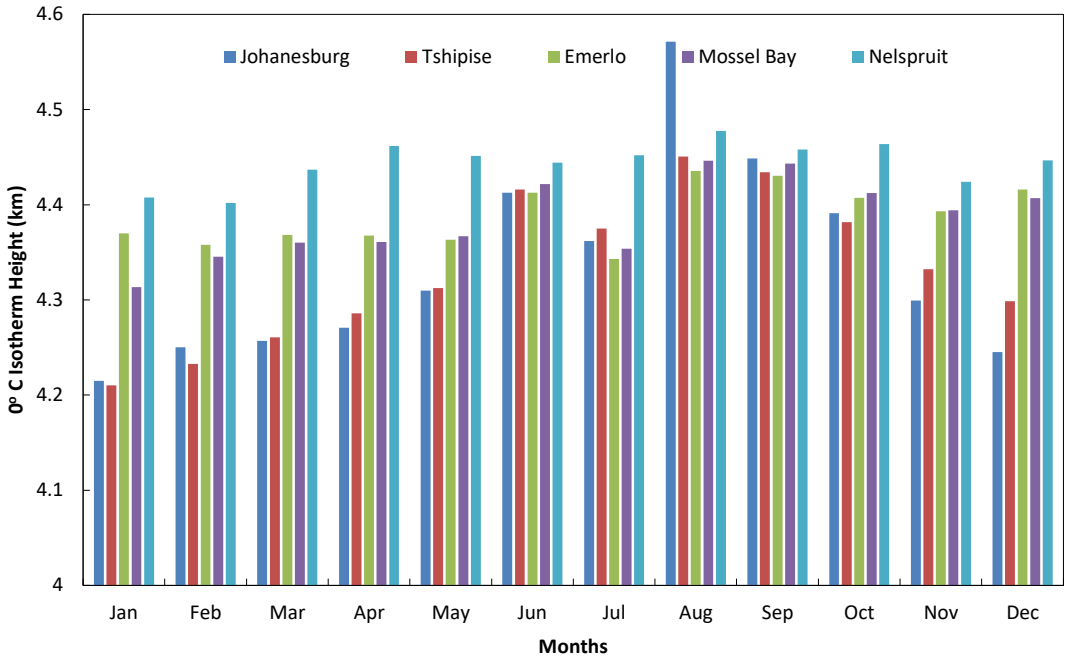

Figure 3.7 The monthly ZDIH measured over Johannesburg, Tshipise, Emerlo, Mossel Bay and Nelspruit.

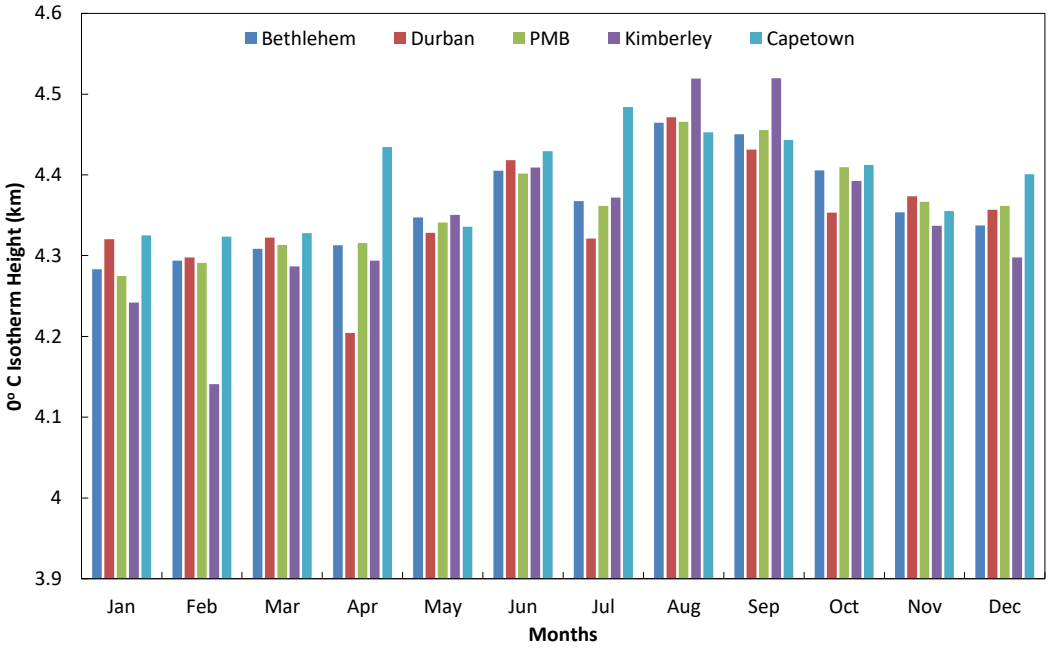

Figure 3.8 The monthly ZDIH measured over Bethlehem, Durban, Pietermaritzburg, Kimberley and Cape Town.

Figure 3.9 also presents the monthly ZDIH measured over Bhisho, Polokwane, Klerksdorp and Lichtenburg respectively. It was observed that Lichtenburg recorded highest ZDIH value, then followed by Klerksdorp, Polokwane and Bhisho while Polokwane recorded lowest ZDIH value, then followed by Klerksdorp, Lichtenburg, and Bhisho.

In Figure 3.10, the monthly ZDIH measured over Umthatha, Pretoria, Ladysmith and Brandvlei are presented. It could be observed that Brandvlei recorded highest ZDIH value of about 4.4255 km, then followed by Umthatha, Ladysmith, and Pretoria; while Pretoria recorded lowest value of ZDIH, then followed by Ladysmith, Brandvlei, and Umthatha.

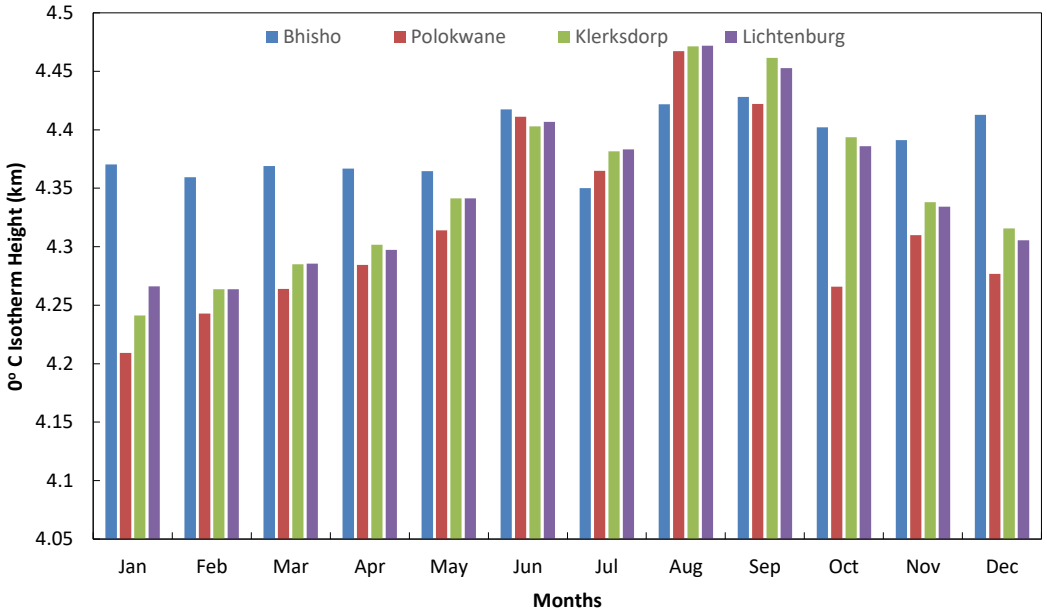

Figure 3.9 The monthly ZDIH measured over Bhisho, Polokwane, Klerksdorp and Lichtenburg.

Figure 3.11 presents the comparison of the 5-year average of ZDIH observed over all the selected locations. It can be seen that Nelspruit recorded the highest ZDIH distribution, then followed by Cape Town, Emerlo, Bhisho, and Mossel Bay with about 4.444, 4.394, 4.389, 4.388, 4.385 km respectively. While Polokwane

recorded the lowest ZDIH distribution, then followed by Pretoria, Tshipise, Johannesburg, Ladysmith and Kimberley with about 4.3194, 4.3195, 4.3325, 4.336, 4.3445, 4.3467 km.

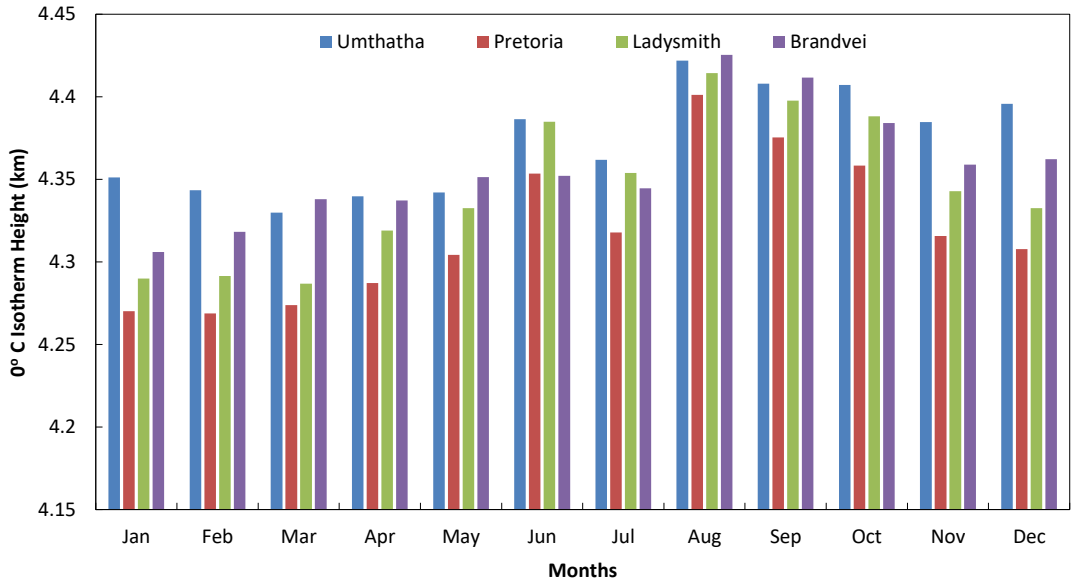

Figure 3.10 The monthly ZDIH measured over Umthatha, Pretoria, Ladysmith and Brandvlei.

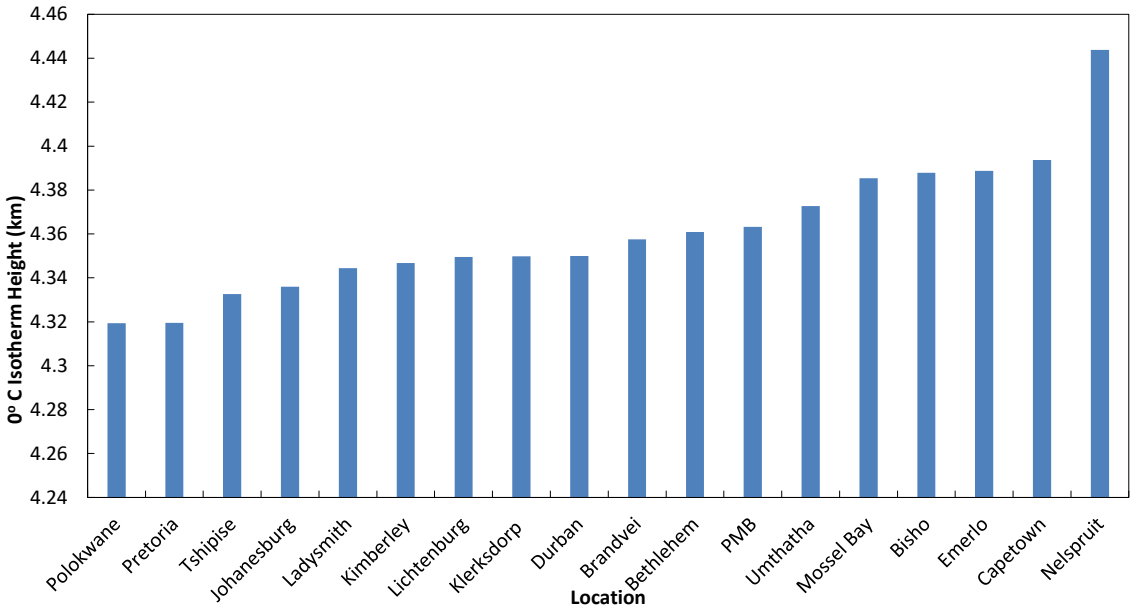

Figure 3.11 Comparison of the 5-year average of ZDIH over the study locations

3.7 Development of Contour Map for South Africa

Contour map for rain height was developed over the location of study based on the measured ZDIH data in this section. Contour maps are developed to meet the recent challenges in the rapid growth of the satellite communication systems and to make provisions for locations where direct measurements are not available. The contour maps were developed based on the **kriging method** in a data field to produce a weighted rain height estimation at each grid point. Kriging is known as a geostatistical interpolation method that can consider both the degree of variation between known data points and its distance, when estimating the values in an unknown area. The mathematical expression to compute the value of Z at grid node A, can be given as [156]:

$$z_A = \sum_{i=1}^{n} W_i Z_i \tag{3.3}$$

where Z_A is the estimated value of the grid node A, n is the number of neighboring data values used in the estimation, Z_i is the value at a location i with weight, W_i. The method in (3.3) was adopted due to the smooth production of rain height data field, which implies a highly consistent and predictable of rain height data variation field as compared to other methods used for the interpolation of the rain height between the actual observations. The information presented in this section is required regarding the height at which the rain extended during the period of precipitation [157]. The data presented here comprises of the longitude between 19º to 31º and the latitude from -35º to -24º. Results obtained from these maps will be needed for satellite system designers because it corresponds to the rain height prediction which is very important in several satellite applications.

3.7.1 Annual Mean Distribution of ZDIH

Figure 3.12 presents the 5-year annual mean of ZDIH distribution observed over South Africa. It can be observed that ZDIH ranges between 4.305 and 5.105 km.

The Northern part of South Africa (Limpopo) recorded the lowest average of ZDIH between 4.305 km and about 4.315 km; the remaining parts of the country recorded between 4.315 km and 4.385 km; except Gauteng and some parts of the Free State and North West with highest values between 4.385 and 5.105 km.

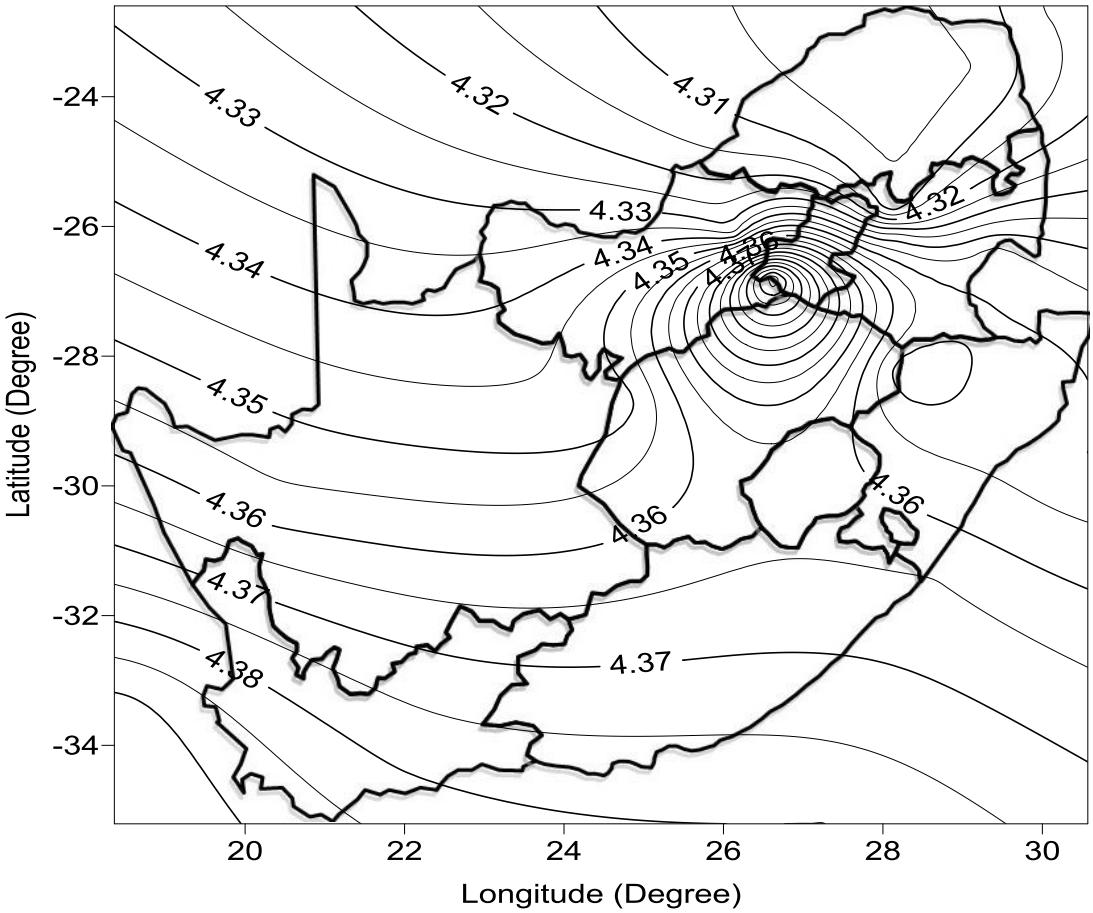

Figure 3.12 A 5-year mean contour map depicting the variability of measured ZDIH across the South African region.

3.7.2 ITU-R Recommendation Predictions

This sub-section presents the rain height prediction model in conjunction with ITU-R Recommendation as predicted in [153], (that is, ZDIH prediction as a function of latitudes), and rain height prediction as a function of ZDIH [146], as described in (3.2). Figure 3.13 reveals a steady increase from the southern part of the country towards the northern area with about 0.05 km increase, and; it can be

seen that the lowest value recorded was about 3.65 km and the highest value was about 4.80 km. As shown in Figure 3.14, the lowest rain height of about 4.670 km was recorded in the Northern part and it increases towards the Southern part, at a rate of about 0.005 km and the highest recorded was about 4.750 km. Hence, the ITU-R model estimated in this region needs to be revised due to the poor estimation of rain height for several locations in the South African region. For example, ITU-R P.839-4 mainly overestimates the actual measurement while ITU-R P. 839-2 underestimates the measurement.

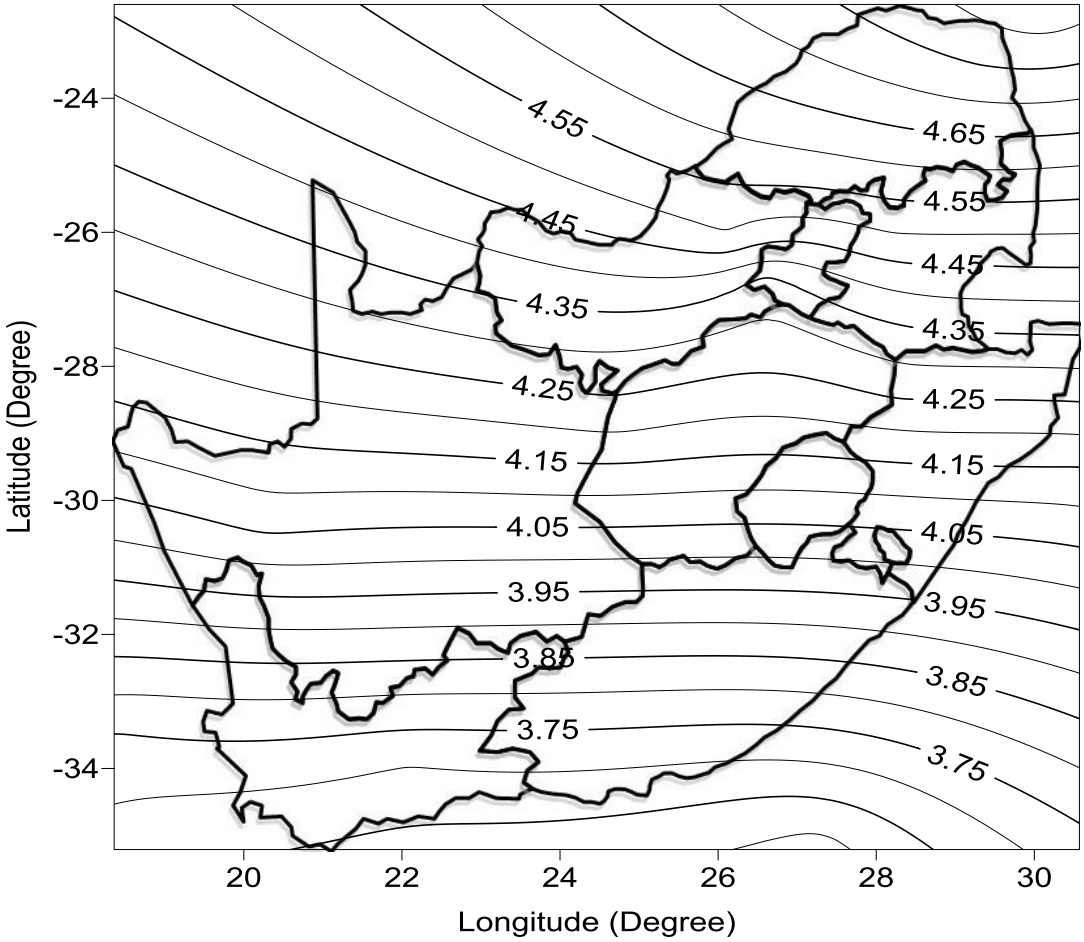

Figure 3.13 A 5-year mean contour map depicting the variability of ZDIH prediction based on ITU-R P.839-2 across the South African region

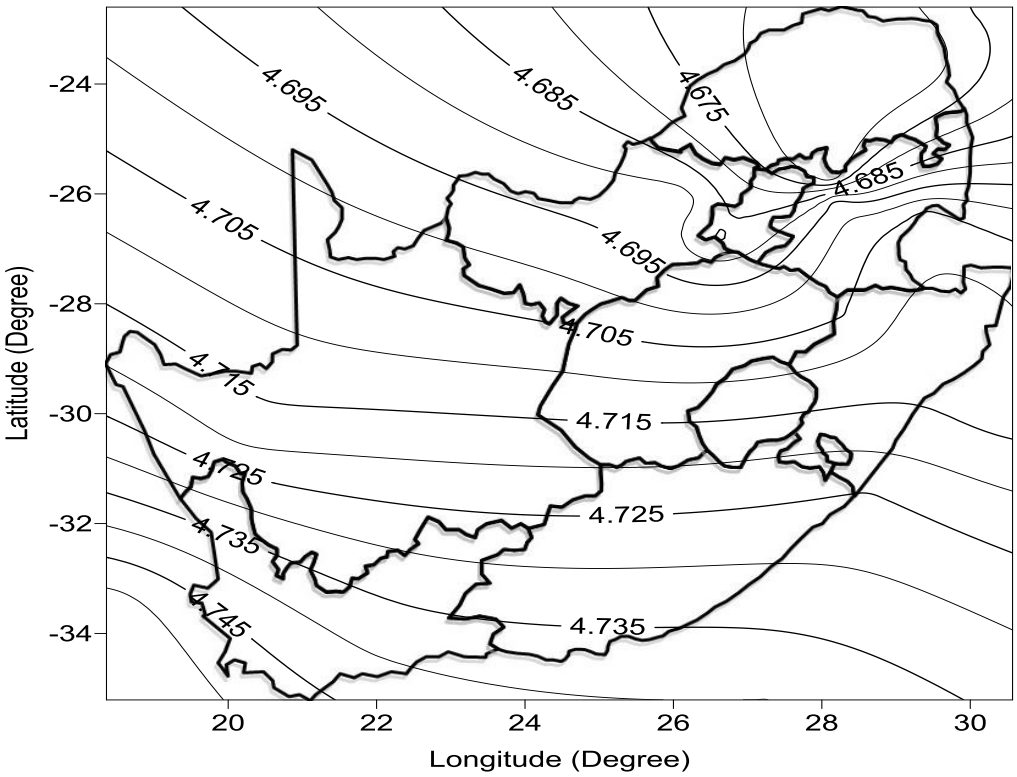

Figure 3.14 A 5-year mean contour map depicting the variability of ZDIH prediction based on ITU-R P.839-4 across the South African region.

3.7.3 Rain Height based on ZDIH at different Percentage of Exceedences

The contour maps in this subsection are very crucial to satellite communication systems engineers, because it will cater for better knowledge of the availability of time in higher frequency bands (such as in EHF and SHF). Figure 3.15 and 3.16 presented the contour map of ZDIH distribution exceeded 0.1% and 0.01% of time respectively across South Africa. This percentage of time is important for satellite applications such as internet multimedia.

It can be observed in Figure 3.15 that the rain height based on ZDIH varies between 4.385 km and 4.485 km for 0.1% of time. Also, Figure 3.16 shows that ZDIH ranges between 4.52 and 4.70 km for 0.01% of time. Hence, the results from this section will be very useful for better estimation of rain attenuation over South Africa.

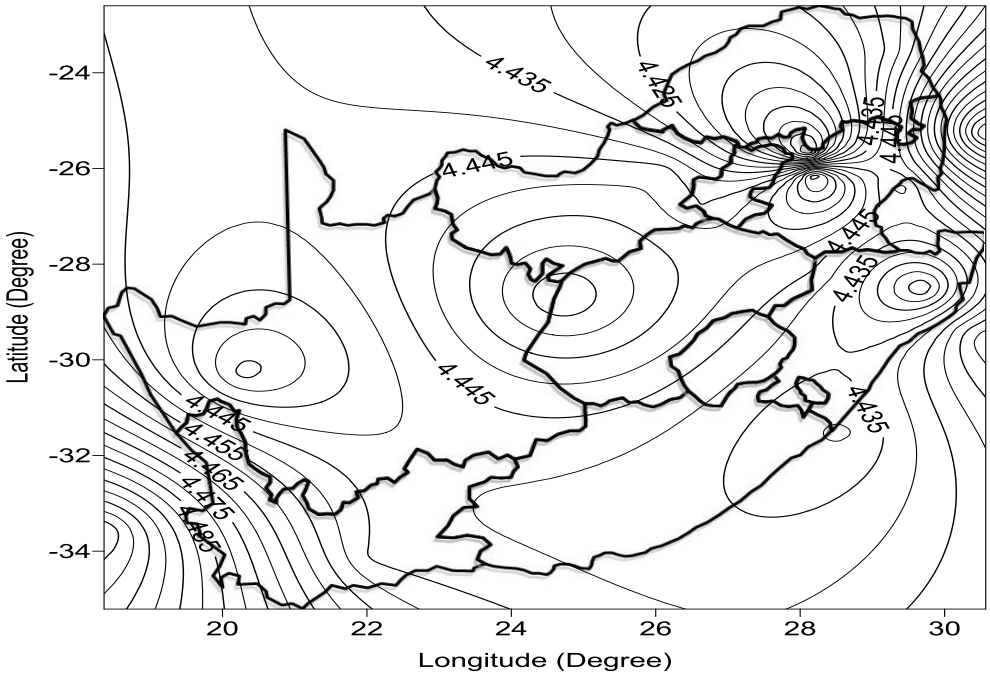

Figure 3.15 A 5-year mean contour map depicting the variability of ZDIH exceeded 0.1% of time across the South African region

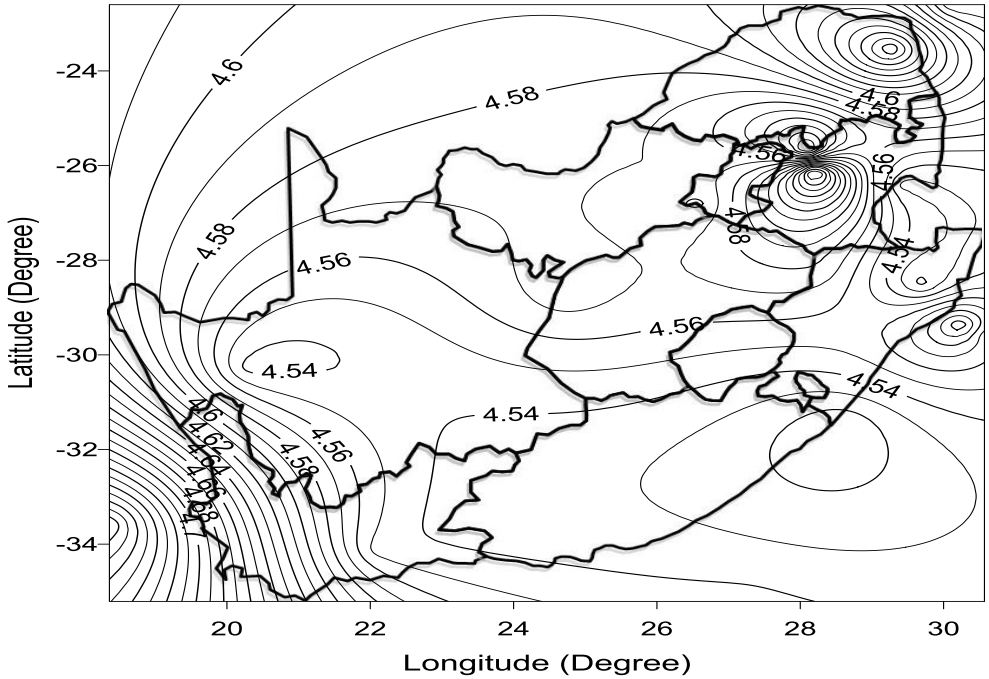

Figure 3.16 A 5-year mean contour map depicting the variability of ZDIH exceeded 0.01% of time across the South African region.

3.8 Modeling of the Rain Height

Effect of radio wave propagation due to atmospheric parameters is in general random functions of space and time. Propagation phenomena can, therefore, be analyzed and computed by means of statistical models. These statistical models differentiated by one or more parameters which can be used to characterize these phenomena with adequate accuracy. Also, accurate analyses of the data can be performed using appropriate statistical techniques and tools to consider the strengths and limitations of the data. Any measured data can be classified as deterministic or random, which can assist in the description of existing mathematical relations, if at all it exists. Also, if data can be described in term of mathematical relations, it is known as deterministic data which will always produce the same output from the initial state. For those data that cannot be described by definite mathematical relations (that is, those data with unexpectable results of any measurement), they are known as random data. The physical phenomena reflected in random data are usually time-varying (or space-varying) events are classified as random processes. Data used in this work as related to one of the atmospheric parameters is classified as a random data. Random variables play an important role virtually in every field of study, such as in engineering, physics, chemistry, management, biological and social sciences.

This section focuses on statistical modeling of ZDIH data that include clustering, stratification, and weights. Also, the models used in this work have developed the effective methods for handling missing exposure data. These models are typically specified by a Probability Density Function (PDF) which consists of continuous and discrete variables respectively. This is assumed to have properly normalized the sum or the integral that takes over all the relevant values for which PDF is defined. Due to the fact that the data obtained in this research contain a continuous variable; therefore, this section will focus and discuss only the continuous variable used in this research.

There are several statistical models available such as Gaussian, Burr, Lognormal, Dagum, Weibull, Erlang, Gamma, Beta, Generalized Extreme, Logistic, Log-logistics, among others. Hence, Dagum and Log-logistic distributions with three parameters were used in this work, which modeled best among other statistical models on the ZDIH data used in this research. The distributions are therefore presented as follows:

3.8.1 Dagum Distribution

Dagum distribution was introduced by [158], for modeling data as a substitute to the Pareto and Log-normal models. This distribution has been comprehensively used for modeling in diverse data, such as meteorological data, income and wealth, among others. Three-parameter Dagum distribution PDF and CDF are known to be continuous random variable distributions [17, 133, 158-164] and is designated as Dagum and expressed in (3.4) and (3.5) respectively:

$$f(x;k,\beta,\alpha) = k\beta\alpha x^{-\alpha-1}(1 + \beta x^{-\alpha})^{k-1} \tag{3.4}$$

$$F(x;k,\beta,\alpha) = (1 + \beta x^{-\alpha})^{-k} \tag{3.5}$$

where α and k are the shape parameters (k and α> 0), β is the scale parameter (β> 0) and x is the value of ZDIH $(x > 0)$.

3.8.2 Log-logistic Distribution

This type of probability distribution is the one which its distribution logarithm has a logistic distribution. Also, it's one of the continuous probability distributions for non-negative random variables, which gained attention due to its important uses in the applied situation [165-169]. Here, three-parameter Log-logistics PDF, $f(x)$, and CDF, $F(x)$, are used with an expression given as:

$$f(x) = \frac{\propto}{\beta}\left(\frac{x-\gamma}{\beta}\right)^{\alpha-1}\left(1 + \left(\frac{x-\gamma}{\beta}\right)^{\alpha}\right)^{-2} \tag{3.6}$$

$$F(x) = \left(1 + \left(\frac{\beta}{x - \gamma}\right)^{\alpha}\right)^{-1} \tag{3.7}$$

where α is a shape parameter (α> 0), while β is the scale parameter (β> 0), γ is the location parameter, and x is the value of ZDIH ($x > 0$).

3.8.3 Parameter Estimations of the Statistical Models

In order to improve the results of the modeling approach of the statistical models, it is essential to employ a systematic method in order to estimate the parameters of the model used, such as method of moments estimation, Bayesian method of estimation, and maximum likelihood estimation, among others. Also, as it is widely known that statistical parameter of a statistical model is the quantity that indexes the family of the probability distributions, based on empirical data that contains a random component, and also to describe the physical setting in a way by which their value affects the measured data of the distribution. Hence, this research employs the use of Maximum Likelihood Estimation (MLE) for parameter estimations, because it is one of the most systemic methods [170], it is consistent in estimation, it can provide effective estimation, and it is not unbiased [163]. The MLE of the distributions used in this research is described in sub-section **3.8.3.1** and **3.8.3.2.**

3.8.3.1 Dagum Maximum Likelihood Estimation

Let $x_1, \ldots, x_n$ be a ZDIH data size,n, from the Dagum distribution with parameters $k,\ \beta$ and $\propto$.

From (3.6), the likelihood is given as:

$$L(k, \beta, \alpha) = (\beta k \alpha)^n \prod_{i=1}^{n} x^{-\alpha-1}(1 + \beta x^{-\alpha})^{-k-1} \tag{3.8}$$

And the log-likelihood function is also given as:

$$l(k,\beta,\alpha) = n\,(e-(b))\sum_{i=1}^{n} c\sum_{i=1}^{n} d \tag{3.9}$$

where $b = \alpha - 1, c = \ln x - (k+1), \quad d = \ln(1+\beta x^{-\alpha})$ and $e = \log k + \log \beta + \log \alpha$.

The maximum likelihood estimators of $\hat{k}_{MLE}$, $\hat{\beta}_{MLE}$, and $\hat{\propto}_{MLE}$ of the parameters $k, \beta,$ and α can be derived numerically by maximizing with respect to $k, \beta,$ and α, the log-likelihood function (3.9). As a result of this, the log-likelihood function is maximized by solving in $k, \beta, \alpha,$ and x, the non-linear equations will be as follows:

$$\frac{\partial}{\partial k} l(k,\beta,\alpha) = \frac{n}{k} - \sum_{i=1}^{n} \ln(1+\beta x^{-\alpha}) = 0 \tag{3.10}$$

$$\frac{\partial}{\partial \beta} l(k,\beta,\alpha) = \frac{n}{\beta} - (k+1)\sum_{i=1}^{n} \frac{x^{-\alpha}}{(1+\beta x^{-\alpha})} = 0 \tag{3.11}$$

$$\frac{\partial}{\partial \alpha} l(k,\beta,\alpha) = \frac{n}{\propto} - \sum_{i=1}^{n} \log x + (k+1)\sum_{i=1}^{n} \frac{x^{-\alpha}}{(1+\beta x^{-\alpha})} = 0 \tag{3.12}$$

3.8.3.2 Log-logistic Maximum Likelihood Estimation

In this estimation, a type-II censored model is adopted and hereby used to obtain the smallest ZDIH observation value, m, from ZDIH data size n. The generalization of the type-II censoring is recognized as progressive type-II censoring. Assumed the unit of X follows the Log-logistic distribution with the itemized parameters in (3.6) and (3.7). It is well recognized that the distribution consists of a decreasing failure rate, where r_1 and r_2 are the first and second failure observed rate, which are arbitrarily removed as they occurred up to the m^{th} failure, which is the final failure rate, the remaining $r_m = n - r_1 - r_2 - \cdots - r_{m-1} - m$ units are removed. Let (X_1, R_1), $(X_2, R_2), \ldots, (X_m, R_m)$ denote the progressively Type-II censored model, where $X_1 < X_2 < \cdots < X_m$, X and R are

continuous random ZDIH data size and pre-fixed censoring scheme. The stated assumptions are also used to define the conditional likelihood function for the type-II progressively censored model as well-defined by [171, 172], which is as follows:

$$L(r) = C\prod_{i=1}^{m} f(x_i)(1-F(x_i))^{r_i} \tag{3.13}$$

where

$$C = n(n-\ r_1-\ 1)(n-r_1-\ r_2-\ 2)\ \ldots\left(n-\sum_{i=1}^{m-1} r_i-\ m+1\right) \tag{3.14}$$

$$r_i = 0;\ i = 1, 2, \ldots., m-1 \tag{3.15}$$

and $r = x/R$ is the dual generalized order of statistics in (3.7).

Consequently, the constant, C in (3.13) is the number of which the m in type-II progressively censored statistics could be selected.

The conditional likelihood function of the Log-logistic distribution can be given as follows:

$$L(r) = C\prod_{i=1}^{m}\left\{\frac{\frac{\propto}{\beta}\left(\frac{x_i-\gamma}{\beta}\right)^{\alpha-1}}{\left(1+\left(\frac{x_i-\gamma}{\beta}\right)^{\alpha}\right)^{2}}\right\}\left\{\frac{1}{1+\left(\frac{x_i-\gamma}{\beta}\right)^{\alpha}}\right\}^{r_i} = C\ \frac{\alpha^m}{\beta^m}\prod_{i=1}^{m}\left\{\frac{\left(\frac{x_i-\gamma}{\beta}\right)^{\alpha-1}}{\left(1+\left(\frac{x_i-\gamma}{\beta}\right)^{\alpha}\right)^{2+r_i}}\right\} \tag{3.16}$$

With an assumption that the removed item numbers are independent, and consists the identical probability mass function given as:

$$P(R_1 =\ r_1)\ = \binom{g}{r_1} p^{r_1}(1-r)^{g-r_1} \tag{3.17}$$

$$r_1 = 0, 1, 2, \ldots, g \tag{3.18}$$

and

$$P(R_i, R_{i-2}) = \binom{g - \sum_{l=1}^{i-1} r_l}{r_i} p^{r_i} (1-p)^{g - \sum_{l=1}^{i} r_i} \tag{3.19}$$

where,

$$R_i = r_{i-1} = \frac{r_i}{R_{i-1}}, \qquad r_i = 0,1,2,3 \ldots\ g - (r_1 + r_2 + \ldots + r_{i-1}); \tag{3.20a}$$

$$R_{i-2} = r_1 = r_{i-2} \ldots . R_1;\ g = n - m \text{ and } i = 1,2,3 \ldots\ m - 1. \tag{3.20b}$$

Suppose that R_i is independent of x_i, thus, it's written as:

$$P(R, p) = P(R_{m-1}) P(R_{m-2}) * P\left(R_2 = \frac{r_2}{R_1} = r_1\right) * P(R_1 = r_1) \tag{3.21}$$

where $R_{m-1} = r_1 = \frac{r_{m-1}}{R_{m-2}} = r_{m-2} \ldots R_1$ and $R_{m-2} = r_i = \frac{r_{m-2}}{R_{m-3}} = r_{m-3} \ldots R_1$

Therefore,

$$P(R, p) = \frac{(g)!}{(g - y)!\, t!} p^y (1-p)^{(g)(m-1) - y(m-i)} \tag{3.22}$$

where $y = \sum_{i=1}^{m-1} r_i$ and $t = \prod_{i=1}^{m-1} r_i$

With an assumption that r_i is independent of x_i for the entire i, the likelihood function of progressive type-II censoring with random removals can be defined as follows:

$$L(r, p) = L\,(r) P(R, p) \tag{3.23}$$

where $L(r)$ is the likelihood function for a progressive type-II censored scheme as defined in (3.16).

Let

$$z_i = \frac{x_i - \gamma}{\beta} \tag{3.24}$$

$$i = 1, 2, \ldots, m \tag{3.25}$$

The maximum likelihood function is given as follows from (3.23)

$$L(r, p) = P(q)^m \prod_{i=1}^{m} Q p^y (1-p)^{(g)(m-1)-y(m-i)} \tag{3.26}$$

$$P = \frac{C(g)!}{(g - y)!\, t!} \tag{3.27}$$

where

$$q = \frac{\propto}{\beta} \text{ and } Q = \frac{{z_i}^{(\propto - 1)}}{(1 + {z_i}^{\propto})^{2 + r_i}} \tag{3.28}$$

3.8.4 Probability Density Function of the Proposed Models on ZDIH

In this sub-section, the probability density function employed in this work is observed over 4 selected locations in 4 provinces in South Africa and discussed in this work. The selected locations are modeled to test the validity of the ZDIH data, which can further be used to extrapolate the ZDIH data across the remaining locations in South Africa. The PDF plot of each distribution is superimposed on the histogram as shown in Figure 3.17. It can be observed from Figure 3.17 that the two distribution models describe the rain height patterns very well.

Figure 3.17 presents the fitting PDF to the measured ZDIH over the studied locations. It can be seen in the figure that the Dagum model recorded the peak compared to the Log-logistic distribution as presented in Figures 3.17 (a), 3.17 (c) and 3.17 (d), with the peak of about 1.850, 0.093 and 0.158 respectively; while in Figure 3.17 (b) Log-logistic has the highest peak of about 0.168. Also, it can be noticed from the figures that ZDIH extends from about 3.579 to 4.585 km; 4.233 to 5.430 km; 4.158 to 4.728 km; and 3.892 to 4.944 km over Durban, Cape Town,

Johannesburg and Kimberley respectively. This implies that ZDIH varies from location to location.

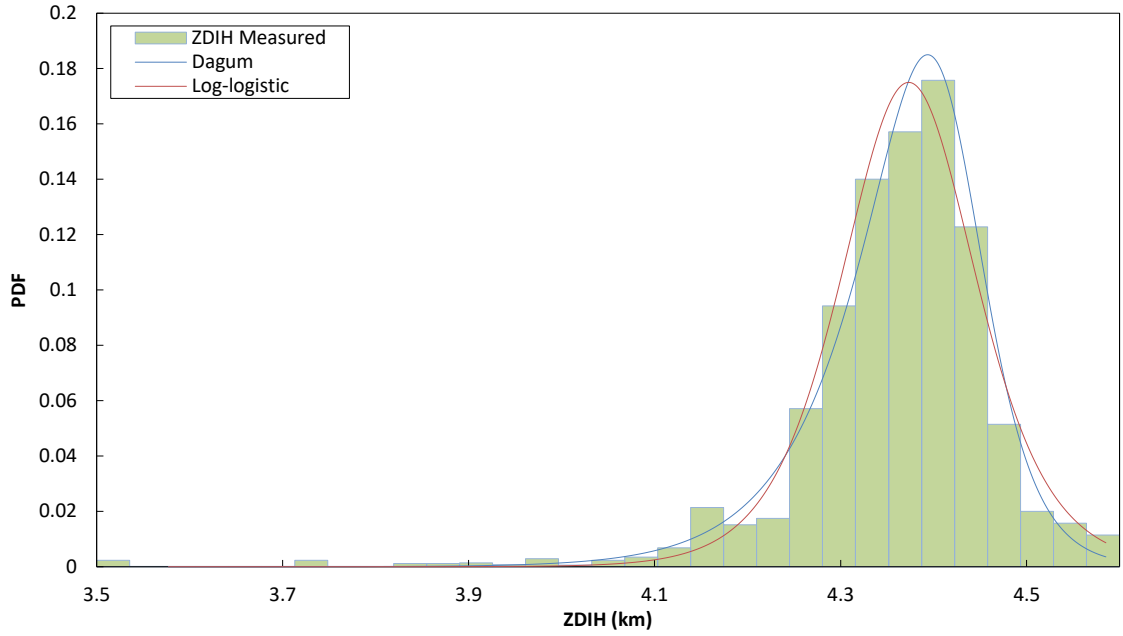

Figure 3.17(a) PDF comparison of measured and modeled (Dagum and Log-logistic) ZDIH data over Durban.

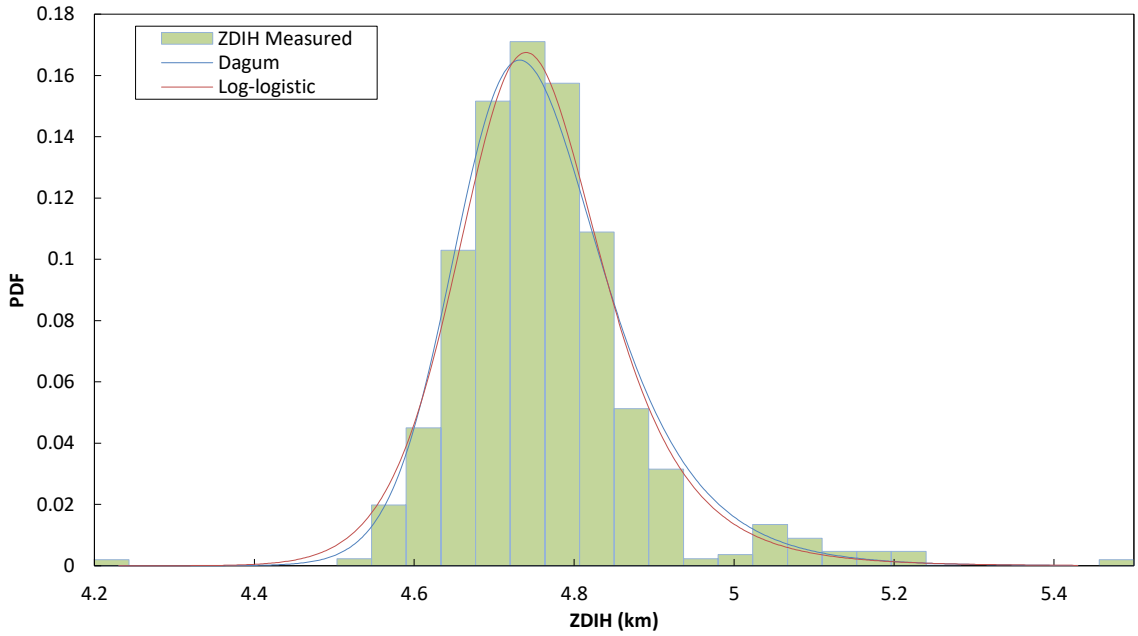

Figure 3.17(b) PDF comparison of measured and modeled (Dagum and Log-logistic) ZDIH data over Cape Town.

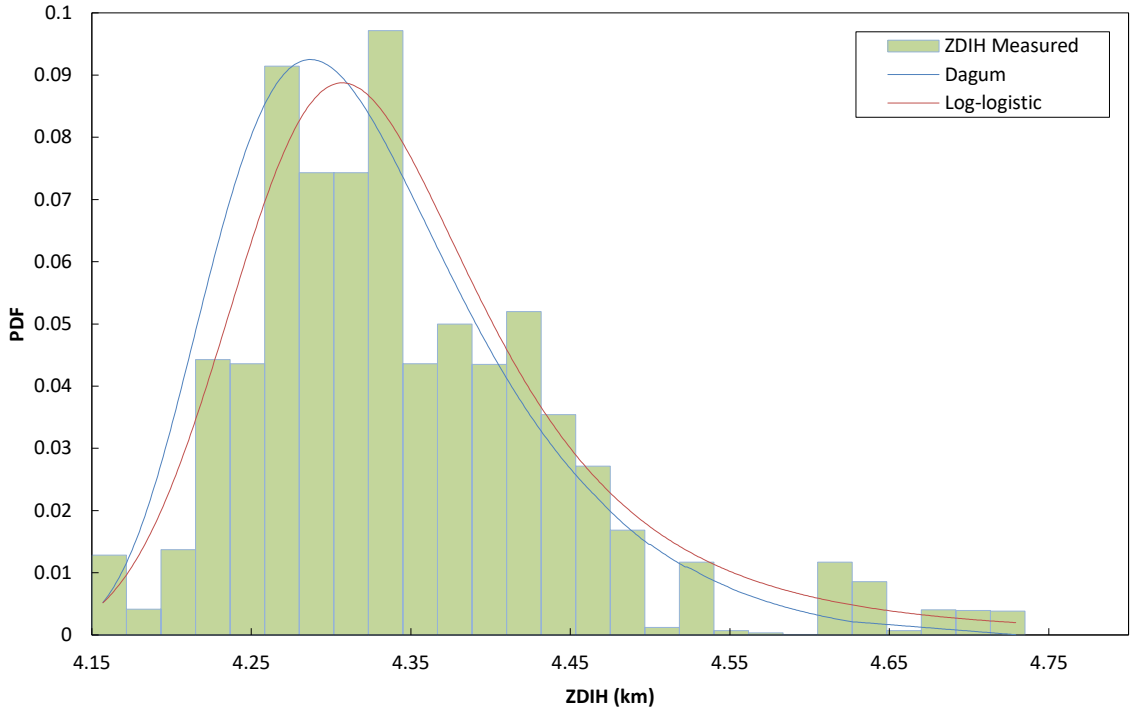

Figure 3.17(c) PDF comparison of measured and modeled (Dagum and Log-logistic) ZDIH data over Johannesburg.

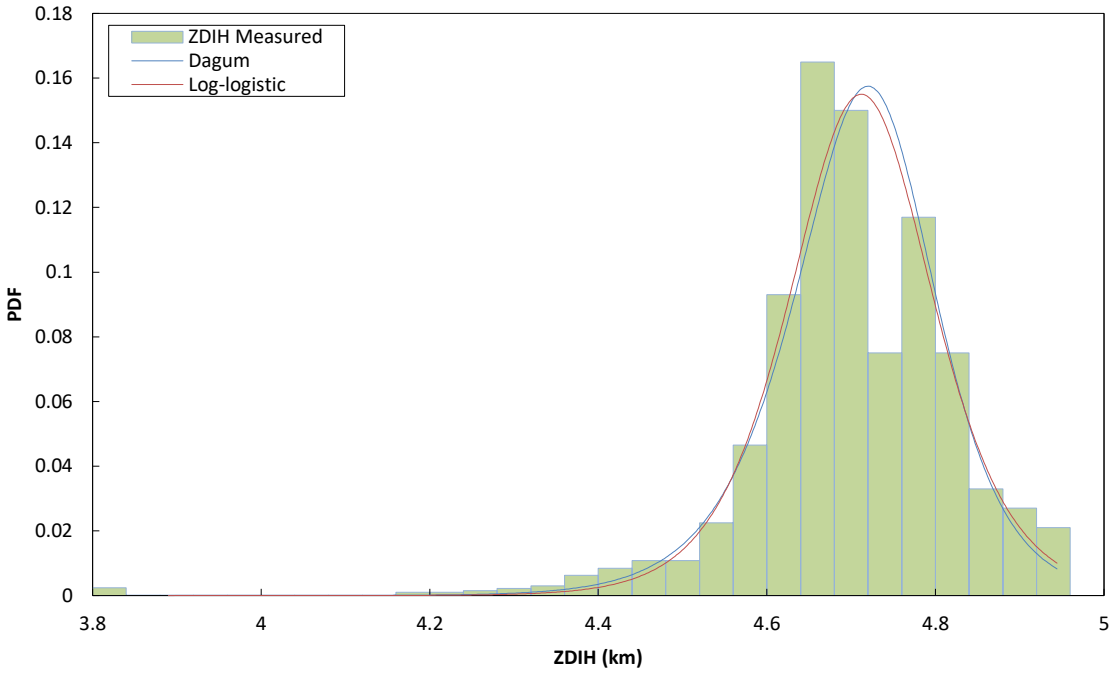

Figure 3.17(d) PDF comparison of measured and modeled (Dagum and Log-logistic) ZDIH data over Kimberley.

3.8.5 Parameters Estimation of the Statistical Models

The results of the parameters estimated from the observed distribution models over the studied locations are estimated using MLE as stated in sub-section 3.8.3. Table 3.4 presents the estimated parameters and their values.

Table 3.4 presents the MLE parameters estimation for the observed models for each location observed. It can be seen from the table that both shape, scale and location parameters vary widely over the observed locations. For example, k and α shape parameters vary from 0.44542 and 56.287 to 101.47 and 131.65, respectively, over the locations of study; β from 3.9504 to 4.6613 in Dagum model; while α, β, and γ vary between 4.2945 and 8.3114E+8, 0.71086 and 4.035E+7, 4.0392 and 4.0350E+7, respectively in the log-logarithm model over the studied locations. These estimated parameters values also imply that ZDIH is strongly location dependent.

Table 3.4 Model parameters estimation for the distributions

Location		**Durban**	**Cape Town**	**Johannesburg**	**Kimberley**
Dagum	k	0.44542	2.6036	101.47	0.71483
	α	131.65	62.223	56.287	87.659
	β	4.4216	4.6613	3.9504	4.3782
Log-logistics	α	8.3114E+8	11.727	4.2945	5.9240E+8
	β	4.0350E+7	0.71086	0.24478	3.3479E+7
	γ	4.0350E+7	4.0392	4.0878	3.3479E+7

3.8.6 Performance Evaluation of the Models Distribution

In this thesis, the performance evaluation of the PDF examined is essential in order to determine the model that best suits for each location of study. Therefore, three statistical goodness of fits was used to appraise the distribution function that best fit ZDIH measured data over the studied locations. They are bias error (Be), Root Mean Square Error (RMSE) and Kolmogorov-Smirnov (K-S) test as depicted as follows:

$$Be = \frac{1}{n}\sum_{i=1}^{n}\left(x_a(i) - x_p(i)\right)^2 \tag{3.29}$$

$$RMSE = \sqrt{\frac{1}{n}\sum_{i=1}^{n}\left(x_a(i) - x_p(i)\right)^2} \tag{3.30}$$

$$K - S\ test = \max_{1\le i\le n}\left((f(x_i) - \frac{i-1}{n}, \frac{i}{n} - f(x_i)\right) \tag{3.31}$$

where n is the total number of data points, i is the cumulative rank of the data points, $f(x)$ is the density function of the fitted data, x_a is the measured value of ZDIH and x_p is the predicted value of ZDIH.

However, since it is widely known that lower values of Bias error, RMSE and K-S test indicate a higher effectiveness of the distribution model function, this is adopted in this work. The metrics are used to illustrate the performance evaluation of ZDIH distribution over the observed locations as presented in Table 3.6. It can be seen from Table 3.6 that Dagum model performs better in Durban and Cape Town, while Log-logistic shows better performance in Johannesburg and Kimberley. Also, Dagum shows an improvement over Durban with about 0.012%, 0.47%, and 0.58%; and Cape Town with about 0.00039%, 0.02%, and 0.42% in Bias error, RMSE, and K-S test, respectively, while Log-logistic over Johannesburg is about 0.0021%, 0.08%, and 5.48%; and Kimberley are about 0.0048%, 0.15%, and 0.68% in Bias error, RMSE, and K-S test respectively.

Table 3.5 Performance Evaluation of the Proposed Distribution Models at the selected locations in South Africa

Statistical distributions	**Performance Evaluation using statistical goodness of fit**		
	Bias error	**RMSE**	**K-S test**
Dagum Durban	9.589E-5	0.0098	0.0361
Log-logistic Durban	2.112E-4	0.0145	0.0419
Dagum Johannesburg	1.768E-4	0.0133	0.0978
Log-logistic Johannesburg	1.561E-4	0.0125	0.0430
Dagum Cape Town	1.587E-4	0.0126	0.0452
Log-logistic Cape Town	1.626E-4	0.0128	0.0494
Dagum Kimberley	2.954E-4	0.0172	0.0525
Log-logistic Kimberley	2.473E-4	0.0157	0.0457

3.9 Chapter Summary

The effect of hydrometeors on communication system plays a major role in the design and applications. The ZDIH, among other parameters, is significant in the prediction of accurate rain attenuation for Earth-satellite communication systems and useful in other applications such as hydrology and remote sensing applications. Chapter three has given the review of rain height across the globe and its importance to communication systems. The description and collection of the rain height data used in this research were also given. Also, the observed results from the measurements of rain height over the studied locations in South Africa such as cumulative distributions, development of contour map and modeling of rain height with parameters estimation using maximum likelihood estimation technique were also presented.

The next chapter will address modeling of tropospheric attenuation at frequencies above 10 GHz for satellite communication systems.

CHAPTER FOUR

Tropospheric Attenuation Modeling

4.1 Introduction

The communication within the SHF and EHF bands are of great interest to satellite system service providers and system designers these days, due to the wide bandwidths obtainable at these frequency ranges. Such bandwidths are preferred in supporting applications such as Microwave Video Distribution Services (MVD), and Local Multipoint Distribution Services (LMDS), among others. Nevertheless, signal transmissions in these bands are impaired by various climatological conditions, which impose severe restrictions on the line-of-sight (LOS) radio systems. Scattering and absorption of signal energy by means of other tropospheric parameters such as clouds, atmospheric gases which can be regarded as secondary effects is significant at higher frequency bands and their effect on communication systems cannot be ignored. However, for the design of low margin systems, especially those aforementioned frequencies and at low elevation angles, the scintillation effects must be accounted for, in order to complete a link budget accurately. Hence, this chapter presents the attenuation due to gases, cloudiness, and scintillation over four selected locations in South Africa. These selected locations are considered with the same condition stated in section 3.8.4 and also considered in the next chapter, in order to test the validity of the ZDIH data, which can further be used to extrapolate the ZDIH data across the remaining locations in South Africa.

4.2 Atmospheric Gaseous Attenuation

The presence of different atmospheric gases in the atmosphere may interrupt satellite signals, traversing through Earth-satellite links [39]. The interruption may arise as a result of the atmospheric constituents of the molecular absorption, which strongly depends on the transmission frequency of signals [39]. In the

transmission medium, propagated signals also suffers signal degradation due to water vapor and dry air elements [42, 49]. It must be noted that water particles can either absorb or scatter electromagnetic signals compared to the presence of oxygen. For the purpose of this, the simplified approximated model of gaseous attenuation was adopted from the techniques recommended by ITU-R [55]. The slant path attenuation depends on various meteorological conditions due to the distribution of temperature, pressure, and humidity along the propagation path. Thus, the effective path length varies from location to location, months of the year, the height of the station above the sea level, and elevation angle. The total gaseous attenuation (dB) can be derived as [55]:

$$A_G = \sum_{n=1}^{k} a_n \gamma_n \tag{4.1}$$

where γ_n is the specific attenuation of the n^{th} layer, while k is the total number of the layers.

The specific attenuation, γ_n, (dB/km), is given as:

$$\gamma_n = \gamma_o + \gamma_w = 0.1820 f (N''_o(f) + N''_w(f)) \tag{4.2}$$

where γ_o and γ_w are the specific attenuation due to dry air (oxygen) and water vapour respectively; f, $N''_o(f)$, and $N''_w(f)$ are the frequency (GHz) and the imaginary parts of the frequency-dependent complex refractivities respectively; and,

$$N''_o(f) = \sum_{io} S_i F_i + N''_D(f) \tag{4.3}$$

$$N''_w(f) = \sum_{iw} S_i F_i \tag{4.4}$$

where S_i is the strength of the i-th oxygen or water vapour line, F_i is the oxygen or water vapour line shape factor, and $N"_D(f)$ is the dry continuum due to pressure-induced nitrogen absorption and also the Debye spectrum. These are further expressed as:

$$S_i = a_1 \times 10^{-7}\, p\, \theta^3 \exp[a_2(1-\theta)] \quad \text{for oxygen} \tag{4.5}$$

$$S_i = b_1 \times 10^{-1} e\, \theta^{3.5} \exp[b_2(1-\theta)] \quad \text{for water vapor} \tag{4.6}$$

$$N"_D(f) = fp\theta^2 \left[\frac{6.14 \times 10^{-5}}{d\left[1+\left(\frac{f}{d}\right)^2\right]} + \frac{1.4 \times 10^{-12}\, p\, \theta^{1.5}}{1+1.9 \times 10^{-5} f^{1.5}} \right] \tag{4.7}$$

where $p, e, \theta, \text{and } d$are dry air pressure (hPa), water vapour partial pressure (hPa), equivalent to $300/T$, and the width parameter for the Debye spectrum respectively, while T is the temperature (K). $e,\ d,\ F_i$ arefurther expressed as:

$$d = 5.6 \times 10^{-4}(p+e)\ \theta^{0.8} \tag{4.8}$$

$$e = \frac{\rho T}{216.7} \tag{4.9}$$

$$F_i = \frac{f}{f_i}\left[\frac{\Delta f - \delta(f_i - f)}{(f_i - f)^2 + \Delta f^2} + \frac{\Delta f - \delta(f_i + f)}{(f_i + f)^2 + \Delta f^2}\right] \tag{4.10}$$

where f_i is the oxygen or water vapour line frequency and Δf is the width of the line and given as:

$$\Delta f = a_3 \times 10^{-4}(p\, \theta^{(0.8 - a_4)} + 1.1 e\, \theta) \quad \text{for oxygen} \tag{4.11a}$$

$$\Delta f = b_3 \times 10^{-4}(p\, \theta^{b_4} + b_5\, e \theta^{b_6}) \quad \text{for water vapor} \tag{4.11b}$$

where, the line width, Δf, is further modified to explanation of Zeeman splitting of oxygen lines and Doppler lengthening of water vapour lines as:

$$\Delta f = \sqrt{\Delta f^2 + 2.25 \times 10^{-6}} \quad \text{for oxygen} \quad (4.12a)$$

$$\Delta f = 0.535\Delta f + \sqrt{0.2217\Delta f^2 + \frac{2.1316 \times 10^{-12} {f_i}^2}{\theta}} \quad \text{for water vapor} \quad (4.12b)$$

Also, δ is a corrections factor that arises due to the interference effects in oxygen lines, and given as:

$$\delta = (a_5 + a_6\theta) \times 10^{-4}(p + e)\,\theta^{0.8} \quad \text{for oxygen} \quad (4.13a)$$

$$\delta = 0 \quad \text{for water vapor} \quad (4.13b)$$

The parameters for $a_1, a_2, a_3, a_4, a_5, a_6,$ and $b_1, b_2, b_3, b_4, b_5, b_6$ are spectroscopic data for oxygen and water vapour attenuation respectively. A typical illustration of specific attenuation due to atmospheric gases had earlier been presented in Figure 2.6 [55].

4.2.1 Prediction of Gaseous Attenuation

The radio frequency energy can be absorbed up to some extent as it passes through water vapor, clear air and smog [173]. The impact of the two parameters, water vapor and dry air, that constitute the absorptions due to gaseous attenuation on the operational frequencies, for an Earth station above sea level and the transmitting or receiving, at an elevation angle towards the zenith angle is presented in this section. Figure 4.1 shows that the gaseous attenuation (water vapor and dry air) which reveals that the attenuation occurs at a specific region across the frequency bands (between 1 GHz and 350 GHz) over the observed locations in South Africa, using ITU-R model. The illustration presented in Figure 4.1 shows a similar pattern over the 5 selected heights considered in this study, although with different values. Further results revealed that, as the frequency increases, attenuation values also increase with the heights. It must be noted that the lowest height corresponds to the surface ground of each of the study locations.

In addition, as the frequency increases above 20 GHz, the atmospheric constituents reached individual points of resonance and the absorption became very high. The attenuation is also significant at the frequency about 60 GHz, which could be due to the effect of water vapor and majorly dry air on signals at that particular frequency. This implies that the effect of resonances is more pronounced at higher frequency. These frequency bands correspond to resonances of water vapor and dry air respectively, and are not employed for downlinks and uplinks. Hence, satellites direct links may utilize the absorptive bands by bypassing the atmosphere.

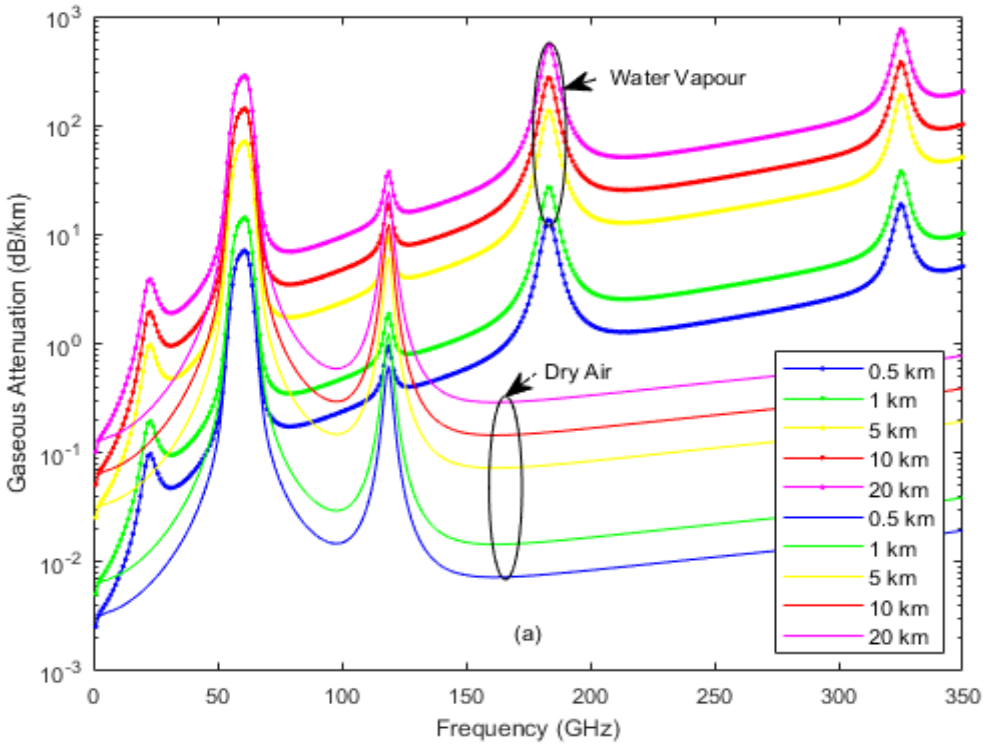

Figure 4.1(a) Influence of gaseous attenuation on frequency at different heights over Durban.

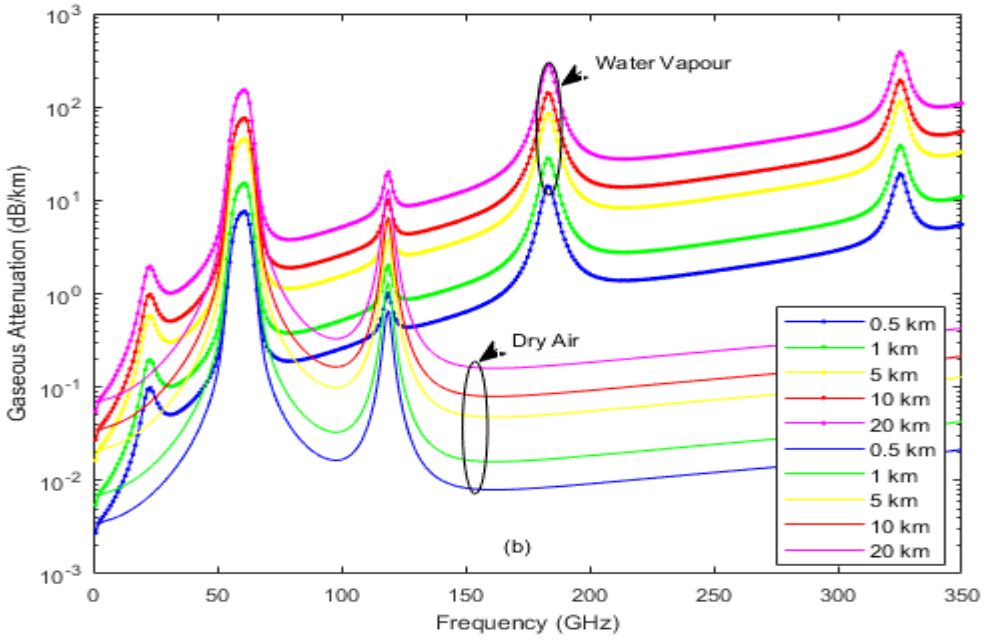

Figure 4.1(b) Influence of gaseous attenuation on frequency at different heights over Cape Town.

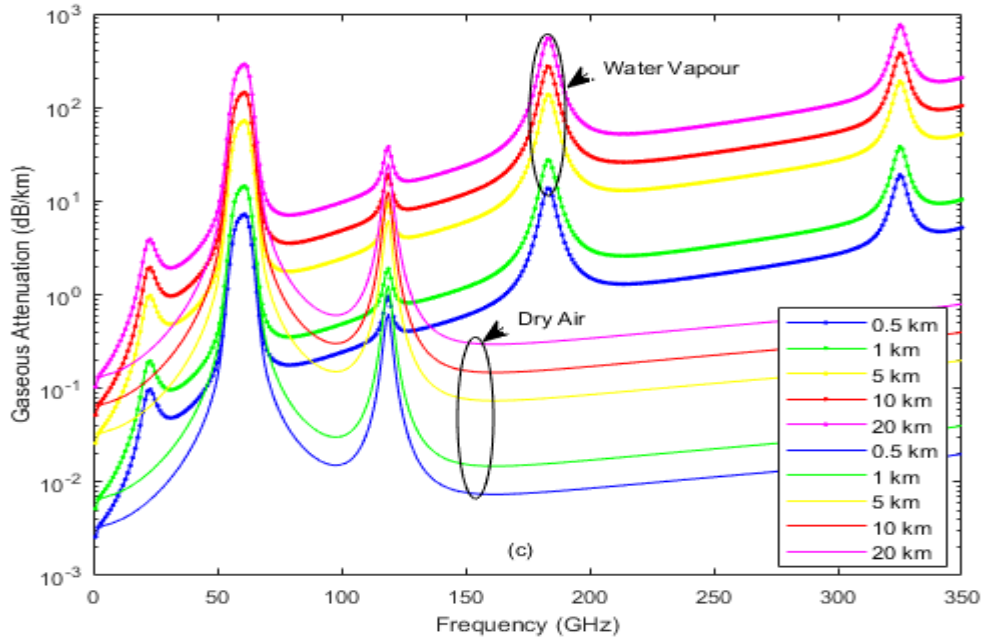

Figure 4.1(c) Influence of gaseous attenuation on frequency at different heights over Johannesburg.

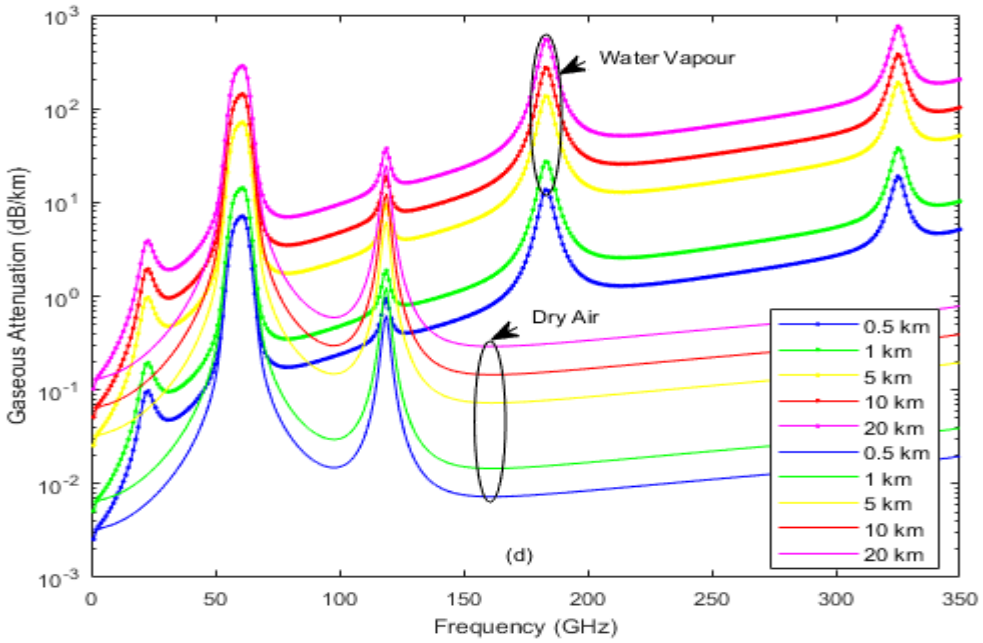

Figure 4.1(d) Influence of gaseous attenuation on frequency at different heights over Kimberley.

4.3 Cloud Attenuation

The cloud can be referred as the compilation of smaller rain droplets, or ice that are suspended in the air and usually located at an elevation above the surface of the Earth [174]. The absorption and scattering of electromagnetic signals operating above 10 GHz frequencies can be influenced by cloud content of liquid water due to its intensity that is lesser than that of rain. This section presents the technique for deriving cloud attenuation, as recommended by ITU-R in [58], which required liquid water content (LWC) parameter, and valid for the frequencies up to 200 GHz.

In order to obtain the attenuation due to cloudiness (dB) of a probability given value, the total columnar content of the liquid water statistics, L (kg/m^2), or equivalent of precipitable water (mm) of a location must be known. The L used in this study was obtained from TRMM-PR. The cloud attenuation can, therefore, be obtained using:

$$A = \frac{LK_l}{\sin\theta} \tag{4.14}$$

where θ is the elevation angle and K_l is the specific attenuation coefficient ((dB/km)/(g/m^3)) which is derived from the specific attenuation within the cloud or fog, and can be expressed as:

$$\gamma_c = K_l M \tag{4.15}$$

where M is the liquid water density in the cloud or fog (g/m^3). A mathematical model based on the Rayleigh scattering, which uses a double-Debye model for the dielectric permittivity $\varepsilon(f)$ of water, can be used to calculate the value of K_l, for the frequencies up to 1000 GHz. The typical diagram of specific attenuation by water droplets at several temperatures (between -8^o C and 20^o C) as a function of frequency ranging between 5 and 200 GHz as provided in [58] is presented in Figure 2.7. It must be noted that the corresponding curve related to 0^o C should be used for cloud attenuation prediction); $\varepsilon(f)$ and valid for the frequencies, f (GHz), up to 1000 GHz. Furthermore, K_l can be expressed as:

$$K_l = \frac{0.819f}{\varepsilon"(1 + \eta^2)} \tag{4.16}$$

while,

$$\eta = \frac{2 + \varepsilon'}{\varepsilon"} \tag{4.17}$$

The complex dielectric water permittivity is given by:

$$\varepsilon" = \frac{f(\varepsilon_o - \varepsilon_1)}{f_p[1 + (f/f_p)^2]} + \frac{f(\varepsilon_1 - \varepsilon_2)}{f_s[1 + (f/f_s)^2]} \tag{4.18}$$

$$\varepsilon' = \frac{\varepsilon_o - \varepsilon_1}{[1 + (f/f_p)^2]} + \frac{\varepsilon_1 - \varepsilon_2}{[1 + (f/f_s)^2]} + \varepsilon_2 \tag{4.19}$$

where $\varepsilon_o = 77.6 + 103.3(\theta - 1)$ (4.20)

$\varepsilon_1 = 5.48$ (4.21)

$\varepsilon_2 = 3.51$ (4.22)

And $\theta = 300/\mathrm{T}$ (4.23)

T is the temperature (K), while f_p and f_s are the principal and secondary frequencies (GHz) given as:

$$f_p = 20.09 - 142(\theta - 1) + 294(\theta - 1)^2 \quad (4.24)$$

$$f_s = 590 - 1500\,(\theta - 1) \quad (4.25)$$

4.3.1 Prediction of Cloud Attenuation in South Africa

The presence of rain along the Earth-satellite path is limited (≈ 5 – 10% of time of the year), while cloudiness cause more limited degradation on the system, which can be characterized with higher occurrence probability (that is, about 40 – 80% of time) according to [175, 176]. Hence, clouds are the important cause of attenuation, especially in the higher frequencies. It is important to examine the effect of clouds by predicting cloud attenuation of the electromagnetic signals, especially in the SHF and EHF bands. This section presents an assessment of the specific attenuation coefficient based on Rayleigh scattering by water droplets, at several temperatures as a function of frequency and also the cloud attenuation prediction over the four selected locations in South Africa using the ITU-R model as earlier presented in section 4.3.

Figure 4.2 shows the values of K_l at frequency range from 10 to 200 GHz, together with the temperatures between -8^o C and 20^o C. It can be seen that the specific attenuation coefficient increases as the frequency increases over the studied locations although the temperatures intercepted each other from about 90 GHz

and above. The curve corresponding to 0º C is used for prediction of cloud attenuation in this thesis as speculated by [58]. This implies that the liquid water in the cloud along the satellite path is very important, especially in the applications concerning low elevation links.

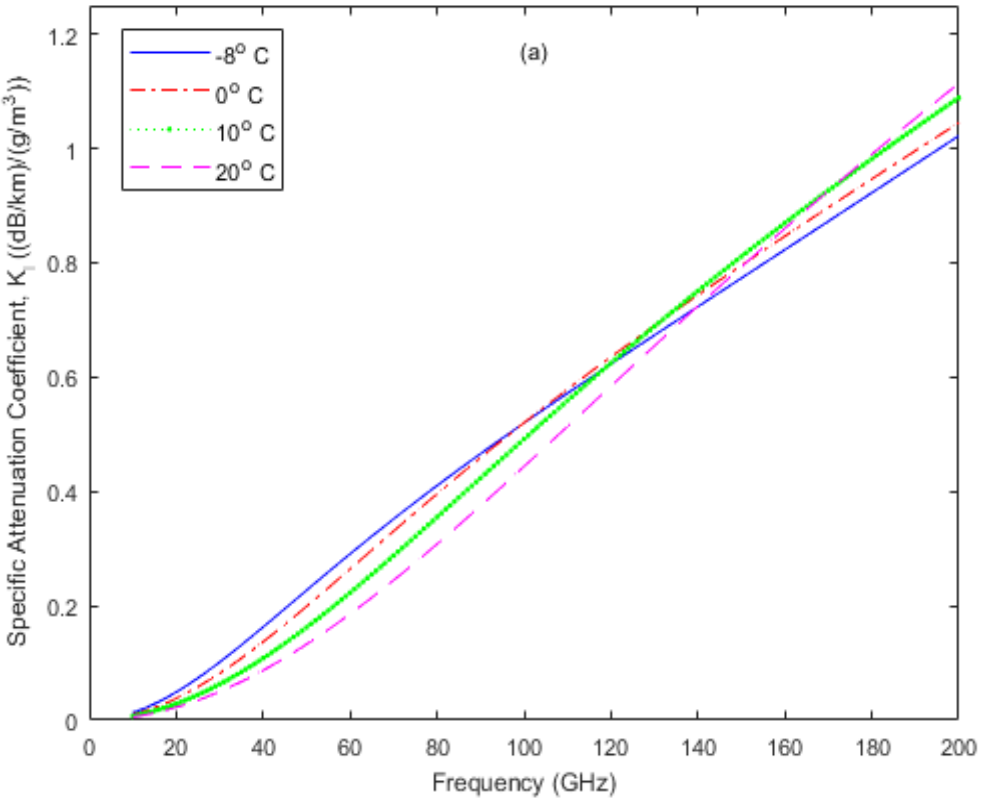

Figure 4.2(a) Specific attenuation coefficient by water droplets at several temperatures as a function of frequency over Durban.

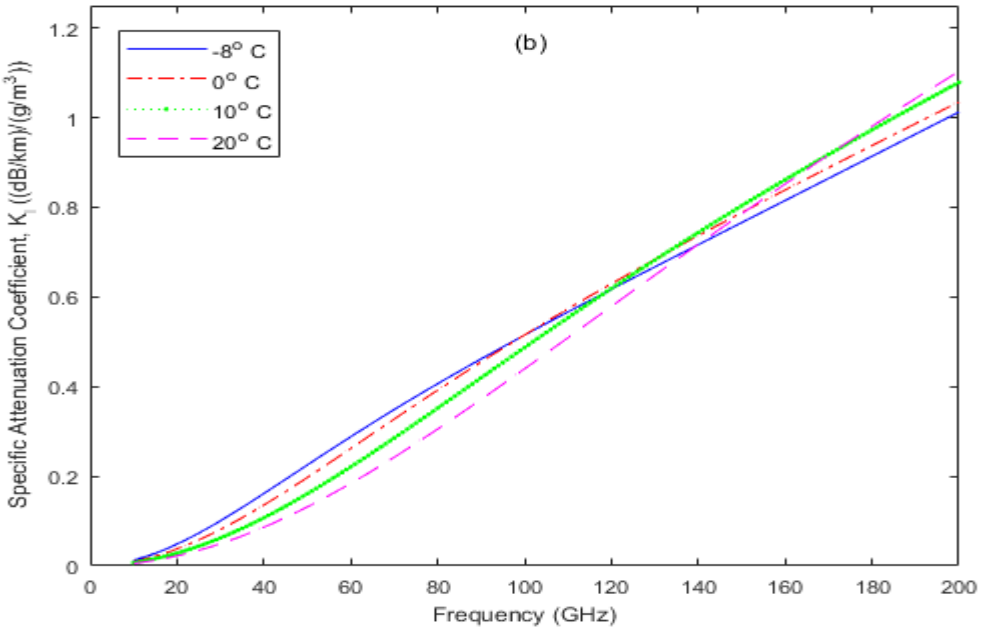

Figure 4.2(b) Specific attenuation coefficient by water droplets at several temperatures as a function of frequency over Cape Town.

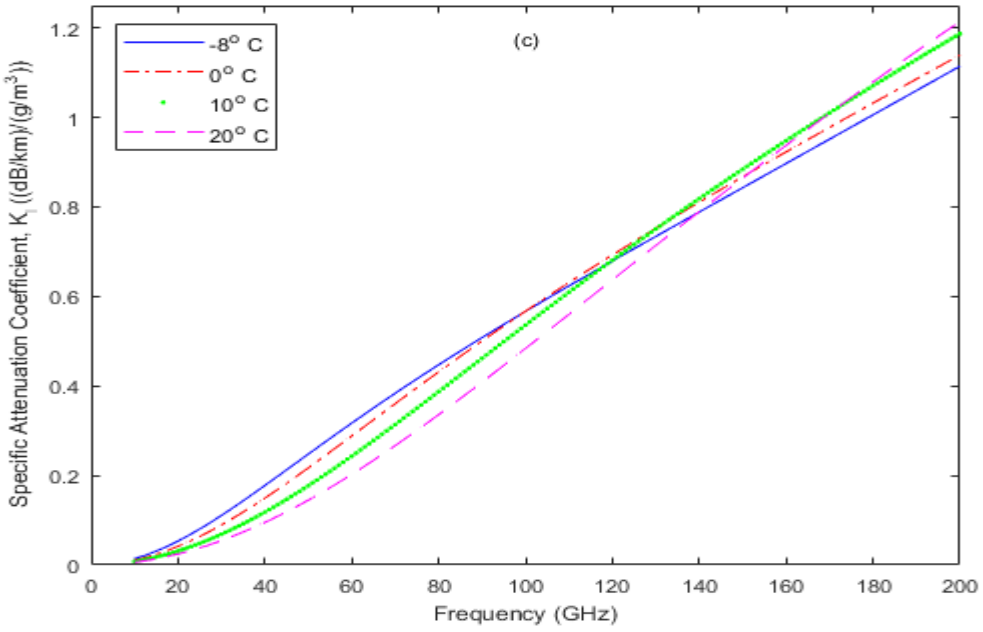

Figure 4.2(c) Specific attenuation coefficient by water droplets at several temperatures as a function of frequency over Johannesburg

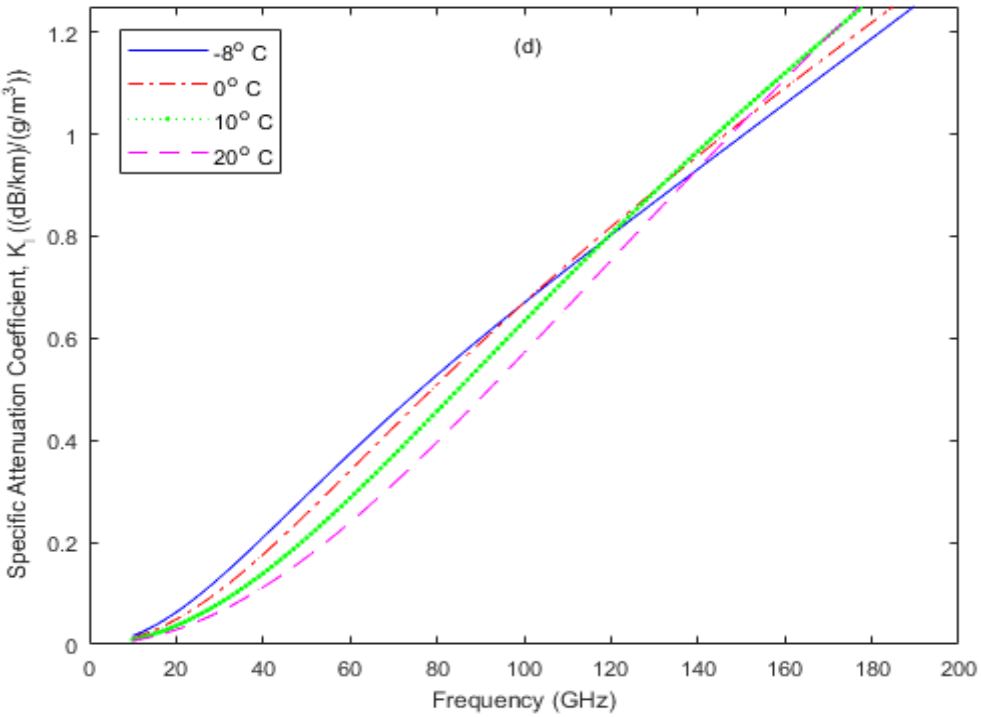

Figure 4.2(d) Specific attenuation coefficient by water droplets at several temperatures as a function of frequency over Kimberley.

Figure 4.3 presents the cloud attenuation prediction over the 4 selected locations in South Africa. It can be observed generally from Figure 4.3 that cloud attenuation increases as the frequency increases and Durban recorded lowest cloud attenuation, followed by Cape Town then Johannesburg, and Kimberley recorded highest cloud attenuation value. Although, cloud attenuation is almost negligible over the locations observed at frequency ranges between 12 GHz and 40 GHz, which shows less than 1 dB/km over the observed locations, while about 1 dB and above was observed at frequencies from above 60 GHz. For example, the cloud attenuation of about 0.4059, 0.4332, 0.4578, and 0.5292 dB/km at 40 GHz was recorded, while at 60 GHz, it was about 0.8727, 0.9233, 0.9810, and 1.1362 dB/km over Durban, Cape Town, Johannesburg and Kimberley respectively. This implies that the effect of cloudiness due to LWC on radio signals has its own

impact and the differences in the attenuation observed may be due to the effect of LWC and other atmospheric parameters observed over the locations.

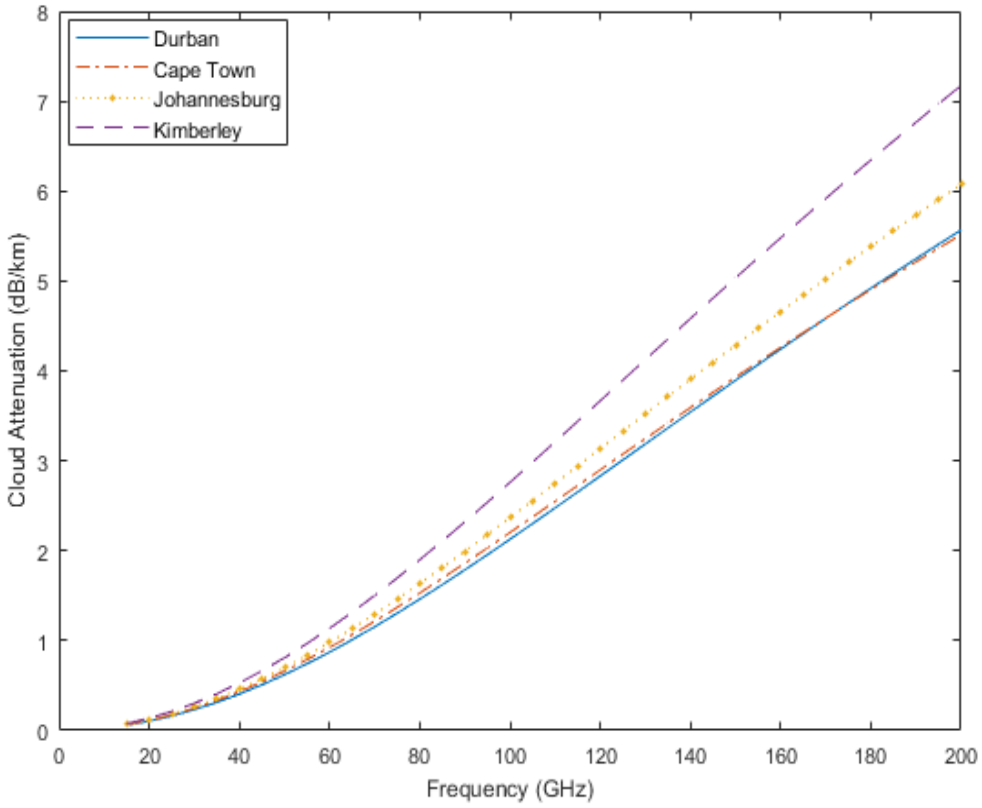

Figure 4.3 Cloud attenuation prediction over the 4 selected locations in South Africa.

4.4 Amplitude of Tropospheric Scintillation

In satellite communications, scintillation results from rapid variations or fluctuations in the phase and signal amplitude due to changes in the refractive index of the Earth's atmosphere, polarization and angle of arrival of the radio wave signal caused by the time-varying irregularities in the propagation channel. The scintillation magnitude is also dependent on the variation of the refractive index, which increases with frequency and path length and decreases according to the decrement of the antenna beam width, due to the aperture averaging. The model for prediction of amplitude tropospheric scintillation consists of three methods [142], which are: prediction of fading among systems at free-space elevation

angle above or below 5°, fading ≥ 25 dB, and the transition region between the earlier stated methods.

However, the method considered in this research is the statistics of amplitude scintillations at an elevation angle greater than 5°. This is a general technique for the prediction of the cumulative tropospheric scintillation and it's based on monthly or longer averages of relative humidity, the temperature of a specific location, and the application is recommended up to at least about 20 GHz [142].

The parameters required for the tropospheric scintillation model are:

1. t: average ambient temperature (° C) at the location of study for a period of one month or longer;
2. H: average surface relative humidity (%) at the location of study for a period of one month or longer;
3. f: frequency (GHz);
4. θ: angle of elevation greater than 5°;
5. D: physical diameter of the Earth-station antenna, (m);
6. η: antenna efficiency.

Also, the step by step require for the model are:

Step 1: For the value of t, obtain the saturation water vapor pressure, e_s (hPa), as specified in [52];

Step 2: Calculate the wet term of the radio refractivity, N_{wet}, conforming to e_s, as specified in [52];

Step 3: Calculate the standard deviation of the reference signal amplitude, σ_{ref} as in (4.26);

$$\sigma_{ref} = 3.6 \times 10^{-3} + 10^{-4} \times N_{wet} \quad (4.26)$$

Step 4: Obtain the effective path length, L (m):

$$L = \frac{2h_L}{\sqrt{\sin^2\theta + 2.35 \times 10^{-4}} + \sin\theta} \tag{4.27}$$

where h_L is the height of the turbulent layer, which is 1000 m.

Step 5: estimation of the effective antenna diameter, D_{eff}(m), from the geometrical diameter, D, and the antenna efficiency, η, as given in (4.28):

$$D_{eff} = \sqrt{\eta} D \tag{4.28}$$

Step 6: Calculate the antenna averaging factor:

$$g(x) = \sqrt{3.86(x^2 + 1)^{11/12} \times \sin\left[\frac{11}{6}\tan^{-1}\frac{1}{x}\right] - 7.08x^{5/6}} \tag{4.29a}$$

where

$$x = 1.22\, {D_{eff}}^2 \left(\frac{f}{L}\right) \tag{4.29b}$$

If the argument of the square root is negative (that is, $x \geq 7$), the predicted scintillation fade depth for the time percentage will be zero and the following steps are not required.

Step 7: Obtain the standard deviation of the signal for the appropriate period and propagation path:

$$\sigma = \sigma_{ref} f^{7/12} \frac{g(x)}{(\sin\theta)^{1.2}} \tag{4.30}$$

Step 8: calculate the factor of the percentage of time for the percentage of time, p, between the range 0.01%< $p \leq 50\%$

$$a(p) = -0.061(\log_{10} p)^3 + 0.072(\log_{10} p)^2 - 1.17 \log_{10} p + 3 \quad (4.31)$$

Step 9: calculate the fade depth (dB) exceeded for the percentage of time:

$$A(p) = a(p)\sigma \quad (4.32)$$

4.4.1 Estimation of Tropospheric Scintillation over South Africa

In satellite communications field, the meteorological condition in the troposphere influences radio wave propagation due to constant motion caused by the energy received from the sun, which warms the Earth's surface and the resultant convective activity agitates in the tropospheric layer. This section presents the magnitude of tropospheric scintillation effects using the wet refractivity over the four selected locations in South Africa as a principal input parameter in the ITU-R model [142], as earlier presented in section 3.9. Scintillation consists of positive signal level termed as enhancement and negative signal level known to as fade. The enhancements of scintillation affect the satellite signal uplink by increasing the intermodulation noise in the transponder consumed by the multicarrier; while the scintillation fading affects the uplink power control systems or the Earth station tracking systems [177].

Over the four selected locations studied in this section, the scintillation was measured based on the five-year average of wet refractivity, relative humidity, the temperature at the ground level. Generally, different patterns of scintillation fading observed may be due to the meteorological conditions of the locations of study. The cumulative distribution of amplitude scintillation (amplitude enhancement and fading) function is presented in Figure 4.4. It can be seen from Figure 4.4 that the scintillation estimated from refractivity statistics of the selected locations followed the same pattern, although, with different scintillation values.

The deviation between the enhancement and fading occurred at about 30%, 25%, and 8% of time over Durban, Cape Town and Kimberley respectively, while

Johannesburg began with deviation of 100% and intercepted at 50% and 0.4% of time respectively; and thereafter increases towards the lower percentages of time. The deviation occurrence may be due to the commencement and the formation of convective rain type, as well as the liquid water content along the propagation path [178, 179]. Also, any scintillation intensity above 0.04 dB could be considered as a scintillation event, and this agrees with the work of [179-181]. This implies that the scintillation effects of any specific location should be accounted for, in order to enhance the link budget of the low margin system at the lower elevation angle and higher frequency bands.

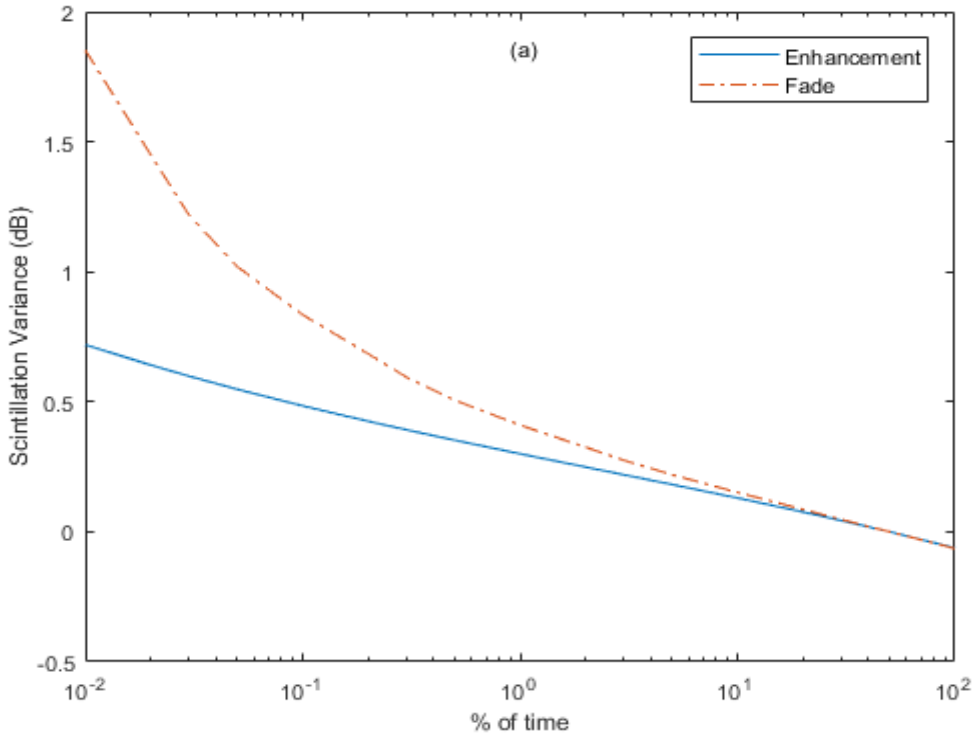

Figure 4.4(a) 5-year Annual mean cumulative distribution of signal level over Durban.

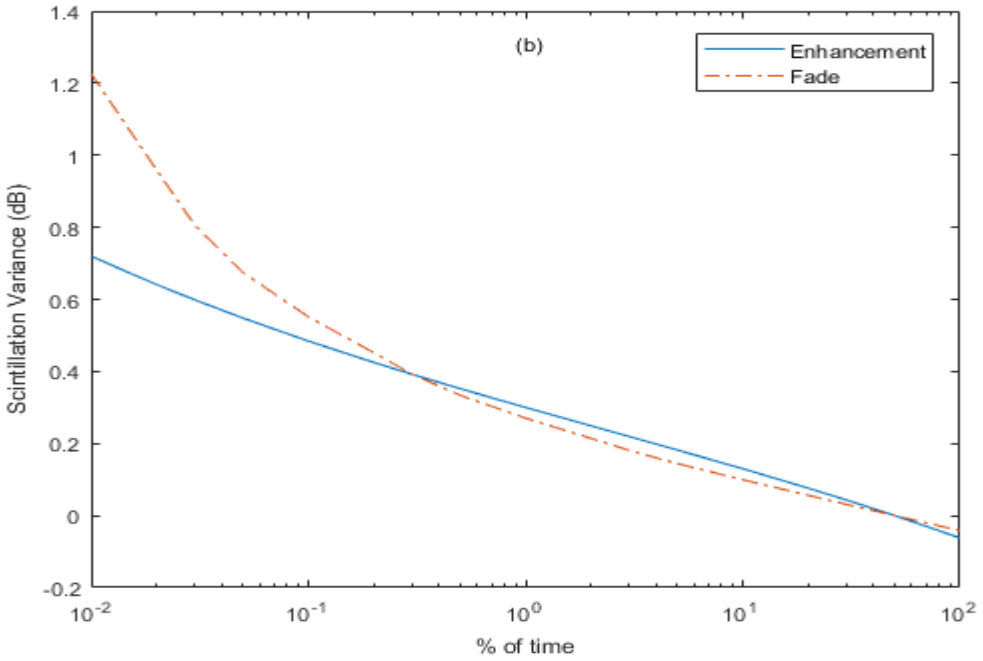

Figure 4.4(b) 5-year Annual mean cumulative distribution of signal level over Cape Town

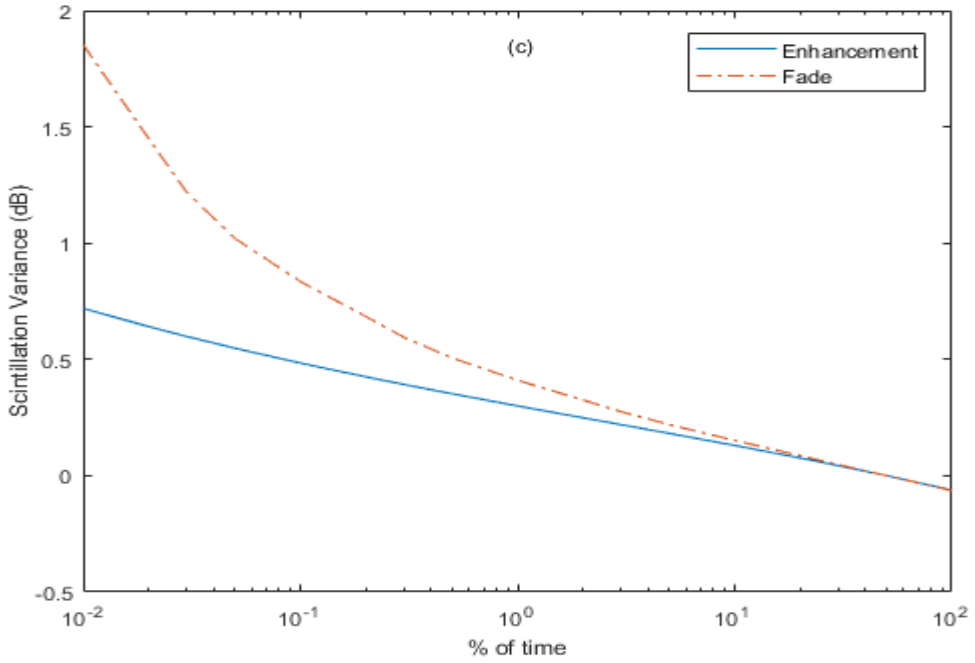

Figure 4.4(c) 5-year Annual mean cumulative distribution of signal level over Johannesburg.

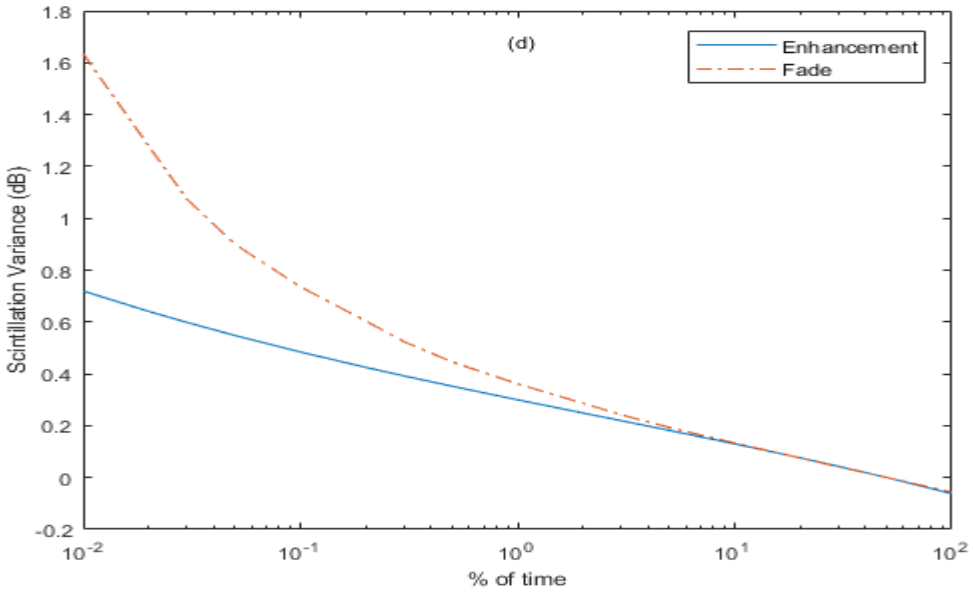

Figure 4.4(d) 5-year Annual mean cumulative distribution of signal level over Kimberley.

4.5 Chapter Summary

Effect of tropospheric parameters on satellite communication links at higher frequencies require attention for effective use of satellite systems. Hence, this chapter has reviewed the available global models and utilized it for the predictions of gaseous attenuation, cloud attenuation and tropospheric scintillation over South Africa.

The results of the predictions of the gaseous attenuation indicated that the resonances are more conspicuous at higher frequencies which may be due to the effect of dry air and water vapor on the radio wave signals. The cloud attenuation prediction shows that the presence of LWC in the cloud contributes to the losses of radio signals at higher frequencies. Also, the effect due to tropospheric scintillations also shows its significance in terms of the enhancement and fading observed, and the scintillation intensity observed was above 0.04 dB, which agrees to the scintillation effect needed to be accounted for especially for link design [179-181].

CHAPTER FIVE

Adaptation of Rain Height in Attenuation Estimation

5.1 Introduction

The rapid growth of telecommunication services, both in the satellite and the terrestrial links using higher frequency bands above 10 GHz (such as SHF and EHF) has highlighted the need for estimating the effects of hydrometeor such as rain, clouds, fog, among others. The demand for ultra-wide bandwidth for high quality, high speed, and multimedia transmission were driven by the use of higher radio frequency spectrum. Nevertheless, attenuation and fading due to rainfall have long been known as a major limitation to reliable communication systems functioning at higher frequencies. The presence of rainfall in radio wave propagation can yield major impairments to SHF and EHF propagation. With the increased demand for direct-to-user satellite services, SHF and EHF bands have become a preferred alternative for several new systems, as it offers a large bandwidth required to support the anticipated need for capacity. While offering a solution to the problem of spectrum congestion, SHF and EHF bands suffer from fading due to rainfall. And fade depth (dB) is commonly caused by rain. However, rain fade has an adverse effect on the quality of service (QoS) in the satellite communication applications. Hence, the need for accurate rain attenuation. This chapter presents an application of measured rain height in rain attenuation prediction, combined attenuation and QoS over the 4 selected locations considered in chapter four.

5.2 Rain Attenuation Prediction

Statistical estimation of rain attenuation is essential for any communication system. This section looks into the concept of rain attenuation prediction techniques. There are several existing techniques for the prediction of rain

attenuation over the microwave paths. These techniques can be grouped into two classes, which are:

1. Empirical techniques: this technique is based on database measurements over some stations in different climatic zones within a specified region, and
2. Physical techniques: this is an attempt to reproduce the physical behaviour involved in the attenuation process.

Some researchers pointed out that, not all required inputs for these techniques are available, mostly when there is a need for the use of these techniques [182]. Therefore, there is a high rate in the use of the empirical techniques. The models that belong to this group contain a set of equations, which are statistical in nature to model the behaviour of the attenuation. It also considered several variables, such as rain rate, rain height, and the Earth–station latitude, among others.

However, in the prediction of rain attenuation, the following procedures should basically be considered:

1. Obtaining the point rainfall rate for the physical site under analysis. This can be done using local rain data (1-minute integration time is recommended) or through global precipitation maps and climatic models;
2. Estimating the rain height (that is the height at which no liquid rain is expected). Also, this can be done with the use of local measurements (such as radar data as used in this research);
3. Estimating the attenuation per unit length (that is, specific attenuation);
4. Estimating the length of the slant path (along the Earth station - satellite) affected by the rain cell;
5. Estimating the total attenuation along the path. This can be estimated from the product of the specific attenuation and the effective slant path length.

Several researchers have proposed different models for prediction of attenuation along a path. This started way back from a few decades ago by [183], who presented a rain attenuation model. Two decades after, [184] published a revised model of [183] and concluded that there is a tendency for the measured attenuations to exceed the maximum conceivable levels predicted by the theory. A decade later, [185] looked afresh at the model predictions and then compared them with the measured values taking the data available and found out that there is an average similarity between model predictions and measurements. He later anticipated another model called, two-component model and followed by the revised version. Several other models also include CCIR model, simple attenuation model (S.A.M) by [186], Dutton et al. model [187], Excell model, MismeWaldteufel, Garcia model, ITU-R model, Flavin model, Bryant model, DHA model, Moupfouma Model, CETUC model among others [188]. However, only a few of the predicted models can be applied to the different regions due to their global recognition, out of which the ITU-R model [142] is the most recognized one and is being utilized in this research.

5.2.1 Rain Attenuation for Satellite Links

As stated in section 5.2, that ITU-R model is utilized in this work as produced in [142]. This recommendation is used for various predictions of the radio wave propagation that are needed in planning Earth-space systems. The recommendation stated that, it is necessary to have an appropriate propagation data and prediction techniques for proper planning of Earth-space systems. Also, these procedures have been developed in order to allow the most important propagation parameters needed for planning Earth-space systems and these procedures are compatible with any natural variability of propagation phenomenon and adequate for recent applications in system planning. The analysis of the model adopted in this research is presented below.

The rain attenuation prediction model has been estimated on the basis of the lognormal distribution, using similar principles of [29]. Both rain rate and path attenuation distributions generally conform to the lognormal distribution. Inhomogeneities of rain in vertical and horizontal directions are accounted for in this prediction. The model can also be applied for the estimation of the frequencies up to 55 GHz, at a given location for Earth-satellite links. Table 5.1 presented the input parameters required for long-term statistics of the rain attenuation. Also, Figure 5.1 presents the typical representation of an Earth-satellite path, which shows the parameters required for the process of the prediction; where A denoted frozen precipitation, B is rain height, C is liquid precipitation, and D is the Earth-space path.

Table 5.1 List of input parameters necessary for the rain attenuation prediction model

ITU-R Model	$\varphi(^{o})$	h_s(km)	$\theta(^{o})$	f(GHz)	k, α	$R_{0.01}$(mm/h)	h_R(km)	R_e(km)
P.618-12	√	√	√	√	√	√	√	√

where φ is the latitude of the Earth station (degree), h_s is the altitude of the Earth's station (km), θ: elevation angle of the link (degree), f is the frequency of the link (GHz), k and α are the frequency and the polarization dependent coefficients respectively as given by [63], $R_{0.01}$ the point of rainfall rate at 0.01% of time of an average year of observation (mm/h), h_R is the rain height (km) according to [146], and R_e is the effective radius of the Earth (km).

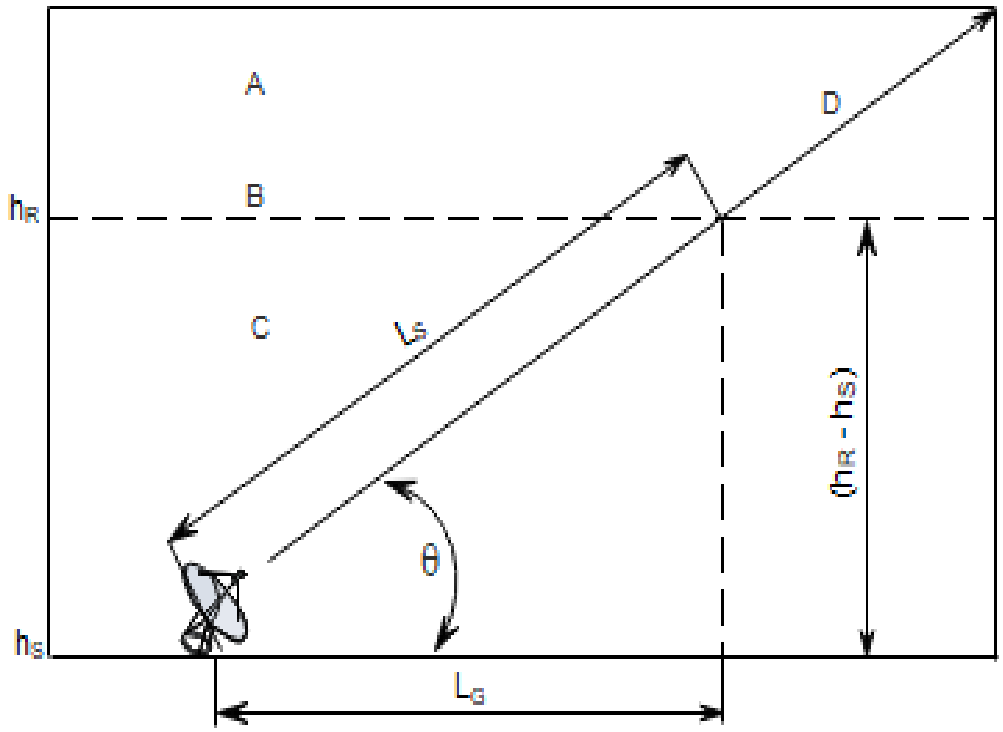

Figure 5.1 The typical representation of an Earth-satellite path [142].

Also, the following steps are the procedure for calculating the rain-induced attenuation distribution for the satellite links:

Step 1: Rain height determination h_R, as given in (3.2) [146];

Step 2: Calculate the slant-path length, L_s, below the rain height in km using the expression in (5.1) for $\theta \geq 5^o$.

$$L_s = \frac{(h_R - h_s)}{\sin\theta} \tag{5.1}$$

However, for $\theta < 5^o$, (5.2) can be used:

$$L_s = \frac{2(h_R - h_s)}{\left(\sin^2\theta + \frac{2(h_R - h_s)}{R_e}\right)^{1/2} + \sin\theta} \tag{5.2}$$

where R_e is 8500 km and if $h_R - h_s$ is ≤ 0, the predicted rain attenuation will be equal to zero for any percentage of time. Therefore, the following steps will not be required.

Step 3: The horizontal projection of the slant path length, L_G, can be computed from:

$$L_G = L_s \cos\theta \tag{5.3}$$

Step 4: The rainfall rate, $R_{0.01}$, (mm/h), exceeded for 0.01% of an average year, is thereby obtained from the 1 min integration rain rate data, and this is used for calculating the specific attenuation due to rain, γ_R, (dB/km); and if the predicted rainfall attenuation for any percentage of time is zero, the following steps will not be required.

Step 5: Obtain the specific attenuation, γ_R, (dB/km), using the frequency-dependent coefficients from [63].

$$\gamma_R = k(R_{0.01})^{\alpha} \tag{5.4}$$

Step 6: The horizontal path adjustment factor, $r_{0.01}$, for 0.01% of the time is also given as:

$$r_{0.01} = \frac{1}{1 + 0.78\sqrt{\frac{L_G \gamma_R}{f}} - 0.38(1 - e^{-2L_G})} \tag{5.5}$$

Step 7: Calculate the adjustment factor vertically, $v_{0.01}$,for 0.01% of time using:

$$v_{0.01} = \frac{1}{1 + \sqrt{\sin\theta}\left(31\left(1 - e^{-(\theta/(1+\chi))}\right)\frac{\sqrt{L_G \gamma_R}}{f^2} - 0.45\right)} \tag{5.6}$$

where

$$\zeta = \tan^{-1}\left(\frac{h_R - h_s}{L_G r_{0.01}}\right) \quad \text{degrees} \tag{5.7}$$

For $\zeta > \theta$,

$$L_R = \frac{L_G \, r_{0.01}}{\cos\theta} \quad \text{km} \tag{5.8}$$

Else,

$$L_R = \frac{h_R - h_s}{\sin\theta} \quad \text{km} \tag{5.9}$$

If $|\varphi| < 36^o$,

$$\chi = 36 - |\varphi| \quad \text{degrees} \tag{5.10}$$

Else,

$$\chi = 0 \quad \text{degrees} \tag{5.11}$$

Step 8: The effective path length, L_e (km), is given by:

$$L_e = L_R v_{0.01} \tag{5.12}$$

Step 9: The predicted attenuation exceeded for 0.01%, $A_{0.01}$ in dB, of an average year can also be obtained from:

$$A_{0.01} = L_e \gamma_R \tag{5.13}$$

Step 10: The estimated attenuation to be exceeded for other percentages of an average year, A_p, ranges from 0.001% to 5%, can be estimated from the attenuation to be exceeded for 0.01% for an average year by the expression:

$$A_p = A_{0.01} \left(\frac{p}{0.01}\right)^{-(0.655 + 0.033 \ln(p) - 0.045 \ln(A_{0.01}) - \beta(1-p)\sin\theta)} \tag{5.14}$$

where p is the percentage probability of interest, β for $p \geq 1\%$ is equal to zero and for $p < 1\%$ is given by:

If $p \geq 1\%$ or $|\varphi| \geq 36^o$, $\beta = 0$ (5.15)

If $p < 1\%$ and $|\varphi| < 36^o$ and $\theta \geq 25^o$, $\beta = -0.005(|\varphi| - 36)$ (5.16)

Otherwise, $\beta = -0.005(|\varphi| - 36) + 1.8 - 4.25 \sin\theta$ (5.17)

5.2.2 Prediction of Rain-Induced Attenuation over South Africa

In designing satellite communication link procedures, the estimation of rain-induced attenuation margin is essential. Raindrops can either scatter or absorb the propagated wave signal, which can cause degradation to the reliability and performance of the communication links [189].

Hence, it is compulsory to study the behaviour of rain heights when determining the rain attenuation exceeding the percentage of time levels (such as 0.1% and 0.01%) during uplink and downlink services. Since rain attenuation data obtained using measured rain height on satellite communication systems, especially at SHF and EHF bands are scarce in South Africa and other subtropical locations. Hence, this sub-section presents the prediction of rain-induced attenuation based on the results from rain height measurement carried out over four locations in South Africa. The cumulative distribution of rain-induced attenuation was estimated using the equations discussed in sub-section 5.2.1, along with the measured rain height in comparison with the rain height predicted by the ITU-R.

Also, as shown in Table 5.1, the model comprises of a large number of input parameters and all the required parameters listed in sub-section 5.2.1 were covered extensively in this thesis. Therefore, Figure 5.2 presents the rain-induced attenuation predicted for satellite communication systems over (a) Durban, (b) Cape Town, (c) Johannesburg, and (d) Kimberley. It could be generally observed that rain-induced attenuation increases as the frequency increases while the percentage of time decreases. This observation is in good agreement with the work done over some tropical regions such as [140, 141]. It can be seen from the figure that the rain-induced attenuation shows the same trend over the locations of study though with different values. For example, the rain-induced attenuation estimated values recorded at 12 GHz between the probability levels required for the design of multimedia applications and low-margin communication systems. At 0.1%, 0.01% and 0.001% of time, rain-induced attenuation of about 10.921,

19.922 and 24.450 dB/km was observed from the measured rain height, while about 10.621, 19.425, and 23.902 dB/km was estimated using ITU-R predicted value over Durban, respectively. At Cape Town, rain-induced attenuation about 11.069, 22.110, and 30.046 dB/km was estimated for measured rain height while about 10.044, 20.247 and 27.766 dB/km for ITU-R predicted value, respectively. Also, about 7.351, 14.179, and 18.440 for measured rain height while about 7.593, 14.601 and 18.931 dB/km for ITU-R predicted value over Johannesburg; and about 7.633, 15.017 and 19.976 dB/km rain-induced attenuation for measured rain height while about 7.462, 14.711 and 19.611 dB/km over Kimberley, respectively. Another significant observation in Figure 5.2 is that, the ITU-R predicted values underestimated the measured ZDIH over Durban, Cape Town, and Kimberley, while it overestimated in Johannesburg. It is concluded that there is disparity between measured and predicted (ITU-R) rain height values. For example, at 0.01% of time, there is a significant of more than 3 dB rain attenuation, which may be detrimental to propagation of the signal of any location. This implies the importance of measured ZDIH by providing accurate ZDIH observed across South Africa locations. The attenuation predicted at 0.001% percentage of time is the lowest and very crucial to communication and multimedia applications.

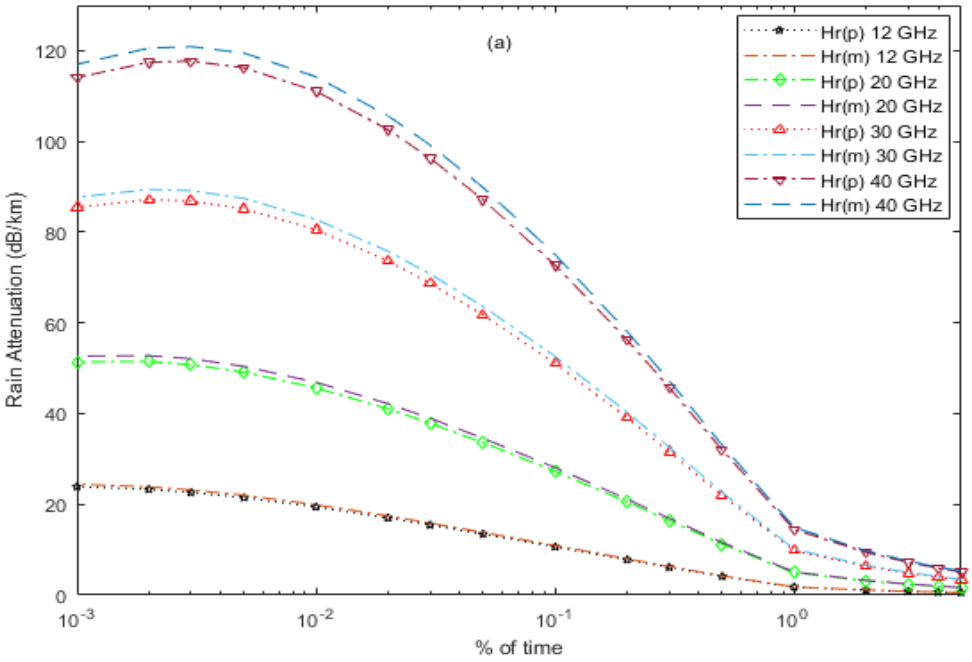

Figure 5.2(a) Rain-induced attenuation prediction (dB/km) over Durban

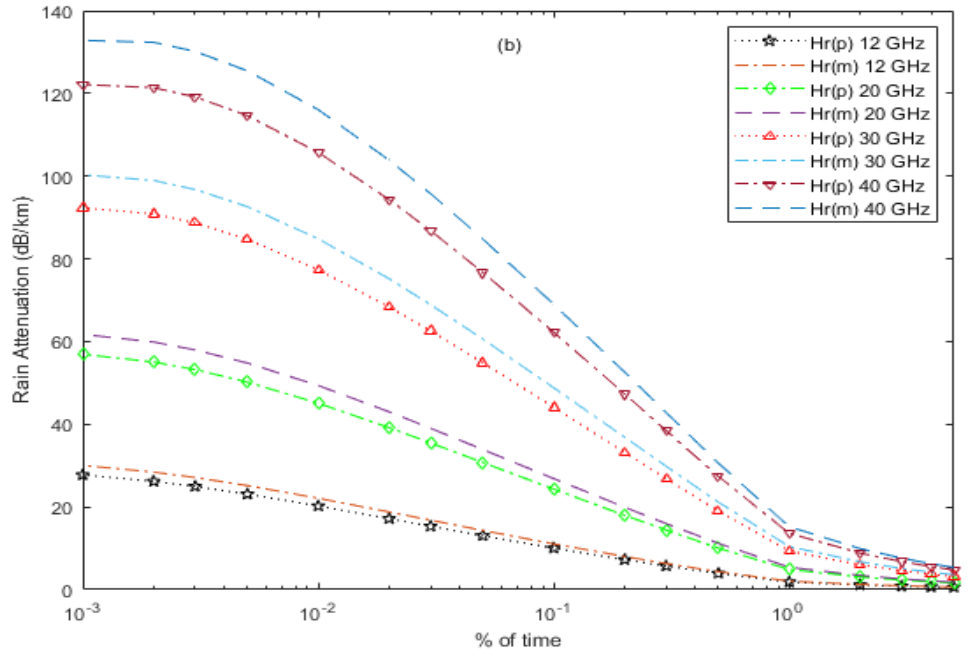

Figure 5.2(b) Rain-induced attenuation prediction (dB/km) over Cape Town

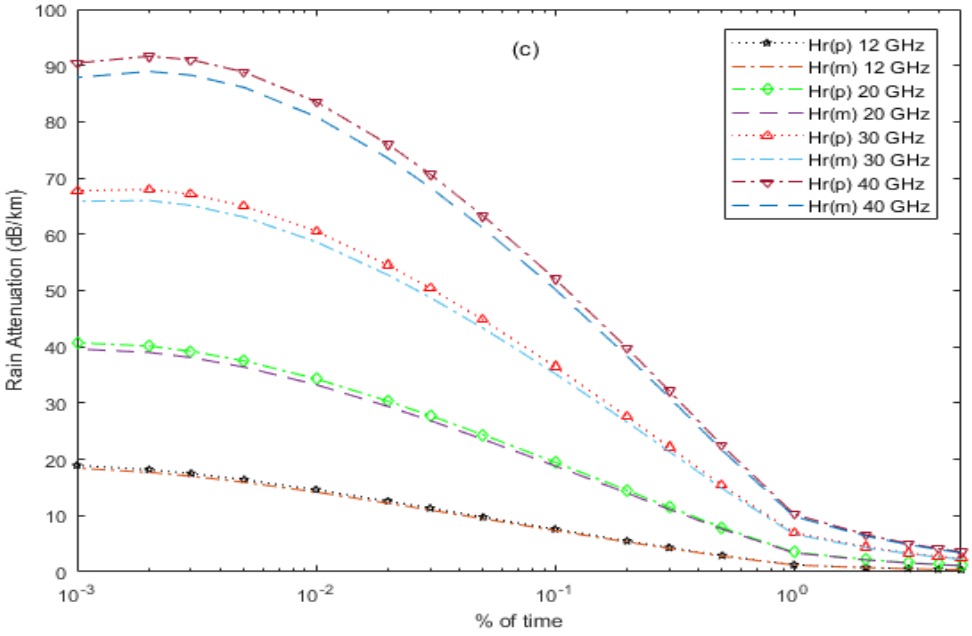

Figure 5.2(c) Rain-induced attenuation prediction (dB/km) over Johannesburg

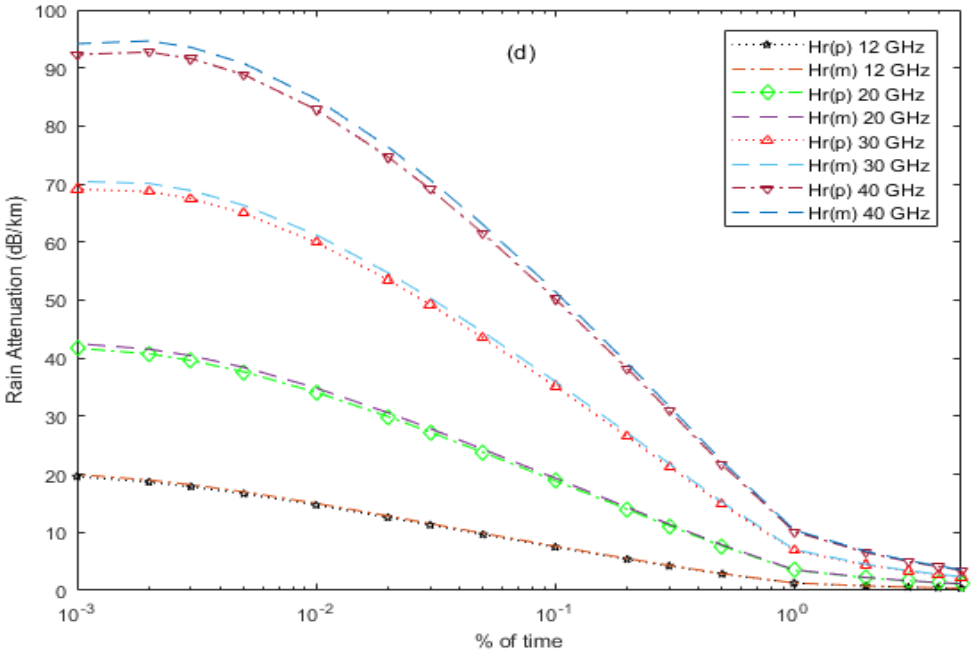

Figure 5.2(d) Rain-induced attenuation prediction (dB/km) over Kimberley.

5.3 Atmospheric Total Attenuation

For the efficient design and the optimum use of Earth-satellite links operating at higher frequencies (that is, above 10 GHz), an accurate attenuation estimation due to multiple sources occurring simultaneously (known as total attenuation) in the atmosphere must be considered, especially for the systems operating in the higher frequency bands. The total attenuation signifies the collective effect of gas, rain, clouds and scintillation. However, the techniques and the predictions for estimating attenuation due to these collective effects (attenuation due to gases, rain, cloudiness, and scintillation) has been studied extensively in this research. Hence, the study of the statistical attenuation combination and the prediction is important, because this effect is detrimental at aforementioned frequencies, especially for the low fade margin systems. The general method for predicting total attenuation can be given as [142]:

$$A_T(p) = A_{W+O}(p) + \sqrt{(A_R(p) + A_C(p))^2 + A_S(p)^2} \tag{5.18}$$

where p is the attenuation probability exceeded in the range between 50% and 0.001%, $A_R(p)$ is a fixed probability of rain attenuation (dB), $A_{W+O}(p)$ is the fixed probability of gaseous attenuation (that is, water vapour and oxygen), $A_C(p)$ is the fixed probability of cloud attenuation, and $A_S(p)$ is the fixed probability of tropospheric scintillation.

5.3.1 Estimation of Total Attenuation for South Africa

The effect of propagation impairments on satellite communication systems, especially in higher frequency bands (SHF and EHF) includes gaseous attenuation, rain attenuation, cloud attenuation, and tropospheric scintillation [29, 190]. These impairments are combined together to form the total (combined) attenuation. This phenomenon is important in the satellite systems design, and to obtain a total propagation attenuation estimation, this is made possible based on the climatology data banks of any location of interest, according to the predictive

models and ITU-R Recommendations [191] as presented in this section 5.3. In this research, the total attenuation studied is based on four selected locations in South Africa against the distance of the satellite radar up to about 200 m. The results presented here are based on the availability of the data measurement over the latitudinal locations selected.

Figure 5.3 presents the total attenuation prediction for 12, 20, 30, and 40 GHz over Durban, Cape Town, Johannesburg, and Kimberley respectively. It can be observed from Figure 5.3 that the total attenuation estimated over the selected locations follows the same pattern, although with different values of total attenuation at each of the selected locations over the frequencies considered. For example, the total attenuation at the propagation path of 180 m over Durban were about 0.761, 1.623, 2.755, 3.694 dB at 12, 20, 30, and 40 GHz respectively. At Cape Town, the total attenuation values were about 0.5995, 1.313, 2.272, and 3.112 dB at 12, 20, 30, and 40 GHz respectively. The trends continue in Johannesburg and Kimberley, although with different total attenuation values occurring at different frequencies. The variations observed in the total attenuation over the selected locations in South Africa may be due to the climatic parameters observed over each of the study locations.

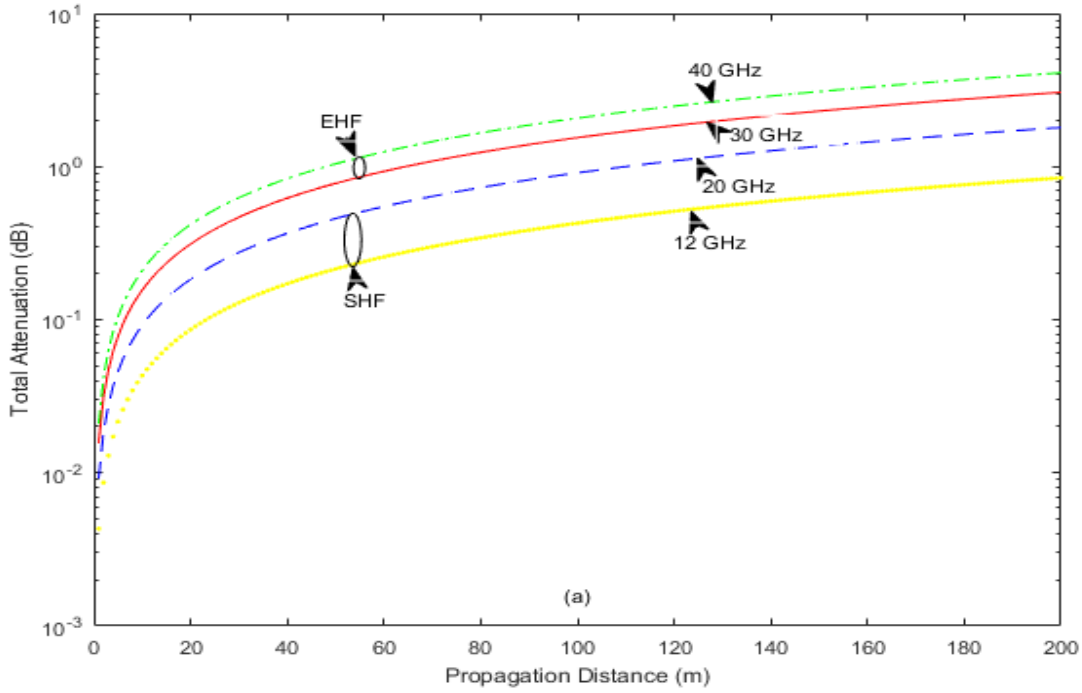

Figure 5.3(a) Total Attenuation Prediction (dB) over Durban

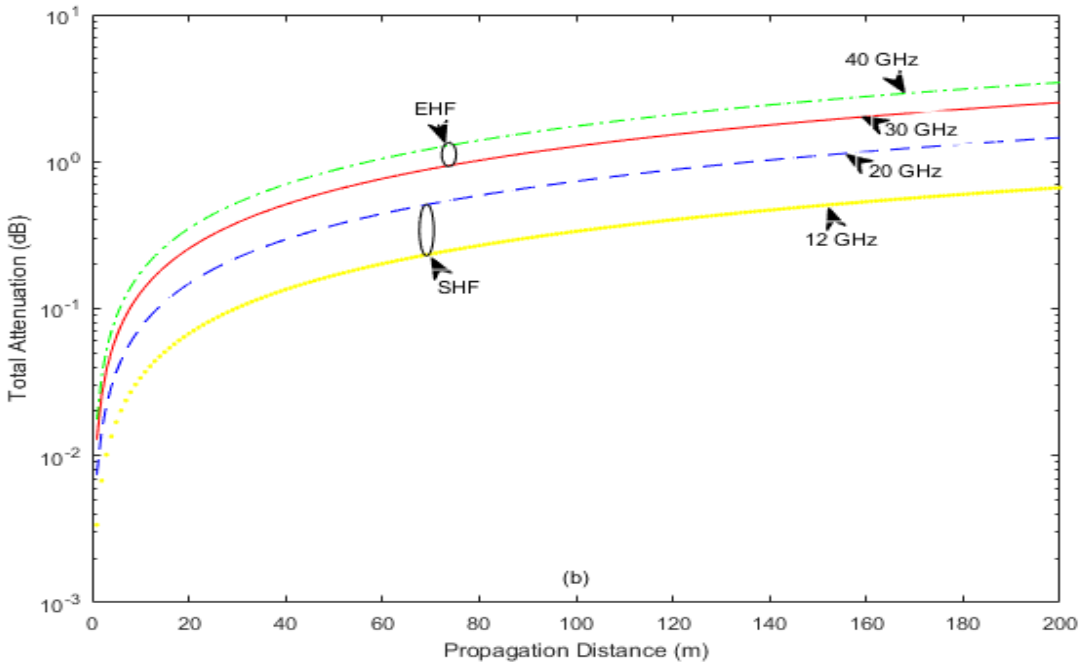

Figure 5.3(b) Total Attenuation Prediction (dB) over Cape Town.

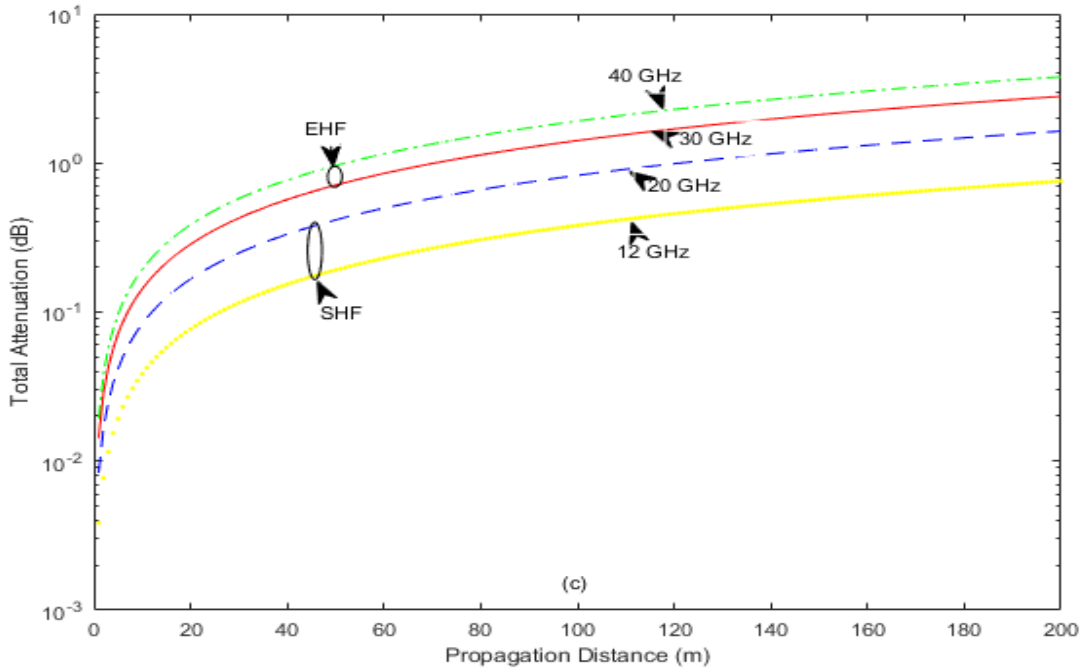

Figure 5.3(c) Total Attenuation Prediction (dB) over Johannesburg.

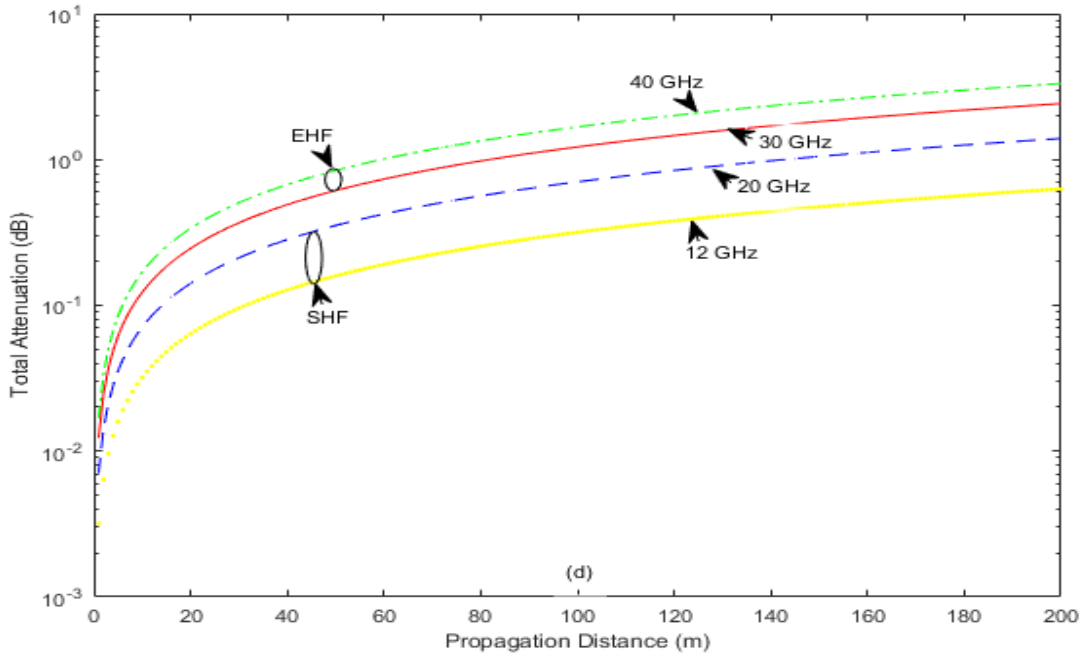

Figure 5.3(d) Total Attenuation Prediction (dB) over Kimberley.

5.4 Signal-to-Noise Ratio Estimation in EHF and SHF over South Africa

The communication system performance can be estimated based on the signal-to-noise ratio achieved at the receiver's end. The general term of the signal-to-noise ratio is the dimensionless ratio of the signal power of a system to the noise power contained in a receiver ends [192]. Also, the Signal-to-Noise Ratio (SNR) can be referred to the signal strength measurement of a satellite signal as a function of background noise and signal degradation [193]. Estimation of SNR is very crucial in satellite systems, in order to provide better QoS to the users. SNR is usually measured in decibels (dB). The following procedure can be used to estimate SNR [194]:

$$SNR = \frac{P_t G_t G_r}{KTBL_{sys}} \left(\frac{\lambda}{4\pi l}\right)^2 \tag{5.19}$$

where P_t is the transmitting power (W), $(\lambda/4\pi l)^2$ is free-space loss (dB), G_t and G_r are the transmitting and receiving antenna gain respectively, K is Boltzmann's constant which = 1.38×10^{-23} (J/K), B is bandwidth (Hz), L_{sys} is the system loss in ratio (unit less), l is the distance between the transmitting and receiving antennas (m), T is the system effective noise temperature (K), which is defined as:

$$T = T_A + T_R \tag{5.20}$$

where T_A is antenna noise temperature (external noise) and T_R is the receiver noise temperature (internal noise), both (K). Also, the parameter L_{sys} is related to the atmospheric loss and the total attenuation. The relationship between the carrier frequency (GHz) and the wavelength (m) is given as:

$$\lambda = \frac{0.3}{f} \tag{5.21}$$

Due to the fact that this research is based on satellite link systems, the following method is adopted for the satellite application.

$$EIRP = P_t G_t \tag{5.22}$$

$$\frac{G}{T} = \frac{G_r}{T_A + T_R} \tag{5.23}$$

where $EIRP$ is equivalent isotropic radiated power, while $\frac{G}{T}$ is the merit figure, let $L_F = \left(\frac{1}{4\pi l}\right)$. Therefore, (5.22) and (5.23) could be rewritten as:

$$SNR = \frac{EIRP(G/T)}{KL_F L_{sys} B} \tag{5.24}$$

The expression of SNR in dB from (5.24) could be written as follows:

$$SNR = EIRP + \frac{G}{T} - L_F - L_{sys} - B + 228.60 \tag{5.25}$$

5.4.1 Prediction of QoS based on SNR at SHF and EHF

Satellite communication systems required an immense value improvement in the quality of service over a location in higher frequencies such as SHF and EHF bands. Signal fidelity of SHF and EHF bands are being distorted by the effect of atmospheric properties such as rain, cloud, gas, and scintillation, which often resulted in the excessive error of digital transmission. Hence, a necessary measure is required to maintain the QoS for satellite communication customers by predicting the SNR, especially those that adaptively adjusts data rate, modulation, signal power and coding. Also, it is important to predict and identify the overall impact of all significant attenuating features on QoS and transmission characteristics along the satellite path of any location. Therefore, this sub-section presents the applications of the equations described in section 5.4 to predict the QoS at SHF and EHF in South Africa.

Figure 5.4 presents the prediction of QoS based on SNR at the higher frequency bands over 4 selected locations. It can be observed that SNR predicted the same trends over the location of study with the difference in values for each of the frequency observed. Also, SNR decreases as the percentage of time decreases and increases with increased frequency. In Figure 5.4a for Durban, SNR values decreases from about 169.40 to about 148.60 dB over the observed frequencies. At 12 GHz, SNR of about 165.098, 163.564, and 162.261 dB are observed at 0.1, 0.01, 0.001% respectively. The trends continue at 30 GHz and 40 GHz frequencies, although with different SNR values occurring at different time percentages. This percentage of times is a useful tool for satellite communication system designers to be able to scale the tropospheric attenuation due to these results. It will also assist in providing the approximated considerable view of total attenuation values that can be calculated over any location of interest in this region.

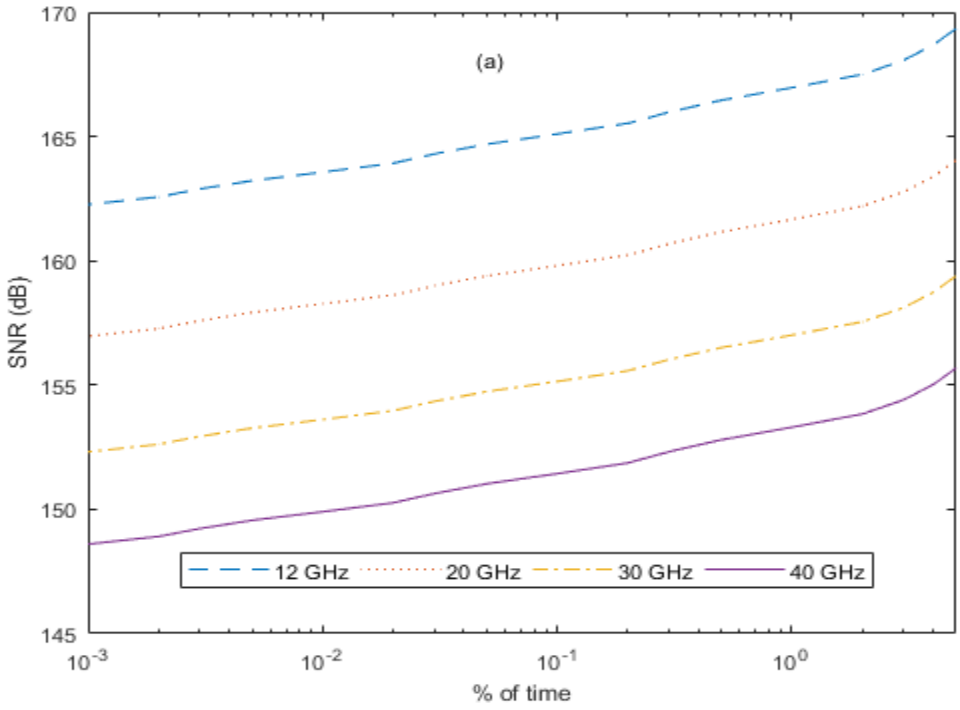

Figure 5.4(a) QoS prediction based on SNR over Durban

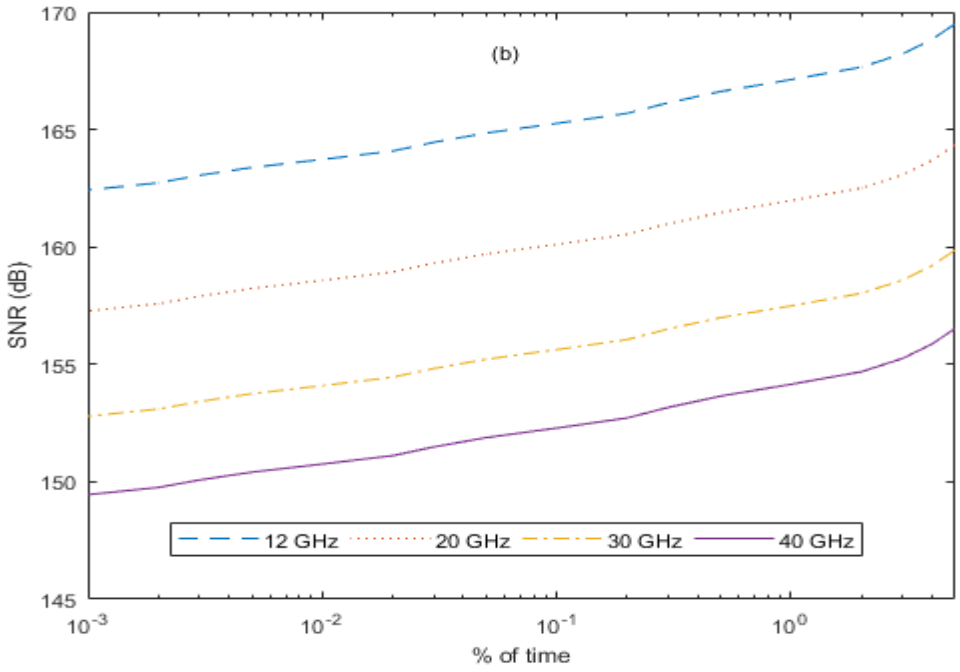

Figure 5.4(b) QoS prediction based on SNR over Cape Town

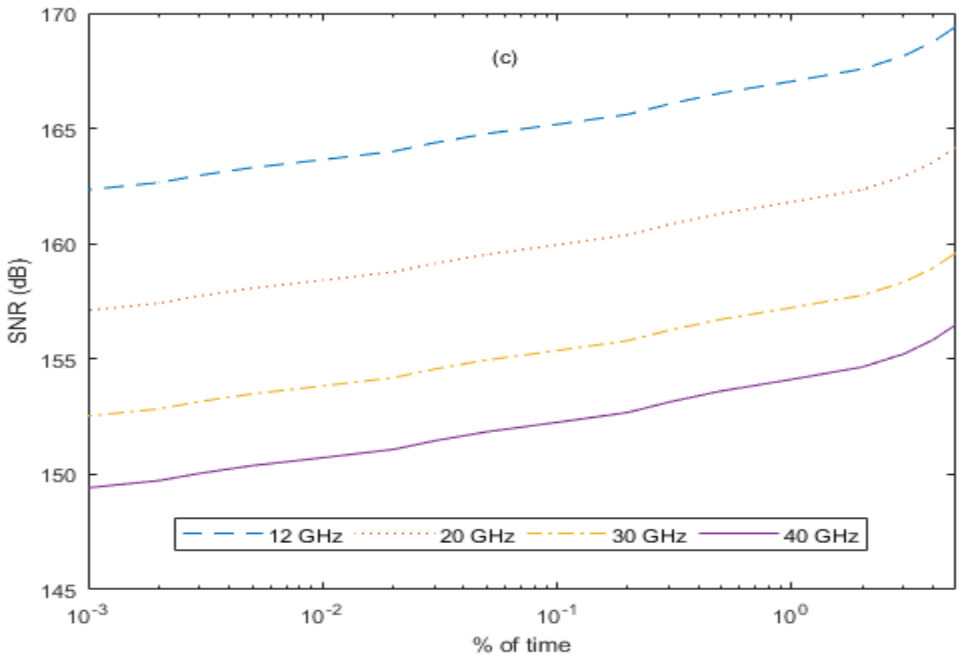

Figure 5.4(c) QoS prediction based on SNR over Johannesburg

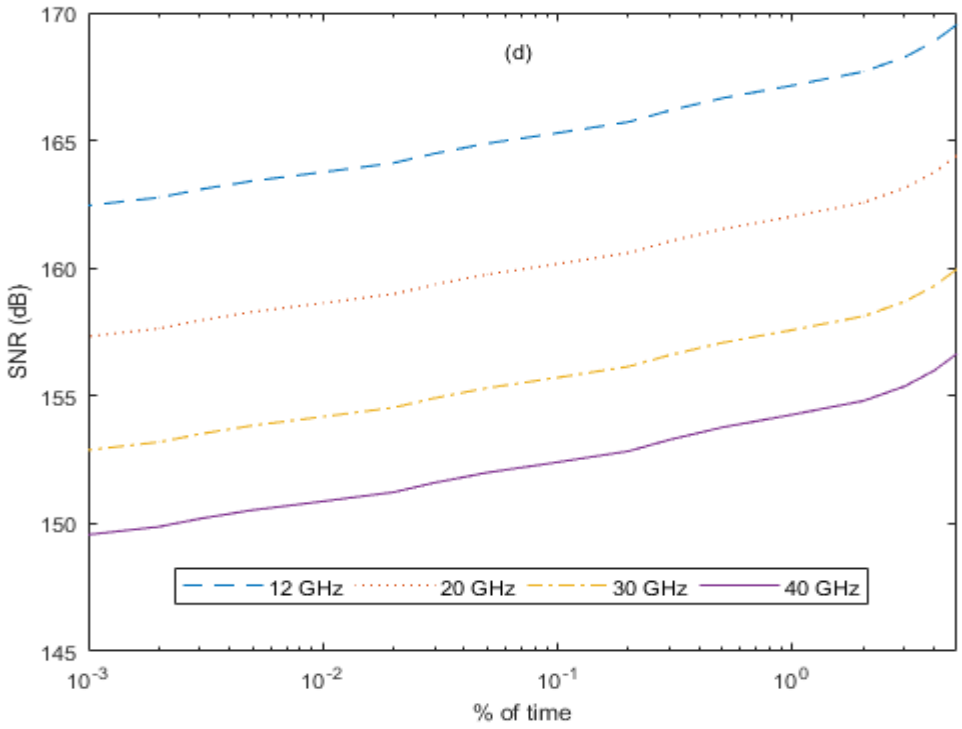

Figure 5.4(d) QoS prediction based on SNR over Kimberley.

5.5 Chapter Summary

In this chapter, the application of rain height for the prediction of rain attenuation is investigated over four selected locations among the study areas in South Africa. The application of rain height, then further tends towards the investigation of the total attenuation, which comprises of tropospheric parameters, that combined gases, rain, clouds and scintillation. Estimation of the performance of the communication systems based on the signal-to-noise ratio is used to cap the chapter.

The rain attenuation prediction based on measured rain height and the predicted values from the ITU-R shows the importance of using local rain height measurement in the designing and development of satellite communication systems. For example, at 0.01% of time there is significant of more than 3 dB when compared rain attenuation obtained using measured rain height and those

obtained using the predicted values from ITU-R. An excess of > 3 dB may be detrimental to signal propagation of any location of interest. It is therefore recommended that the rain height physical information should be obtained from any local database of interest will improve the accuracy of the rain attenuation prediction over a desired location. Also, the total attenuation prediction implies that the collective effect of tropospheric parameters is crucial in effective designing and development of the optimum used of Earth-satellite systems.

CHAPTER SIX

Conclusion and Recommendations

6.1 Introduction

Satellite communication systems and applications continue to be relevant in the newer technologies as well as new ones. The new technologies are achievable at higher frequency bands such as SHF and EHF bands, because they can deliver excellent services to end-users. However, higher frequency bands are susceptible to signal degradation due to atmospheric influences, hence adequate prediction is required to avoid either over- or under-prediction of the propagation effect which can result in the expensive or unreliable design of a communication system in any desired location.

6.2 Conclusions

This section hereby discusses the conclusions drawn from chapter three, four and five from this work.

6.2.1 Chapter Three – Review, Measurement and Modeling of Rain Height

In chapter three, the global review of rain height was presented, where it was shown that rain height varies from one location to another. Rain height is significance in several applications and also very crucial in satellite communication systems applications. The description of rain height distribution based on the measurement of ZDIH across South Africa (a subtropical region) has shown an increasing trend over South Africa over the year of observation. The trend has been linked to global warming experienced over the region. Strong variation of ZDIH distributions in the monthly and seasonal basis was also observed. Contour maps developed were to meet the recent challenges in the rapid growth of the satellite communication systems [136, 195], the results show that average ZDIH ranges from 4.305 km to 5.105 km, as it also increased steadily, with about 0.05 km from southern towards the northern part and about

0.005 km from northern towards southern for ITU-R Rec. P.839-2 and ITU-R Rec. P.839-4 model respectively. Based on the integration of time, ZDIH varies from about 4.385 to 4.485 and 4.52 to 4.70 km for 0.1 and 0.01% of time respectively. Lastly, the rain height modeling based on the ZDIH measurement that was carried out in this chapter, in order to understand the characteristics of the ZDIH pattern over Southern Africa region. Therefore, the cumulative distribution of ZDIH is fitted with the three-parameter Dagum and Log-logistic model. The parameters of the models were estimated using maximum likelihood estimation (MLE) method over the selected locations, it was observed that both models employed, give a proper description of the ZDIH distribution over the locations and shows a wider variation of distribution based on the MLE parameters (shape, scale, and location parameters). Also, the efficiency of the models in this work was optimized by bias error, root means square error and K-S test, which shows that both models were good. The performance analysis based on degree of errors shows that Dagum technique performs better over two locations of study, and log-logistics also perform better over the other 2 locations of study in the four locations of study considered in South Africa.

6.2.2 Chapter Four – Tropospheric Attenuation Modeling

The purpose of this chapter is to investigate the tropospheric attenuation (that is, attenuation due to gases, cloudiness, and scintillation). Results obtained from the predictions show that gaseous attenuation increase for frequencies above 20 GHz. This may be due to the effect of water and dry air on signals at the frequency of about 20, 55 or 60 GHz, where atmospheric constituents reached its individual points of resonance and the absorption effects also became high. Cloud attenuation shows an increase as frequency increases over the observed locations. The predicted scintillation (enhancement and fading) increases as the percentage of time decreases, which may be due to the formation of convective rain type and liquid water content along the satellite propagation paths. These imply that the parameters produced by troposphere have their significant effect

on satellite communication systems which requires proper measurements to determine the accuracy of the effects.

6.2.3 Chapter Five – Adaptation of Rain Height in Attenuation Estimation

Due to the adverse effects of rainfall and the fact that it contributes the highest impairment to the QoS in the application of satellite communication systems. The application of measured rain height is studied in this chapter as an important factor of rain attenuation prediction, which was also combined with several other tropospheric parameters to predict the combined (total) attenuation and therefore used to estimate the performance of the communication systems based on signal to noise ratio along the satellite communication paths. The observed rain-induced attenuation increases as the frequencies increase with a decrease in the percentage of time. Comparison with the established ITU-R values show the difference of about 3 dB, which can be higher as the frequency increases. The implication of this is that local data measurement is essential in improving the accuracy of rain attenuation prediction which are useful in low margin communication systems. The total attenuation predicted which comprises of several attenuations produced by the atmosphere, that is, rain attenuation, gaseous attenuation, cloud attenuation and tropospheric scintillations over the locations of observation shows the same trend though with different values and increases as the frequencies increase together with the increase in propagation paths. Finally, in the chapter, the quality of service based on the signal to noise ratio prediction shows the same trend as well (with different values) and decreases as the percentage of time decreases with increase in frequency.

6.3 Recommendations for Future Work

6.3.1 Measurement Campaign

There is a need for proper estimation of rain height, which requires a suitable equipment that will be capable of measuring real-time and spatial rain height events at optimal resolutions. In this thesis, the work done has been restricted to

measurements using satellite radar (that is, TRMM-PR). For this region is just receiving the attention of rain height measurement, which is very crucial to the development of satellite communication over the region, more investigations can still be done on melting layer over this region using TRMM-PR, such as freezing height level (ZDIH), bright-band height, bright-band intensity, bright-band width, bright-band boundary, rain types, among others. Also, more information on water phase gained through this can be used to investigate the precipitation process, in order to improve other measurement methods, there is a need to use some other equipment for this study over the subtropical region to provide more knowledge on the melting layer, such as other satellite radar, radiosonde, or weather radar. In addition, simultaneous attenuation measurement is necessary to validate the predictions presented in this thesis

6.3.2 Modeling and Simulation

There is a need to further extend the work done over this region (subtropical region) by studying the possibility of modeling rain height distribution, with the use of several estimator techniques with other statistical distribution methods, the method of moments, and kernel estimator. Modeling rain height and their parameters of distributions over a location together with any time series could be used to generate data which can have the same characteristics as the actual data over the region in the future.

6.3.3 Applications

Based on the outcomes obtained from this research, the results can as well be extended to cover several research topics such as the following:

- Evaluation of rain height distribution using different estimator methods over Southern Africa;
- Parameterization of rain height or melting layer for communication satellite systems;

- Comparison of rain height measurement using different equipment such as satellite radar, radiosonde or micro rain radar;
- Measurement of rain rate using satellite radar for comparison with other measurements from ground equipment;
- Development of different methods to mitigate against signal loss due to tropospheric parameters at higher frequencies; and
- Information of melting layer in subtropical regions for terrestrial and satellite communications applications.

REFERENCES

[1] R. M. Frieden and R. Frieden, *Managing Internet-driven change in international telecommunications*. Artech House, 2001.

[2] J. Ojo and P. Owolawi, "Estimation of Effective Transmission Loss Due to Subtropical Hydrometeor Scatters using a 3D Rain Cell Model for Centimeter and Millimeter Wave Applications," *Journal of Infrared, Millimeter, and Terahertz Waves,* vol. 35, no. 12, pp. 1068-1082, 2014.

[3] J. N. Pelton, *Future trends in satellite communications: Markets and Services*. Intl. Engineering Consortiu, 2005.

[4] J. N. Pelton, S. Madry, and S. Camacho-Lara, *Handbook of satellite applications*. Springer Publishing Company, Incorporated, 2017.

[5] Y. H. Lee and S. Winkler, "Effects of rain attenuation on satellite video transmission," in *IEEE 73rd Vehicular Technology Conference (VTC Spring)*, 2011, pp. 1-5: Citeseer.

[6] J. S. Ojo, O. L. Ojo, and C. I. Joseph-Ojo, "Rain height information from TRMM precipitation radar and micro rain radar for radio communication studies in Nigeria," in *IEEE 6th International Conference on Adaptive Science & Technology (ICAST)*, 2014, pp. 1-5: IEEE.

[7] R. K. Crane, *Propagation handbook for wireless communication system design*. CRC press, 2003.

[8] M. P. Hall, L. W. Barclay, and M. T. Hewitt, "Propagation of radiowaves," in *Propagation of Radiowaves*, 1996.

[9] I. A. Adimula, "Rainfall parameters in Ilorin and their application to microwave radio propagation," Ph.D Thesis, University of Ilorin, Nigeria, 1997.

[10] G. Macchiarella, "A comparative analysis of some prediction methods for rain attenuation statistics in Earth-to-space links," *Radio Science,* vol. 20, no. 1, pp. 35-49, 1985.

[11] R. L. Freeman, *Radio system design for telecommunications*. John Wiley & Sons, 2006.

[12] W. Asen and T. Tjelta, "A novel method for predicting site dependent specific rain attenuation of millimeter radio waves," *IEEE Transactions on Antennas and Propagation,* vol. 51, no. 10, pp. 2987-2999, 2003.

[13] F. Moupfouma, "Improvement of a rain attenuation prediction method for terrestrial microwave links," *IEEE Transactions on Antennas and Propagation,* vol. 32, no. 12, pp. 1368-1372, 1984.

[14] G. O. Ajayi, S. Feng, S. M. Radicella, and B. M. Reddy, *Handbook on radio propagation related to satellite communications in tropical and subtropical countries*. Trieste, Italy: International Centre for Theoretical Physics, 1996.

[15] F. Moupfouma and J. Tiffon, "Raindrop size distribution from microwave scattering measurements in equatorial and tropical climates," *Electronics Letters,* vol. 18, no. 23, pp. 1012-1014, 1982.

[16] W. Myers, "Comparison of propagation models," *IEEE Broadband Wireless Access Working Group P.802,* vol. 16, 1999.

[17] E. O. Olurotimi, O. Sokoya, J. S. Ojo, and P. A. Owolawi, "Modeling freezing height level for satellite link communication: Durban, South Africa," in *IEEE AFRICON*, 2017, pp. 342-347.
[18] J. S. Mandeep, "Rain height statistics for satellite communication in Malaysia," *Journal of Atmospheric and Solar-Terrestrial Physics,* vol. 70, no. 13, pp. 1617-1620, 2008.
[19] J. S. Ojo, "Rain height statistics based on 0°C isotherm height using TRMM precipitation data for Earth-space satellite links in Nigeria," *International Scholarly Research Notices Atmospheric Sciences,* vol. 2014, 2014.
[20] H. E. Green, "Propagation impairment on Ka-band SATCOM links in tropical and equatorial regions," *IEEE Antennas and Propagation Magazine,* vol. 46, no. 2, pp. 31-45, 2004.
[21] ITU-R Recommendation P.837-6, "Characteristics of precipitation for propagation modelling," *International Telecommunication Union, Geneva, Switzerland,* 2012.
[22] K. Harb, "Quality of service improvements in weather impacted satellite communication networks," Carleton University Ottawa, 2010.
[23] ITU-R Recommendation V.431, "Nomenclature of the frequency and wavelength bands used in telecommunications," *International Telecommunication Union, Geneva, Switzerland,* vol. 8, 2015.
[24] U. Fiebig and C. Riva, "Impact of seasonal and diurnal variations on satellite system design in V-band," *IEEE Transactions on Antennas and Propagation,* vol. 52, no. 4, pp. 923-932, 2004.
[25] R. L. Olsen, "Worldwide techniques for predicting the multipath fading distribution on terrestrial LOS links: background and results of tests," *IEEE Transactions on Antennas and Propagation,* vol. 47, no. 1, pp. 157-170, 01 1999.
[26] S. Ventouras and C. L. Wrench, "ITU-R total attenuation predictions in comparison with slant path measurements in southern England," *Electronics Letters,* vol. 38, no. 18, pp. 1058-1059, 2002.
[27] S.-C. Wu, "The Impact of Combined Rain Attenuation and Tropospheric Scintillation on the Satellite Communication System," *Electrical Engineering,* 1998.
[28] T. Tjelta and D. Bacon, "Predicting Combined Rain and Wet Snow Attenuation on Terrestrial Links," *IEEE Transactions on Antennas and Propagation,* vol. 54, no. 5, pp. 1677-1682, 2010.
[29] A. Dissanayake, J. Allnutt, and F. Haidara, "A prediction model that combines rain attenuation and other propagation impairments along Earth-satellite paths," *IEEE Transactions on Antennas and Propagation,* vol. 45, no. 10, pp. 1546-1558, 1997.
[30] V. J. Schaefer, J. A. Day, and J. Pasachoff, *A field guide to the atmosphere*. Houghton Mifflin Harcourt, 1998.
[31] NASA/Goddard. (2017). *Earth's Atmospheric Layers*. Available: www.nasa.gov/mission_pages/sunearth/science/atmosphere-layers2.html
[32] E. J. Tarbuck and F. K. Lutgens, "Earth Science," ed: Merrill Publishing Co. Columbus, OH, 1982.
[33] V. E. Derr, "Remote sensing of the troposphere," *National Oceanic and Atmospheric* 1972.
[34] M. Lynch, "Aphanizomenon blooms: Alternate control and cultivation by Daphnia pulex," in *Am. Soc. Limnol. Oceanogr. Spec. Symp*, 1980, vol. 3, pp. 299-304.

[35] M. P. M. Hall, L. W. Barclay, and M. T. Hewitt, "Propagation of radiowaves," 1996: The Institute of Electrical Engineers Press.
[36] S. K. Sarkar, N. C. Mondal, A. B. Bhattacharya, and R. Bhattacharya, "Some studies on attenuation and atmospheric water vapour measurements in India," *International Journal of Remote Sensing,* vol. 19, no. 3, pp. 473-480, 1998.
[37] H. E. Bussey, "Microwave attenuation statistics estimated from rainfall and water vapor statistics," *Proceedings of the IRE,* vol. 38, no. 7, pp. 781-785, 1950.
[38] J. M. Wallace and P. V. Hobbs, *Atmospheric science: an introductory survey*. Elsevier, 2006.
[39] S. D. Ilcev, *Global Mobile Satellite Communications: For Maritime, Land and Aeronautical Applications*. Springer Science & Business Media, 2005.
[40] L. J. Ippolito, *Radiowave propagation in satellite communications*, 1st ed. New York: Van Nostrand Reinhold Company, 1986.
[41] J. E. Allnutt, "Satellite-to-ground radiowave propagation-Theory, practice and system impact at frequencies above 1 GHz," *IEE Electromagnetic Waves Series Stevenage Herts England Peter Peregrinus Ltd.,* vol. 29, 1989.
[42] L. J. Ippolito and L. J. Ippolito Jr, *Satellite communications systems engineering: atmospheric effects, satellite link design and system performance*. John Wiley & Sons, 2017.
[43] D. C. Hogg, "Millimeter-wave communication through the atmosphere," *Science,* vol. 159, no. 3810, pp. 39-46, 1968.
[44] F. C. Medeiros Filho, R. S. Cole, and A. D. Sarma, "Millimetre-wave rain induced attenuation: theory and experiment," in *IEE Proceedings H (Microwaves, Antennas and Propagation)*, 1986, vol. 133, no. 4, pp. 308-314: IET.
[45] D. Cermak, O. Fiser, and V. Schejbal, "Electromagnetic scattering by rain drops," in *Cost*, 2005, p. 280.
[46] R. K. Crane, *Electromagnetic wave propagation through rain*. Wiley-Interscience, 1996.
[47] C. F. Bohren and D. R. Huffman, *Absorption and scattering of light by small particles*. John Wiley & Sons, 2008.
[48] M. N. O. Sadiku, *Elements of electromagnetics*. Oxford University Press, 2014.
[49] L. J. Ippolito Jr, *Satellite communications systems engineering: atmospheric effects, satellite link design and system performance*. John Wiley & Sons, 2008.
[50] H. Sizun and P. de Fornel, *Radio wave propagation for telecommunication applications*. Springer, 2005.
[51] T. Pratt, W. C. Bostian, and J. E. Allnutt, "Satellite communication," *John Wiley and Sons, NJ,* 2003.
[52] ITU-R Reccommendation P.453-11, "The radio refractive index: its formula and refractivity data," *International Telecommunication Union, Geneva, Switzerland,* 2015.
[53] C. E. Mayer, B. E. Jaeger, R. K. Crane, and X. Wang, "Ka-band scintillations: Measurements and model predictions," *Proceedings of the IEEE,* vol. 85, no. 6, pp. 936-945, 1997.
[54] M. Marcus and B. Pattan, "Millimeter wave propagation: spectrum management implications," *IEEE Microwave Magazine,* vol. 6, no. 2, pp. 54-62, 2005.
[55] ITU-R Recommendation P.676-11, "Attenuation by atmospheric gases," *International Telecommunication Union, Geneva, Switzerland,* 2016.

[56] H. J. Liebe, "An atmospheric millimeter wave propagation model," *Natl. Telecommun. and Inform. Admin., Boulder, Colo,* pp. 83-137, 1983.

[57] R. K. Crane, *Propagation handbook for wireless communication system design*. CRC press, 2014.

[58] ITU-R Recommendation P.840-6, "Attenuation due to clouds and fog," *International Telecommunication Union, Geneva, Switzerland,* 2013.

[59] H. J. Liebe, G. A. Hufford, and M. G. Cotton, "Propagation modeling of moist air and suspended water/ice particles at frequencies below 1000 GHz," in *In AGARD, Atmospheric Propagation Effects Through Natural and Man-Made Obscurants for Visible to MM-Wave Radiation*, 1993.

[60] E. Salonen *et al.*, "Study of propagation phenomena for low availabilities," *ESA/ESTEE/Final Report,* 1990.

[61] R. L. Olsen, D. V. Rogers, and D. B. Hodge, "The aR^b relation in the calculation of rain attenuation," *IEEE Transactions on Antennas and Propagation,* vol. 26, no. 2, pp. 318-329, 1978.

[62] W. Zhang and N. Moayeri, "Power-law parameters of rain specific attenuation," *Broadband Wireless Access Working Group,* vol. 16, 1999.

[63] ITU-R Recommendation P.838-3, "Specific attenuation model for rain for use in prediction methods," *International Telecommunication Union, Geneva, Switzerland,* 2005.

[64] J. O. Laws and D. A. Parsons, "The relation of raindrop-size to intensity," *EOS, Transactions American Geophysical Union,* vol. 24, no. 2, pp. 452-460, 1943.

[65] R. Gunn and G. D. Kinzer, "The terminal velocity of fall for water droplets in stagnant air," *Journal of Meteorology,* vol. 6, no. 4, pp. 243-248, 1949.

[66] P. S. Ray, "Broadband complex refractive indices of ice and water," *Applied optics,* vol. 11, no. 8, pp. 1836-1844, 1972.

[67] E. Matricciani and A. Pawlina, "Statistical Characterization of Rainfall Structure and Occurence for Convective and Stratiform Rain Inferred from Long Term Point Rain Rate Data," in *AP2000 Millenium Conference on Antennas and Propagation*, 2000, pp. 1-8.

[68] F. Moupfouma, "More about rainfall rates and their prediction for radio systems engineering," in *IEEE Proceedings H (Microwaves, Antennas and Propagation)*, 1987, vol. 134, no. 6, pp. 527-537: IET.

[69] R. A. Houze Jr, "Stratiform precipitation in regions of convection: A meteorological paradox," *Bulletin of the American Meteorological Society,* vol. 78, no. 10, pp. 2179-2196, 1997.

[70] A. Tokay, D. A. Short, C. R. Williams, W. L. Ecklund, and K. S. Gage, "Tropical rainfall associated with convective and stratiform clouds: Intercomparison of disdrometer and profiler measurements," *Journal of Applied Meteorology,* vol. 38, no. 3, pp. 302-320, 1999.

[71] S. Mandeep and J. E. Allnutt, "Rain attenuation predictions at Ku-band in South East Asia countries," *Progress In Electromagnetics Research,* vol. 76, pp. 65-74, 2007.

[72] A. Tokay and D. A. Short, "Evidence from tropical raindrop spectra of the origin of rain from stratiform versus convective clouds," *Journal of Applied Meteorology,* vol. 35, no. 3, pp. 355-371, 1996.

[73] R. A. Houze Jr, *Cloud dynamics*. Academic Press, 2014.

[74] D. Atlas, C. W. Ulbrich, F. D. Marks, E. Amitai, and C. R. Williams, "Systematic variation of drop size and radar-rainfall relations," *Journal of Geophysical Research: Atmospheres,* vol. 104, no. D6, pp. 6155-6169, 1999.

[75] P. A. Barclay, "Raindrop-size distributions in the Melbourne area," *Institute of Engineering, Armidale, New South Wales, Australia,* 1975.

[76] D. J. Fang and C. H. Chen, "Propagation of centimeter/millimeter waves along a slant path through precipitation," *Radio Science,* vol. 17, no. 5, pp. 989-1005, 1982.

[77] E. A. Mueller and A. L. Sims, "Investigation of the quantitative determination of point and areal precipitation by radar echo measurements," Illinois State Water Survey Div. Urbana 1966.

[78] J. A. Ruffner and F. E. Bair, *The weather almanac: a reference guide to weather, climate, and air quality in the United States and its key cities, comprising statistics, principles, and terminology*. Gale Research Co., 1981.

[79] I. A. Adimula and G. O. Ajayi, "Variations in raindrop size distribution and specific attenuation due to rain in Nigeria," in *Annales des télécommunications*, 1996, vol. 51, no. 1-2, pp. 87-93: Springer.

[80] J. Joss, "The variation of raindrop size distributions at Locarno," in *Proc. Int. Conf. Cloud Physics*, Toronto, Canada, 1968, pp. 369-373.

[81] T. J. O. Afullo, "Raindrop size distribution modeling for radio link design along the eastern coast of South Africa," *Progress In Electromagnetics Research B,* vol. 34, pp. 345-366, 2011.

[82] A. A. Alonge and T. J. O. Afullo, "Seasonal analysis and prediction of rainfall effects in Eastern South Africa at microwave frequencies," *Progress in Electromagnetics Research B,* vol. 40, pp. 279-303, 2012.

[83] AMS Glossary, "Rainfall Rate," *Glossary of Meteorology, 2nd Edition, Allen, America Meteorological Society, Boston, MA, USA,* 2007.

[84] E. O. Olurotimi, O. Sokoya, J. S. Ojo, and P. A. Owolawi, "Observation of bright-band height data from TRMM-PR for satellite communication in South Africa," *Journal of Atmospheric and Solar-Terrestrial Physics,* vol. 160, pp. 24-33, 2017.

[85] M. S. Pontes, L. A. R. da Silva Mello, and R. S. L. Souza, "Statistical behaviour of the effective rain height in the tropics," in *IET Ninth International Conference on Antennas and Propagation*, 1995, vol. 2, pp. 119-122.

[86] AMS Glossary of Metereology, "Drop-size distribution," *Glossary of Meteorology, Allen, America Meteorological Society, Boston, MA, USA*. 2012.

[87] Wikipedia. (2018). *Tropics*. Available: https://en.wikipedia.org/wiki/Tropics

[88] South Africa weather and climate. Available: http://www.sa-venues.com/no/weather.html

[89] J. S. Ojo and P. A. Owolawi, "Development of one-minute rain-rate and rain-attenuation contour maps for satellite propagation system planning in a subtropical country: South Africa," *Advances in Space Research,* vol. 54, no. 8, pp. 1487-1501, 2014.

[90] Y. Karasawa and T. Matsudo, "One-minute rain rate distributions in Japan derived from AMeDAS one-hour rain rate data," *IEEE Transactions on Geoscience and Remote Sensing,* vol. 29, no. 6, pp. 890-898, 1991.

[91] F. Moupfouma and L. Martin, "Modelling of the rainfall rate cumulative distribution for the design of satellite and terrestrial communication systems," *International Journal of Satellite Communications,* vol. 13, no. 2, pp. 105-115, 1995.
[92] J. Chebil and T. A. Rahman, "Development of 1 min rain rate contour maps for microwave applications in Malaysian Peninsula," *Electronics Letters,* vol. 35, no. 20, pp. 1772-1774, 1999.
[93] C. Ito and Y. Hosoya, "Proposal of a global conversion method for different integration time rain rates by using M distribution and regional climatic parameters," *Electronics and Communications in Japan (Part I: Communications),* vol. 89, no. 4, pp. 1-9, 2006.
[94] P. Rice and N. Holmberg, "Cumulative time statistics of surface-point rainfall rates," *IEEE Transactions on Communications,* vol. 21, no. 10, pp. 1131-1136, 1973.
[95] M. O. Fashuyi, P. A. Owolawi, and T. J. Afullo, "Rainfall rate modelling for LoS radio systems in South Africa," *Trans. of South African Inst. of Elect. Engineers (SAIEE),* vol. 97, pp. 74-81, 2006.
[96] M. O. Fashuyi, "A study of rain attenuation on terrestrial paths at millimetric wavelengths in South Africa," MSc Thesis, School of Electrical, Electronic and Computer Engineering, University of KwaZulu-Natal, South Africa, 2006.
[97] M. O. Odedina and T. J. Afullo, "Characteristics of seasonal attenuation and fading for line-of-sight links in South Africa," in *Proc. of SATNAC*, 2008, pp. 203-208.
[98] M. O. Odedina and T. J. O. Afullo, "Rain attenuation prediction along terrestrial paths in South africa using existing attenuation models," in *IEEE AFRICON 2007*, 2007, pp. 1-7.
[99] P. A. Owolawi, "Derivation of one-minute rain rate from five-minute equivalent for the calculation of rain attenuation in South Africa," *PIERS Online,* vol. 7, no. 6, pp. 524-535, 2011.
[100] P. A. Owolawi and T. J. Afullo, "Rainfall rate modeling and worst month statistics for millimetric line-of-sight radio links in South Africa," *Radio Science,* vol. 42, no. 6, 2007.
[101] P. A. Owolawi, T. J. O. Afullo, and S. B. Malinga, "Rainfall rate characteristics for the design of terrestrial link in South Africa," in *Proc. of SATNAC*, 2008, pp. 71-76.
[102] South Africa Weather Services. Available: http://www.weathersa.co.za/
[103] T. T. Wilheit, "Some comments on passive microwave measurement of rain," *Bulletin of the American Meteorological Society,* vol. 67, no. 10, pp. 1226-1232, 1986.
[104] J. R. Tesmer and T. T. Wilheit, "An improved microwave radiative transfer model for tropical oceanic precipitation," *Journal of the atmospheric sciences,* vol. 55, no. 9, pp. 1674-1689, 1998.
[105] T. T. Wilheit, "TRMM microwave radiometer algorithms," in *Geoscience and Remote Sensing Symposium, 1993. IGARSS '93. Better Understanding of Earth Environment., International*, 1993, p. 422 vol.2.
[106] TRMM Precipitation Radar Team, "Tropical rainfall measuring mission (TRMM) precipitation radar algorithm instruction manual for version 7," *Japan Aerospace Exploration Agency and NASA,* 2011.
[107] T. Kawanishi *et al.*, "TRMM precipitation radar," *Advances in Space Research,* vol. 25, no. 5, pp. 969-972, 2000.
[108] T. Kozu *et al.*, "Development of precipitation radar onboard the Tropical Rainfall Measuring Mission (TRMM) satellite," *IEEE Transactions on Geoscience and Remote Sensing,* vol. 39, no. 1, pp. 102-116, 2001.

[109] M. Aris, N. Azlan, and J. Din, "Rain height statistics from spaceborne radar for satellite communication in Malaysia," *Jurnal Teknologi (Sciences & Engineering),* vol. 58, no. 1, pp. 1-5, 2012.
[110] Q. Cao *et al.*, "Statistical and physical analysis of the vertical structure of precipitation in the mountainous west region of the united states using 11+ years of spaceborne observations from TRMM precipitation radar," *Journal of Applied Meteorology and Climatology,* vol. 52, no. 2, pp. 408-424, 2013.
[111] M. Thurai, E. Deguchi, T. Iguchi, and K. Okamoto, "Freezing height distribution in the tropics," *International Journal of Satellite Communications and Networking,* vol. 21, no. 6, pp. 533-545, 2003.
[112] J. Awaka, T. Iguchi, and K. Okamoto, "Early results on rain type classification by the Tropical Rainfall Measuring Mission (TRMM) precipitation radar," in *Proc. Eighth URSI Commission F Open Symp*, 1998, pp. 143-146.
[113] T. Iguchi, T. Kozu, R. Meneghini, J. Awaka, and K. Okamoto, "Rain-profiling algorithm for the TRMM precipitation radar," *Journal of Applied Meteorology,* vol. 39, no. 12, pp. 2038-2052, 2000.
[114] A. Funk, C. Schumacher, and J. Awaka, "Analysis of Rain Classifications over the Tropics by Version 7 of the TRMM PR 2A23 Algorithm," *Journal of the Meteorological Society of Japan,* vol. 91, no. 3, pp. 257-272, 2013.
[115] C. Kummerow, W. Barnes, T. Kozu, J. Shiue, and J. Simpson, "The tropical rainfall measuring mission (TRMM) sensor package," *Journal of Atmospheric and Oceanic Technology,* vol. 15, no. 3, pp. 809-817, 1998.
[116] J. Awaka, T. Iguchi, H. Kumagai, and K. i. Okamoto, "Rain type classification algorithm for TRMM precipitation radar," in *IEEE International Geoscience and Remote Sensing*, 1997, vol. 4, pp. 1633-1635.
[117] R. Meneghini *et al.*, "Use of the surface reference technique for path attenuation estimates from the TRMM precipitation radar," *Journal of Applied Meteorology,* vol. 39, no. 12, pp. 2053-2070, 2000.
[118] R. Joaquin, "ITU and ITU-R basics and facts," *International Telecommunication Union, Geneva, Switzerland,* 2014.
[119] ITU-R Recommendations. (2007). *The List of ITU-R Recommendations*. Available: https://www.itu.int/pub/R-REC/en
[120] A. D. Papatsoris, K. Polimeris, and A. A. Lazou, "Development of rain attenuation and rain rate maps for satellite communications system design in Greece," *polis,* vol. 40, no. 51, pp. 25-57, 2008.
[121] K. Chakravarty and A. Maitra, "Rain attenuation studies over an Earth–space path at a tropical location," *Journal of Atmospheric and Solar-Terrestrial Physics,* vol. 72, no. 1, pp. 135-138, 2010.
[122] A. AAM Ali, "Slant path rain attenuation profile obtained from radar data," Universiti Teknologi Malaysia, Faculty of Electrical Engineering, 2009.
[123] A. Y. Abdulrahman *et al.*, "Investigation of the Unified Rain Attenuation Prediction Method With Data From Tropical Climates," *IEEE Antennas and Wireless Propagation Letters,* vol. 13, pp. 1108-1111, 2014.
[124] A. Adhikari and A. Maitra, "Studies on the inter-relation of Ku-band scintillations and rain attenuation over an Earth–space path on the basis of their static and dynamic spectral

analysis," *Journal of Atmospheric and Solar-Terrestrial Physics,* vol. 73, no. 4, pp. 516-527, 2011.

[125] D. Das and A. Maitra, "Time series prediction of rain attenuation from rain rate measurement using synthetic storm technique for a tropical location," *AEU - International Journal of Electronics and Communications,* vol. 68, no. 1, pp. 33-36, 1// 2014.

[126] J. S. Ojo, M. O. Ajewole, and S. K. Sarkar, "Rain rate and rain attenuation prediction for satellite communication in Ku and Ka bands over Nigeria," *Progress In Electromagnetics Research B,* vol. 5, pp. 207-223, 2008.

[127] J. S. Mandeep, "Slant path rain attenuation comparison of prediction models for satellite applications in Malaysia," *Journal of Geophysical Research,* vol. 114, no. D17108, 2009.

[128] E. O. Olurotimi and J. S. Ojo, "Testing rainfall rate models for rain attenuation prediction purposes in tropical climate," in *2014 XXXIth URSI General Assembly and Scientific Symposium (URSI GASS)*, Beijing, 2014, pp. 1-4.

[129] J. S. Ojo and P. A. Owolawi, "Application of synthetic storm technique for diurnal and seasonal variation of slant path Ka-band rain attenuation time series over a subtropical location in South Africa," *International Journal of Antennas and Propagation,* vol. 2015, 2015.

[130] S. H. Lin, "A method for calculating rain attenuation distributions on microwave paths," *Bell System Technical Journal,* vol. 54, no. 6, pp. 1051-1086, 1975.

[131] G. O. Ajayi and F. Barbaliscia, "Prediction of attenuation due to rain: characteristics of the 0^{o} C isotherm in temperate and tropical climates," *International Journal of Satellite Communications,* vol. 8, no. 3, pp. 187-196, 1990.

[132] E. O. Olurotimi, O. Sokoya, J. S. Ojo, and P. A. Owolawi, "Analysis of bright-band height data from TRMM-PR for satellite communication in Durban, South Africa," in *IEEE AFRICON 2015*, Addis-Ababa, Ethiopia, 2015, pp. 1-5.

[133] E. O. Olurotimi, O. Sokoya, J. S. Ojo, and P. A. Owolawi, "Distribution of rain height over subtropical region: Durban, South Africa for satellite communication systems," in *IOP Conference Series: Materials Science and Engineering*, 2018, vol. 321, no. 1, p. 012006: IOP Publishing.

[134] K. Paulson and A. Al-Mreri, "A rain height model to predict fading due to wet snow on terrestrial links," *Radio Science,* vol. 46, no. 04, pp. 1-6, 2011.

[135] K. Paulson and A. Al-Mreri, "Trends in the incidence of rain height and the effects on global satellite telecommunications," *Microwaves, Antennas & Propagation, IET,* vol. 5, no. 14, pp. 1710-1713, 2011.

[136] R. S. Bradley, F. T. Keimig, H. F. Diaz, and D. R. Hardy, "Recent changes in freezing level heights in the Tropics with implications for the deglacierization of high mountain regions," *Geophysical Research Letters,* vol. 36, no. 17, 2009.

[137] S. Das and A. Maitra, "Some melting layer characteristics at two tropical locations in Indian region," in *XXXth URSI General Assembly and Scientific Symposium*, 2011, pp. 1-4.

[138] A. I. O. Yussuff and N. H. H. Khamis, "Comparative analysis of bright band data from TRMM and ground radar data in Malaysia," *International Journal of Networks and Communications,* vol. 3, no. 4, pp. 99-109, 2013.

[139] G. O. Ajayi and P. A. Odunewu, "Some characteristics of the rain height in a tropical environment," in *IET Sixth International Conference on Antennas and Propagation*, 1989, pp. 80-82.

[140] J. S. Ojo, S. E. Falodun, and O. Odiba, "0° C isotherm height distribution for Earth-space communication satellite links in Nigeria," *Indian Journal of Radio and Space Physics,* vol. 43, pp. 225-234, 2014.

[141] J. S. Mandeep, "0°C isotherm height for satellite communication in Malaysia," *Advances in Space Research,* vol. 43, no. 6, pp. 984-989, 2009.

[142] ITU-R Recommendation P.618-12, "Propagation data and prediction methods required for the design of Earth-space telecommunication systems," *International Telecommunication Union, Geneva, Switzerland,* 2015.

[143] ITU-R Recommendation P.620-6, "Propagation data required for the evaluation of coordination distances in the frequency range 100 MHz to 105 GHz," *International Telecommunication Union, Geneva, Switzerland,* 2005.

[144] ITU-R Recommendation P.452-16, "Prediction procedure for evaluation of interference between stations on the surface of the Earth at frequencies above about 0.1 GHz," *International Telecommunication Union, Geneva, Switzerland,* 2015.

[145] ITU-R Radio Regulations Appendix 7, "Method of the determination of the coordination area around an Earth station in frequency range 100 MHz to 105 GHz . 'Propagation in non-ionised media'," *International Telecommunication Union, Geneva, Switzerland,* 2012.

[146] ITU-R Recommendation P.839-4, "Rain height model for prediction methods," *International Telecommunication Union, Geneva, Switzerland,* 2013.

[147] M. Satake, K. Oshimura, Y. Ishido, S. Kawase, and T. Kozu, "TRMM PR data processing and calibration to be performed by NASDA," in *International Geoscience and Remote Sensing Symposium*, 1995, vol. 1, pp. 57-59 vol.1.

[148] T. Kozu, T. Kawanishi, K. Oshimura, M. Satake, and H. Kumagai, "TRMM precipitation radar: Calibration and data collection strategies," in *International Geoscience and Remote Sensing Symposium*, 1994, vol. 4, pp. 2215-2217.

[149] N. Takahashi and T. Iguchi, "Estimation and correction of beam mismatch of the precipitation radar after an orbit boost of the Tropical Rainfall Measuring Mission satellite," *IEEE transactions on geoscience and remote sensing,* vol. 42, no. 11, pp. 2362-2369, 2004.

[150] C. Ho, "Modeling and simulation for realistic propagation environments of communications signals at SHF band," *Annual ITEA Technology Review Conference,* 2005.

[151] M. Zubair, Z. Haider, S. A. Khan, and J. Nasir, "Atmospheric influences on satellite communications," *Przeglad Elektrotechniczny,* vol. 87, no. 5, pp. 261-264, 2011.

[152] M. S. Pontes, R. S. L. Souza, and E. C. B. Miranda, "Radiosonde data of the 0^{o} C isotherm height: Regulating factors in predicting radio wave attenuation due to rain," *Rio de Janeiro, Brazil,* 1990.

[153] ITU-R Recommendation P.839-2, "Rain height model for prediction methods," *International Telecommunication Union, Geneva, Switzerland,* 1999.

[154] H. F. Diaz and N. E. Graham, "Recent changes in tropical freezing heights and the role of sea surface temperature," *Nature [H.W.Wilson - GS],* vol. 383, p. 152, 1996.

[155] G. N. Harris Jr, K. P. Bowman, and D.-B. Shin, "Comparison of freezing-level altitudes from the NCEP reanalysis with TRMM precipitation radar brightband data," *Journal of Climate,* vol. 13, no. 23, pp. 4137-4148, 2000.
[156] Golden Software Support. (2018). *A basic understanding of Surfer gridding methods - Part 1*. Available: https://support.goldensoftware.com/hc/en-us/articles/231348728
[157] ITU-R Recommendation P.839-3, "Rain height model for prediction methods," *International Telecommunication Union, Geneva, Switzerland,* 2001.
[158] C. Dagum, "A model of income distribution and the conditions of existence of moments of finite order," in *Proceedings of the 40th session of the International Statistical Institute*, 1975, vol. 46, pp. 196-202.
[159] C. Kleiber and S. Kotz, *Statistical size distributions in economics and actuarial sciences*. John Wiley & Sons, 2003.
[160] C. Kleiber, "A guide to the Dagum distributions," in *Modeling Income Distributions and Lorenz Curves*: Springer, 2008, pp. 97-117.
[161] C. Dagum, "The generation and distribution of income, the lorentz curve and the gini ratio," *Economie Appliquée,* vol. 33, no. 2, pp. 327-367, 1980.
[162] C. Dagum, *Income distribution models*. Wiley Online Library, 1983.
[163] S. Dey, B. Al-Zahrani, and S. Basloom, "Dagum Distribution: Properties and Different Methods of Estimation," *International Journal of Statistics and Probability,* vol. 6, no. 2, p. 74, 2017.
[164] E. O. Olurotimi, O. Sokoya, J. S. Ojo, and P. A. Owolawi, "Freezing height level distribution over Durban, South Africa for satellite communication," in *Radio and Antenna Days of the Indian Ocean*, Cape Town, 2017, pp. 1-2.
[165] N. L. Johnson, S. Kotz, and N. Balakrishnan, "Distributions in statistics: continuous univariate distributions," *NY: Wiley,* vol. 2, 1970.
[166] N. L. Johnson, S. Kotz, and N. Balakrishnam, "Noncentral χ 2 distributions. Noncentral F distributions," *Continuous univariate distributions,* vol. 2, p. 433, 1995.
[167] P. E. Verde, L. A. Geracitano, L. L. Amado, C. E. Rosa, A. Bianchini, and J. M. Monserrat, "Application of public-domain statistical analysis software for evaluation and comparison of comet assay data," *Mutation Research/Genetic Toxicology and Environmental Mutagenesis,* vol. 604, no. 1, pp. 71-82, 2006.
[168] M. O. Ojo and A. Olapade, "On the generalized logistic and log-logistic distributions," *Kragujevac Journal of Mathematics,* vol. 25, no. 25, pp. 65-73, 2003.
[169] A. E. Mohammed, P. S. Karan, and A. B. Alfred, "A generalized log-logistic model for analysis of survival data," in *Proceedings of the Statistical Computing Section,*, 1992, pp. 113-118: American Statistical Association.
[170] G. Casella and R. L. Berger, "Statistical inference. The Wadsworth & Brooks/Cole Statistics/Probability Series. Wadsworth & Brooks," ed: Cole Advanced Books & Software, Pacific Grove, CA, 1990.
[171] A. C. Cohen, "Progressively censored samples in life testing," *Technometrics,* vol. 5, no. 3, pp. 327-339, 1963.
[172] D. P. Raykundaliya, "Modified maximum likelihood estimation of parameters in the log-logistic distribution under progressive Type II censored data with binomial removals," *International Journal of Engineering, Pure and Applied Sciences,* vol. 2, no. 1, 2017.
[173] B. Elbert, *Introduction to satellite communication*. Artech House, 2008.

[174] B. A. Albrecht, "Aerosols, cloud microphysics, and fractional cloudiness," *Science,* vol. 245, no. 4923, pp. 1227-1230, 1989.
[175] L. Luini and C. Capsoni, "A unified model for the prediction of spatial and temporal rainfall rate statistics," *IEEE Transactions on Antennas and Propagation,* vol. 61, no. 10, pp. 5249-5254, 2013.
[176] L. Luini and C. Capsoni, "Efficient calculation of cloud attenuation for earth–space applications," *IEEE Antennas and Wireless Propagation Letters,* vol. 13, pp. 1136-1139, 2014.
[177] O. Banjo and E. Vilar, "Measurement and modeling of amplitude scintillations on low-elevation earth-space paths and impact on communication systems," *IEEE transactions on communications,* vol. 34, no. 8, pp. 774-780, 1986.
[178] G. Peeters, F. S. Marzano, G. d'Auria, C. Riva, and D. Vanhoenacker-Janvier, "Evaluation of statistical models for clear-air scintillation prediction using olympus satellite measurements," *International Journal of Satellite Communications,* vol. 15, no. 2, pp. 73-88, 1997.
[179] J. S. Ojo, B. Rabiu, S. M. Radicella, and O. O. Obiyemi, "Experimental analysis and comparison of tropospheric scintillation prediction models using eutelsat-36b satellite in a tropical Nigeria," *International Journal of Basic and Applied Sciences,* vol. 7, no. 1, pp. 8-14, 2018.
[180] M. A. Hussein, "Scintillation Effect on Satellite Communications within Standard Atmosphere," *Anbar Journal for Engineering Sciences,* vol. 2, no. 2, pp. 17-27, 2009.
[181] A. C. C. Yee *et al.*, "Development of new tropospheric scintillation prediction model for country in tropical climate," in *IEEE International Conference on Space Science and Communication*, 2011, pp. 93-95.
[182] R. K. Crane and A. W. Dissanayake, "ACTS propagation experiment: attenuation distribution observations and prediction model comparisons," *Proceedings of the IEEE,* vol. 85, no. 6, pp. 879-892, 1997.
[183] J. W. Ryde, "The attenuation and radar echoes produced at centimeter wavelengths by various meteorological phenomena," *Meteorological Factors in Radio Wave Propagation, London,* pp. 169-189, 1946.
[184] R. G. Medhurst, "Rainfall attenuation of centimeter waves: Comparison of theory and measurement," *IEEE Transactions on Antennas and Propagation,* vol. 13, no. 4, pp. 550-564, 1965.
[185] R. K. Crane, "Prediction of the effects of rain on satellite communication systems," *Proceedings of the IEEE,* vol. 65, no. 3, pp. 456-474, 1977.
[186] W. L. Stutzman and W. K. Dishman, "A simple model for the estimation of rain-induced attenuation along earth-space paths at millimeter wavelengths," *Radio Science,* vol. 17, no. 6, pp. 1465-1476, 1982.
[187] E. J. Dutton, H. T. Dougherty, and R. F. Martin Jr, "Prediction of European rainfall and link performance coefficients at 8 to 30 GHz," Institute for Telecommunication Sciences Boulder Colombia 1974.
[188] B. Arbesser-Rastburg, E.-e. Tos-eep, and K. N. l.-A. Noordwijk, "Radiowave propagation modelling for new satcom services at Ku-band and above," *COST 255,* 2002.

[189] A. Chavan and R. D. Patane, "Performance Improvement of Intelligent Weather System for Satellite Networks," *International Journal of Scientific and Research Publications,* vol. 7, pp. 579-583, 2015.

[190] K. Harb, A. Srinivasan, C. Huang, and B. Cheng, "Prediction method to maintain QoS in weather impacted wireless and satellite networks," in *IEEE International Conference on Systems, Man and Cybernetics* 2007, pp. 4008-4013.

[191] ITU-R Recommendation P.530-17, "Propagation data and prediction methods required for the design of terrestrial line-of-sight systems," *International Telecommunication Union, Geneva, Switzerland,* 2017.

[192] D. H. Johnson, "Signal-to-noise ratio," *Scholarpedia,* vol. 1, no. 12, p. 2088, 2006.

[193] I. A. Adegbindin, P. A. Owolawi, and M. O. Odhiambo, "Intelligent Weather Awareness Technique for Mitigating Propagation Impairment at SHF and EHF Satellite Network System in a Tropical Climate," *SAIEE Africa Research Journal,* vol. 107, no. 3, pp. 136-145, 2016.

[194] E. Lutz, M. Werner, and A. Jahn, *Satellite systems for personal and broadband communications*. Springer Science & Business Media, 2012.

[195] P. M. Smith, A. Kar, W. J. Boettinger, J. A. West, C. C. Koch, and W. W. Mullins, "Recent changes in tropical freezing heights and the role of sea surface temperature," *Nature,* vol. 383, p. 12, 1996.

ANNEXURES

ANNEXURE A-1: HDFView Interface showing typical TRMM 2A23 parameters (displayed only ZDIH values)

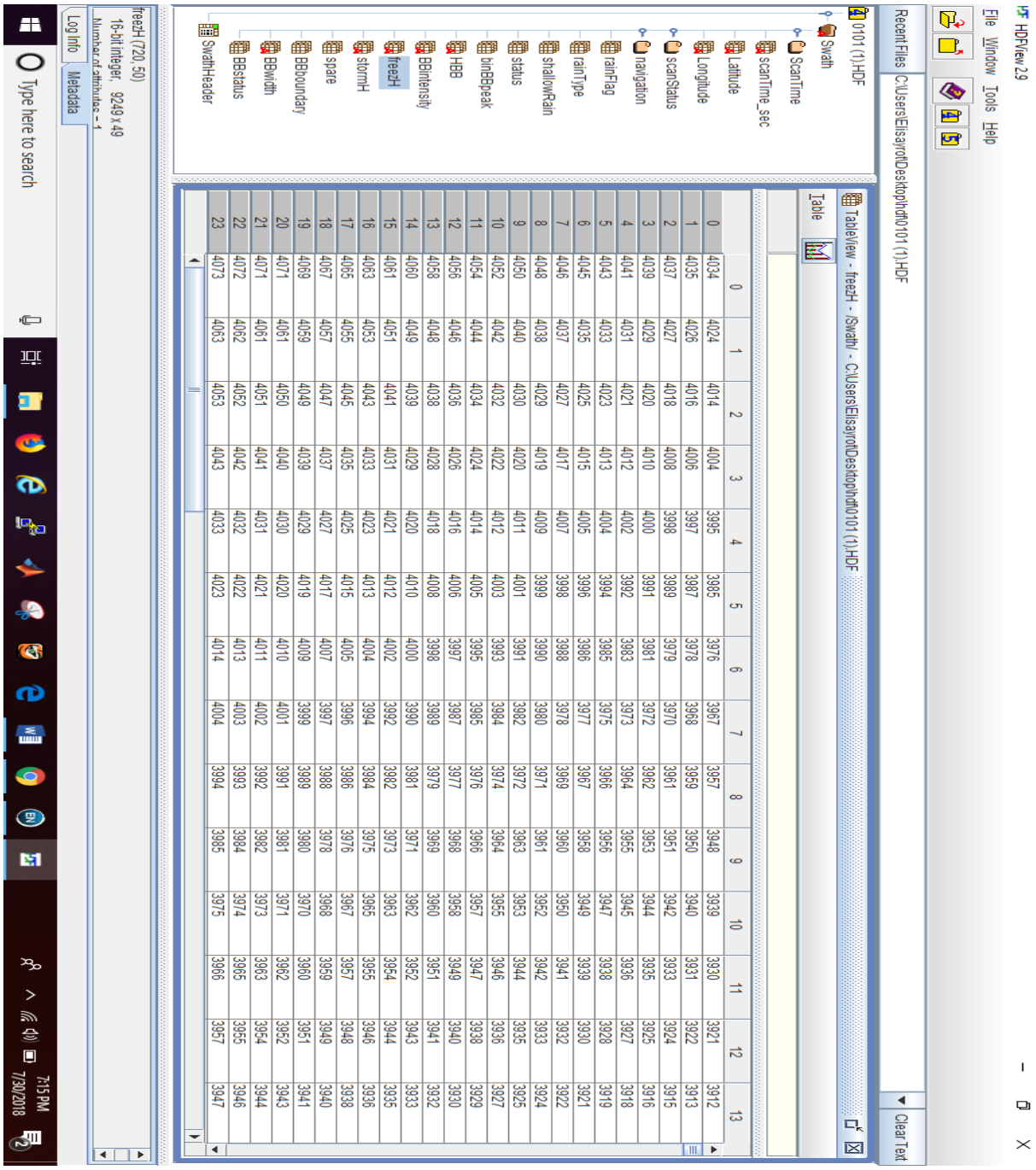

ANNEXURE A-2: Microsoft Excel Interface showing typical TRMM 2A23 parameters (displayed only ZDIH values)

ANNEXURE A-3: TRMM 2A23 parameters on MATLAB Interface (displayed only ZDIH values)